Stony Brook University

Indentation of Transversely Isotropic Materials

A Dissertation Presented

by

Talapady Srivatsa Bhat

to

The Graduate School

in Partial Fulfillment of the

Requirements

for the Degree of

Doctor of Philosophy

in

Materials Science and Engineering

Stony Brook University

August 2012

Stony Brook University

The Graduate School

Talapady Srivatsa Bhat

We, the dissertation committee for the above candidate for the

Doctor of Philosophy degree, hereby recommend

acceptance of this dissertation.

Dr. T. A. Venkatesh – Dissertation Advisor
Assistant Professor, Materials Science and Engineering

Dr. Tadanori Koga- Chairperson of Defense
Assistant Professor, Materials Science and Engineering

Dr. Yizhi Meng
Assistant Professor, Materials Science and Engineering

Dr. Maen Alkhader
Assistant Professor, Mechanical Engineering

This dissertation is accepted by the Graduate School

Charles Taber
Interim Dean of the Graduate School

Abstract of the Dissertation

On the Instrumented Indentation of Transversely Isotropic Materials

by

Talapady Srivatsa Bhat

Doctor of Philosophy

in

Materials Science and Engineering

Stony Brook University

2012

Instrumented indentation, as a tool for characterization of mechanical properties, has well been established in the past decades. Studies have been conducted to understand the behavior of isotropic materials under indentation and techniques to accurately predict isotropic material properties have also been reported. Further, within the isotropic regime, work has been done to predict the indentation hardness without having to investigate the area of contact during indentation. Studies have also reported the prospect of utilizing indentation to predict the fatigue behavior of isotropic materials. This dissertation is made with the intent of extending the use of indentation, as a characterization tool, to the anisotropic regime.

The effect of transverse isotropy on the indentation response of materials is systematically studied here. Extensive computational analysis is performed to elucidate the underlying deformation mechanics of indentation of transversely isotropic materials. Owing to the anisotropy, indentation may be performed parallel or perpendicular to the plane of isotropy of the specimen. It is observed that the indentation response varies significantly for each of these cases. The two cases are treated as unique and an identical systematic analysis is carried for both. The indentation orientations shall henceforth be referred to as transverse and longitudinal indentation for indentation

parallel and perpendicular to the plane of isotropy respectively. A technique is developed capable of extracting the elastic-plastic properties of transversely isotropic materials from interpretation of indentation response in either direction. The technique is rigorously tested for its robustness, accuracy and uniqueness of results. A sensitivity analysis is performed to determine how sensitive the technique is to errors in experimental results. Rigorous studies are performed to understand the variation in pile-up or sink-in during indentation with varying anisotropy in the specimen. As a result of these studies, relations are obtained between the contact area and hardness during indentation and material properties of transversely isotropic materials. Further, utilizing the previously devised technique, relations which directly predict hardness from either known material properties or known indentation response, in either the transverse or longitudinal direction, without actually measuring the area of contact are obtained. Variation of hardness with anisotropy as well as other material properties is thoroughly studied. Fatigue response of transversely isotropic materials to cyclic indentation is studied using computation analysis. Distinct variation in the fatigue response with varying anisotropy is observed and reported.

A systematic investigation into the indentation behavior of materials with residual stress is undertaken. Algorithms are developed to predict the residual stress and material properties for elastic perfectly plastic materials from known indentation response for both isotropic as well as transversely isotropic materials. The algorithms are then tested for their accuracy and sensitivity.

Dedicated To

My Parents

Table of Contents

List of Figures

List of Tables

Acknowledgements

The journey through my PhD has been the most challenging as well as memorable time of my life and it would not have been possible without a considerable amount of help and support from the people around me.

First I would like to thank my guide and mentor, Prof. T. A. Venkatesh for giving me this wonderful opportunity. His academic guidance, inspiration and undying support have been invaluable to me. This work would not have been possible without his encouragement and patience.

I would like to thank the grant which, in part, has funded this work, the National Science Foundation grant DMR-0836763.

Furthermore, I would like to thank Dr. Ronit Kar Gupta for guiding me patiently every time I came up to him for help regarding ABAQUS. I sincerely thank Prof. T. Nakamura for his guidance related to executing ABAQUS codes. I would also like to thank my lab mates Sumantu Iyer, Guang Chen and Ming Tian for our long and fruitful discussions on modeling techniques. I deeply appreciate and thank Debbie Michienzi, Chandrani Roy and Lynn Allopena for their constant help with my official paperwork. I would also like to thank my fellow peers Dr. Gopal Dwivedi, Shayan Byrappa, Gagan Jodhani, Saurabh Patel, Girish Ramakrishnan, for many discussions on the subject matter. My undergraduate colleague and friend Jaya Nagamani and I have had many fruitful discussions on the various aspects of anisotropic materials and I appreciate her help and advice.

I would like to thank my committee members Prof. T. Koga, Prof. Maen Alkhader and Prof. Yizhi Meng for their support and time. I would also like to thank my fellow friends at Stony Brook University for their inspiration and constant support.

I am grateful to the Department of Materials Science and Engineering for having faith in me and giving me the opportunity to pursue my PhD.

The person responsible for my growth and development as a person and as a researcher, my father, Dr. T Balakrishna Bhat has guided, encouraged and advised me constantly through my PhD and I am deeply grateful to him for the ideas that spawned from our discussions and for his inspirational words.

Finally I would like to thank my loving mother, my role model and brother Chakrapani, my sister Vidyadayini, my younger brother Madhav and friends all over the world as every contribution has been invaluable to me.

1 Introduction

The exponential growth of science and technology in the past few decades has led to a rapid miniaturization of devices and structures. The dimensions and structure of engineered materials has shrunk from the macro scale down to the micro and nano scale. It has often been observed that the properties of materials vary significantly from their macroscopic counterparts as we delve into micro and nano sizes. It is thus imperative to develop tools for the characterization of the mechanical properties at small length scales in an accurate and systematic manner. Instrumented indentation analysis provides a simple and convenient method to accurately characterize the mechanical behavior of materials at all scales.

Instrumented indentation as an analysis tool has rapidly gained interest owing to its versatility and simplicity. In particular, in systems where conventional testing methods fail, indentation method has shown an excellent alternative way for material characterization for e.g. [1, 2].

Many attempts have been made to tap the potential of instrumented indentation as a characterization tool. Analytical, experimental and computational techniques have been utilized to elucidate the contact mechanics during indentation. These studies have been successful in utilizing indentation response parameters to predict material

properties within the isotropic regime for e.g. [3-5]. Most miniature structures however display a certain degree of anisotropy due to the effect of confinement and specific microstructures imposed during fabrication. However, in spite of the extensive research in the isotropic regime, there has been little work on the indentation response of anisotropic materials.

To this end, this study attempts to lay the foundations for extensive investigation into the indentation response of anisotropic materials. Here, computational and experimental approaches are utilized to further the research done on isotropic materials to understand the mechanics and indentation response of transversely isotropic materials.

Instrumented indentation on a transversely isotropic material can be performed either parallel or perpendicular to the plane of isotropy of the material. The indentation response for each of these two cases is distinct. This study investigates both these cases. Using dimensional analysis, closed-form functions are developed correlating material properties to indentation response. Coefficients of these functions are then accurately determined using finite element analysis, modeling the indentation response for sharp indenters with cone half angles of 50, 60 and 70.3 degrees over a large range of material properties. An approach similar to the investigation carried out by studies on isotropic materials is utilized to generate

- A forward analysis that predicts the indentation response from known empirical constitutive relations of the material,
- A reverse analysis that predicts the materials empirical constitutive relations from known indentation response.

In addition, the hardness of a material is an important parameter widely utilized to describe mechanical characteristics of materials. The challenge with respect to prediction of hardness lies in accurately measuring the area of contact during indentation. Prior to this, other studies have attempted the prediction of the hardness of isotropic materials for e.g. [6, 7]. This study aims at devising algorithms to predict transversely isotropic materials hardness during indentation, perpendicular as well as parallel to the plane of isotropy, from known empirical constitutive relations or known indentation response parameters without actually having to investigate the area of contact during indentation.

Fatigue analysis of engineered components is an essential part of investigating a structure. Cyclic indentation has been used in the past to study the fatigue behavior of materials [8-12]. This study aims at extending the theory of indentation fatigue behavior to anisotropic materials.

In addition to anisotropy one other material processing artifact found in materials is residual stress. The determination of the extent of residual stress in miniature components using conventional techniques poses significant issues. Here again, indentation provides a convenient and simple alternative to conventional testing techniques. In this study, indentation is used to develop relations correlating indentation response with residual stress and material properties for elastic perfectly plastic materials with isotropic or transversely isotropic properties and specific forward and reverse algorithms are developed.

The main objective of this work is to develop computational tools for the study of transversely isotropic materials. The computational modeling focuses on instrumented indentation using single, dual and triple indentation with sharp indenters. The thesis is organized as follows:

- Chapter 2 presents a systematic analysis of triple indentation parallel and perpendicular to the plane of isotropy of transversely isotropic materials. Forward and reverse algorithms are formulated and a comprehensive analysis of the uniqueness and sensitivity of the proposed algorithms is undertaken.
- Chapter 3 presents an argument which uses the algorithms proposed in the previous chapter to the determination of hardness of transversely isotropic materials for indentation parallel and perpendicular to the plane of isotropy. A technique to predict the hardness without actually having to measure the area of contact under the indenter is proposed. Once again the accuracy and sensitivity of the technique is verified.
- Chapter 4 delves into the fatigue response of transversely isotropic materials when subject to cyclic indentation. Previously developed indentation fatigue law for isotropic materials is extended to the transversely isotropic regime. A study is done on the variation of indentation fatigue response parameters with varying anisotropy.
- Chapter 5 presents an investigation of the change in indentation response of isotropic and transversely isotropic materials with existing equibiaxial residual stresses. A systematic analysis is performed and algorithms are developed to predict the residual stress and material properties for elastic perfectly plastic

isotropic materials from known indentation response. Further, algorithms are then developed to predict the residual stress and transversely isotropic plastic properties of materials from known indentation response and elastic modulus. The algorithms are then tested for their accuracy, and sensitivity.

- Chapter 6 concludes this thesis with a summary of the work done and a brief discussion on the significance of this work.
- Chapter 7 delves into the future possibilities and promises of the field of indentation analysis.

2 Computational modeling of the forward and reverse problems in the indentation of transversely isotropic materials

2.1 Introduction

Indentation based methods for property assessment and characterization have received considerable attention in recent times owing to their simplicity and versatility. Furthermore, within the context of thin-films, coatings, and small-volume materials where conventional methods of property evaluation are not readily applicable, there is a greater motivation for developing several small-scale test methods such as those based on the indentation technique for property determination and assessment as well.

A large number of studies have focused on the determination of several mechanical and functional properties of substrate materials such as hardness, and also elastic, plastic, fracture, and piezoelectric properties using indentation-based methods [3, 5-7, 13-25]. A combination of analytical modeling [26, 27], computational modeling [3, 5, 6, 13, 14, 17, 19-21, 28-33] and experiments [1, 15] have been invoked to obtain a better understanding of the indentation response of a wide variety of materials that include metals, alloys, ceramics, polymers, metallic glasses, foams and composites. Owing to the complexity in the deformation behavior associated with the indentation process, analytical modeling approaches are, in general, unable to capture the

complete indentation characteristics of a wide variety of materials. Consequently, many recent efforts have focused on developing computational approaches to accurately capture the indentation response of select classes of materials.

In the computational approach, the indentation problem is generally divided into two parts: (i) the “forward problem” – where the characteristics of the indentation response are predicted from known elastic and plastic properties of the substrate material; and (ii) the “reverse problem” – where the elastic and plastic properties are estimated from experimentally measured indentation response. Based on the forward and reverse analyses, several forward and reverse algorithms have been developed to map the materials’ elastic and plastic properties with their corresponding indentation response characteristics.

In developing and applying the forward and reverse algorithms to a broad class of materials, two questions are generally identified as being important [4, 29, 31, 34-41]:

(i) Indentation – Uniqueness: Does a unique set of material properties map to a unique set of indentation response parameters, both in the forward and the reverse analyses?

(ii) Indentation – Sensitivity: How accurate should the experimental measurements of the indentation parameters be in order to obtain reasonable estimates of the mechanical properties of the indented substrate materials?

Consequently, methods that rely on multiple indentations to address potential non-uniqueness issues with the indentation analysis [34, 35, 37, 39-42] and those that

provide reduced sensitivity for a robust estimation of mechanical properties have also been developed [4, 32, 38, 39]. Furthermore, several studies have also considered the effects of pile-up and sink-in that may occur in indentation experiments as well [28, 30, 43].

However, much of the prior studies have focused on developing the forward and reverse indentation analyses of isotropic materials and very few studies [44] have attempted to obtain an understanding of the indentation of anisotropic (e.g., transversely isotropic) materials. As there are several engineering 'bulk' and 'thin film' materials which are transversely isotropic that exhibit varying degrees of elastic and plastic anisotropy, there is a compelling need to understand the indentation behavior of such transversely isotropic materials. Hence, the objectives of the present study described in this chapter are as follows.

(i) To develop a multiple indentation-based framework for capturing the indentation response of transversely isotropic materials.

(ii) To formulate a forward algorithm to predict the indentation response of transversely isotropic materials and a reverse algorithm to obtain the material elastic and plastic properties from measured indentation responses.

(iii) To assess the issues of uniqueness and sensitivity within the context of the indentation of transversely isotropic materials.

The present chapter is organized as follows. Theoretical background information about the mechanical properties of transversely isotropic materials and the fundamentals of indentation are presented in section 2.2. A framework based on dimensional analysis and computational modeling for understanding the indentation

response of transversely isotropic materials is formulated in section 2.3. The results of the indentation simulations, the forward and reverse indentation algorithms, and the uniqueness and sensitivity issues associated with the forward and reverse analyses are discussed in section 2.4. A comparison between forward-reverse analysis and experimental data from literature, for both isotropic and transversely isotropic materials, is made in section 2.5. Principal conclusions are highlighted in section 2.6.

2.2 Background on transversely isotropic materials and instrumented indentation

2.2.1 Mechanical properties of transversely isotropic materials

A transversely isotropic material is one with physical properties symmetric about an axis normal to a plane of isotropy. A partial list of engineering materials that exhibit transverse isotropy is provided in Table 2.1 [45]. In the present study, two classes of indentations are identified (Fig. 2-1):

(i) Longitudinal indentations where in the indentations are perpendicular to the plane of isotropy; and

(ii) Transverse indentations where in the indentations are parallel to the plane of isotropy;

2.2.1.1 Elastic properties

The elastic properties of a transversely isotropic material can be described using five independent constants. Let us assume an x-y-z coordinate system as shown in Fig.2-1a. Also let us assume the x-z plane to be the transverse plane of isotropy. The

compliance matrix of a transversely isotropic material can then be expressed in the form of the Young's moduli, shear moduli and the Poisson's ratios as:

$$\begin{bmatrix} \varepsilon_{11} \\ \varepsilon_{22} \\ \varepsilon_{33} \\ \gamma_{12} \\ \gamma_{23} \\ \gamma_{13} \end{bmatrix} = \begin{bmatrix} 1/E_T & -\nu_{LT}/E_L & -\nu_T/E_T & 0 & 0 & 0 \\ -\nu_{TL}/E_T & 1/E_L & -\nu_{TL}/E_T & 0 & 0 & 0 \\ -\nu_T/E_T & -\nu_{LT}/E_L & 1/E_T & 0 & 0 & 0 \\ 0 & 0 & 0 & 1/G_L & 0 & 0 \\ 0 & 0 & 0 & 0 & 1/G_L & 0 \\ 0 & 0 & 0 & 0 & 0 & 1/G_T \end{bmatrix} \begin{bmatrix} \sigma_{11} \\ \sigma_{22} \\ \sigma_{33} \\ \sigma_{12} \\ \sigma_{23} \\ \sigma_{13} \end{bmatrix} \quad \text{Eq 2-1}$$

Table 2.1 : List of transversely isotropic engineering materials that exhibit varying degrees of elastic and plastic anisotropy.

Material	**E_0 (GPa)**	**E_L/E_T**	**σ_0(MPa)**	**σ_L/σ_T**	**n**	***ν***
Annealed tool steel	192	1	610	1.4	0.1	0.3
Al Castings 242-0T21	71	1	155	1.5	0.16	0.3
Malleable Iron	210	1	285	1.54	0.01	0.3
2124 Al 15% SiC Whiskers	105	1.2	480	1.5	0.1	0.3
Ti-15V-3Cr-3Al-3Sn	164	1.3	1200	1.35	0	0.4
Zirconium	112	1.3	230	1.4	0.1	0.35
Ductile Iron ASTM A 476-70	210	1	483	1.33	0.1	0.3
Be-Cu Alloy 50C UNS C81800	110	1	238	2	0.18	0.3
Al 6092 17.5 SiC whiskers	121	1.05	452.5	1.15	0.1	0.33
Titanium	123.82	1.37	200	1.57	0.07	0.35

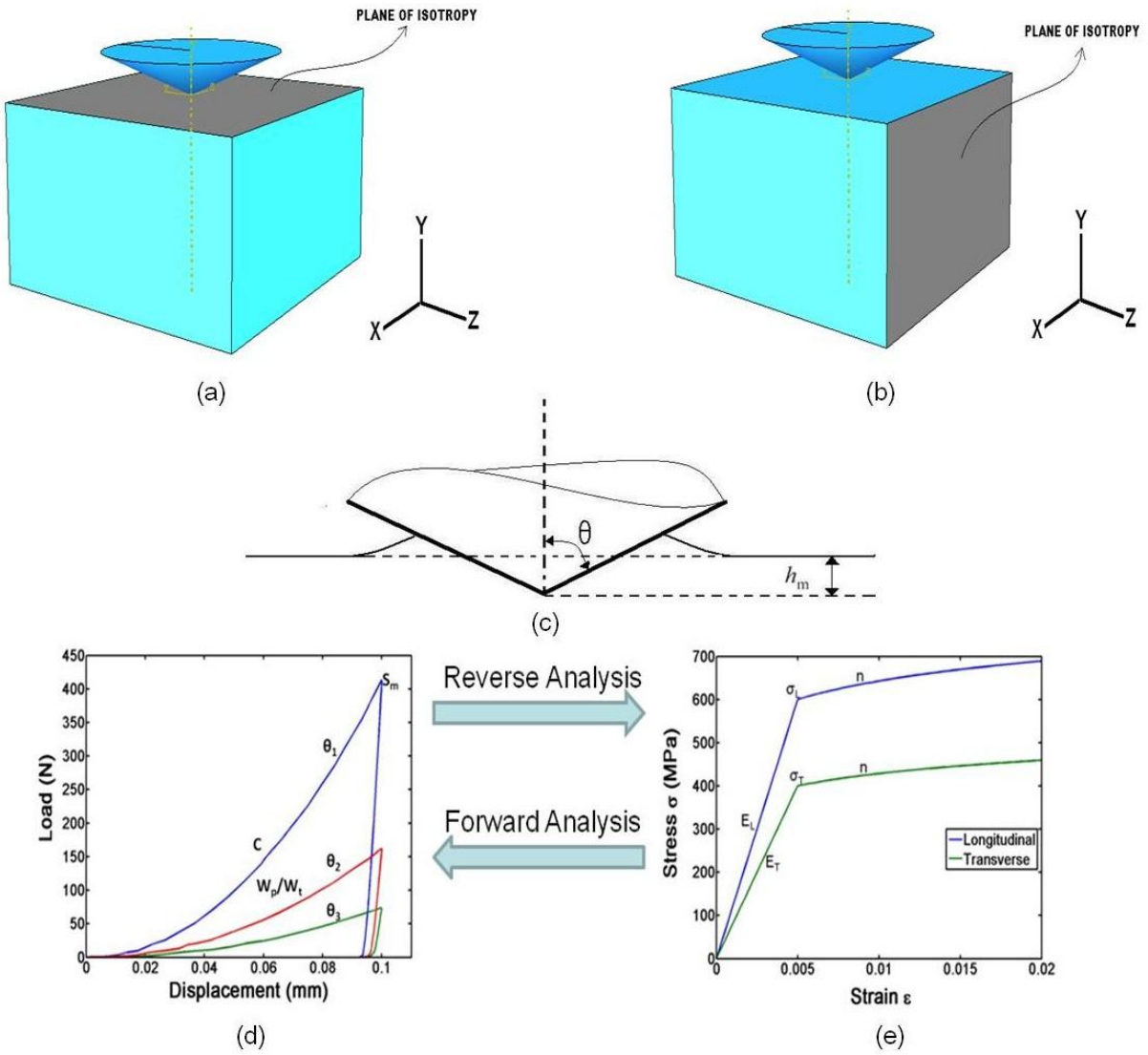

Figure 2-1: Schematic illustrating (a) longitudinal indentation and (b) transverse indentation of a transversely isotropic material. (c) Indentation with a typical conical indenter with an indenter cone half angle θ and the corresponding depth of penetration h_m (d), (e) Characteristic indentation responses of transversely isotropic materials obtained through triple indentations (with three indenters) and the elastic and plastic properties of the transversely isotropic substrate material determined through the reverse analysis.

$$\frac{E_L}{E_T} = \frac{\nu_{LT}}{\nu_{TL}} \qquad \text{Eq 2-2}$$

The in-plane shear modulus can be expressed as

$$G_T = \frac{E_T}{2(1+\nu_T)} \qquad \text{Eq 2-3}$$

Also, G_L is the out-of-plane shear modulus for planes x-y and y-z.

The Poisson's ratios ν_T, ν_{TL}, and $\nu_{LT,}$ are, respectively, given as $-\frac{\varepsilon_{33}}{\varepsilon_{11}}$, $-\frac{\varepsilon_{11}}{\varepsilon_{22}}$, and $-\frac{\varepsilon_{22}}{\varepsilon_{33}}$. Thus, five independent elastic constants - E_L, E_T, ν_T, ν_{TL}, and G_L (or alternately E_0, E_L/E_T, ν_T, ν_{TL}, and G_L) fully describe the elastic properties of a transversely isotropic material, where, E_0 is the average Young's modulus $(E_L+E_T)/2$.

2.2.1.2 Plastic properties

The plastic properties of a transversely isotropic material can be defined with the help of Hill's criterion for orthotropic materials. Hills criterion for yielding (1948) can be modified for transversely isotropic materials as:

$$f(\sigma) = \sqrt{(P(\sigma_{11}-\sigma_{22})^2 + P(\sigma_{22}-\sigma_{33})^2 + Q(\sigma_{33}-\sigma_{11})^2 + 2R\tau_{12}^2 + 2R\tau_{23}^2 + 2S\tau_{31}^2)} - \sigma_0 = 0. \qquad \text{Eq 2-4}$$

Here, σ_0 is the reference stress taken as $(\sigma_{0L}+ \sigma_{0T})/2$, and P, Q, R and S are the dimensionless constants that are related to σ_0 as:

$$P = \frac{1}{2}\left(\frac{\sigma_0}{\sigma_{0L}}\right)^2; \quad Q = \frac{1}{2}\left(2\frac{\sigma_0^2}{\sigma_{0T}^2} - \frac{\sigma_0^2}{\sigma_{0L}^2}\right); \quad R = \frac{1}{2}\left(\frac{\sigma_0}{\tau_{0L}}\right)^2; \quad S = \frac{1}{2}\left(\frac{\sigma_0}{\tau_{0T}}\right)^2; \qquad \text{Eq 2-5}$$

where, σ_{0L}, σ_{0T}, τ_{0L} and τ_{0T} are the yield stresses along the respective (i.e., longitudinal and transverse) directions. To reduce further complications the post-yielding behavior is restricted to isotropic power law hardening with a single hardening exponent 'n' for both longitudinal and transverse directions. For uniaxial stress-strain behavior the post yielding behavior for the longitudinal and transverse directions can be then defined as:

$$\sigma_L = (\sigma_{0L})\left(1 + \left(\frac{E_L}{\sigma_{0L}}\epsilon_L\right)\right)^n; \quad \text{for } \sigma_L > \sigma_{0L}, \text{ and} \qquad \text{Eq 2-6}$$

$$\sigma_T = (\sigma_{0T})\left(1 + \left(\frac{E_T}{\sigma_{0T}}\epsilon_T\right)\right)^n; \quad \text{for } \sigma_T > \sigma_{0T} \qquad \text{Eq 2-7}$$

Thus, we recognize that the elastic and plastic properties of a transversely isotropic material can be described by 10 constants, (five elastic constants, four yielding stresses, and one hardening exponent) if the strain hardening exponent is assumed to be the same for both the transverse and longitudinal directions. However, as pointed out by Nakamura et al. [44] estimating all these ten constants from the indentation analysis is extremely difficult. Hence, in this study an approach suggested by Nakamura et al. is invoked to reduce the total number of material constants that are required to reasonably capture the elastic and plastic properties of transversely isotropic materials to five. The approximations that help reduce the number of material constants from 10 to 5 are highlighted in Eqs. (2-8 to 2-10).

$$\nu_T = 0.3; \qquad \nu_{LT} + \nu_{TL} = 2\nu_T \qquad \text{Eq 2-8}$$

$$G_L = \frac{(E_L + E_T)}{4\left(1 + \left(\frac{\nu_{TL} + \nu_{LT}}{2}\right)\right)} \qquad \text{Eq 2-9}$$

$$\tau_{0T} = \frac{\sigma_0}{\sqrt{3}} \quad \text{and,} \quad \tau_{0L} = \frac{\sigma_0}{\sqrt{3}}\sqrt{\frac{\sigma_{0L}}{\sigma_{0T}}} \qquad \text{Eq 2-10}$$

The approximation of ν_T as 0.3 is reasonable as the Poisson's ratio of most metals falls close to this value. Next, the average of the two out-of-plane Poisson's ratio is taken to be equal to the in-plane Poisson's ratio. The out-of-plane shear modulus - G_L is also approximated in a manner similar to the definition of the in-plane shear modulus - G_T. Finally, the shear yield stresses are approximated in a manner similar to the Von-

Mises yield criterion for isotropic materials. These approximations are valid when the degree of anisotropy is low and the difference between properties in the longitudinal and transverse directions is not too large.

2.2.2 Indentation theory and nomenclature

The instrumented indentation technique of property determination involves indenting a substrate material with a (sharp or spherical) indenter and observing the corresponding force (P) - depth (h) relationships during the loading and unloading cycles. Figure 2-1d shows the typical P-h response of a power law hardening elasto-plastic material to sharp indentation. The loading response is governed by the equation:

$$P = Ch^2 \qquad \text{Eq 2-11}$$

where C is the loading curvature and is constant for a given material and indenter cone angle. The maximum indentation depth h_m occurs at the maximum load of P_m (Fig. 2-1c). The initial unloading slope is defined as,

$$S_m = \frac{dP_u}{dh}|h_m \qquad \text{Eq 2-12}$$

where P_u is the unloading force. The residual depth of the indent, after complete unloading, is termed as h_r. The area under the loading curve is the total work done (W_t) and the area under the unloading curve (W_e) represents the recovered elastic work done by the system. The plastic work done is given as $W_p = W_t - W_e$ and the plastic work ratio (R_w) is given as:

$$R_w = \frac{W_p}{W_t} \qquad \text{Eq 2-13}$$

Thus, we see that several indentation response parameters such as the loading curvature, C, the unloading slope at the maximum depth, S_m, the maximum and residual indentation depths, h_m and h_r and the areas under the loading and the unloading curves, W_p and W_e, can be invoked to determine the elastic and plastic properties of the indented material.

In general, the indentation response (i.e., the P-h response and the stress fields beneath the indenter) of a transversely isotropic material (e.g., with E_L/E_T = 1.5; E_L = 100 GPa and E_T = 150 GPa) varies considerably from its isotropic counterpart for which the elastic and plastic properties are obtained as a simple average of the properties of the transversely isotropic material (e.g., E = 125 GPa) (as illustrated in Figs. 2-2 to 2-3).

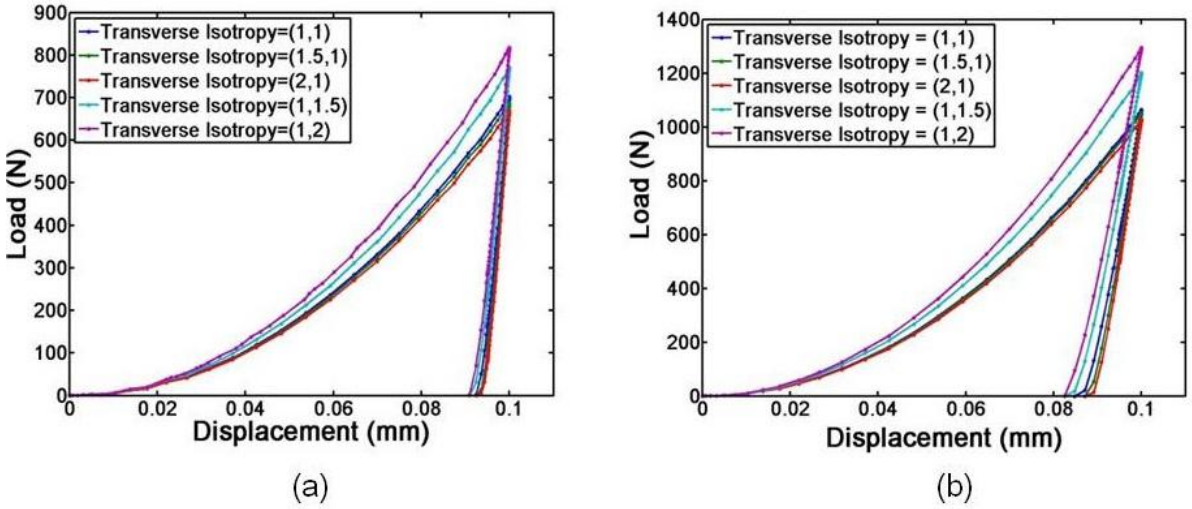

Figure 2-2: A comparison of the load-depth indentation response with varying anisotropy in the substrate material for (a) a material with no strain hardening and (b) a material with strain hardening coefficient, n=3. Here, (x, y) represents x as the degree of elastic anisotropy, and y the degree of plastic anisotropy.

It has been observed in the past that a single indentation experiment, for most cases, yields three independent parameters i.e, C, S_m and R_w. However, as discussed in section 2.2.1, the minimum number of independent constants needed to describe the

mechanical properties of a transversely isotropic material is five. Hence, it is clear that a single indentation experiment cannot be used to uniquely determine all the properties of a transversely isotropic material. Hence, in the present study, three indentations using three indenters with cone half angles of 50, 60 and 70.3 degrees have been used, which yields 9 distinct indentation response parameters for each material. That, the three P-h curves and corresponding nine indentation response parameters can help uniquely determine the elastic and plastic properties of transversely isotropic materials is demonstrated in section 2.4.

2.3 Framework for the indentation analysis of transversely isotropic materials

In the present study, a combination of dimensional analysis and finite element simulations is invoked to develop a framework that establishes the relationships between the elastic and plastic properties of transversely isotropic materials and their indentation responses.

2.3.1 Dimensional analysis

In prior studies, dimensional analysis has been invoked to identify closed form universal functions that capture the indentation behavior of isotropic materials. In the present study, as described below, dimensional analysis is invoked to develop closed form universal functions to capture the indentation behavior of transversely isotropic materials.

For a sharp indenter with a half cone angle of θ, the load required to indent a power law hardening transversely isotropic material can be written as:

$$P = P\left(h, E_0, \sigma, \frac{E_L}{E_T}, \frac{\sigma_L}{\sigma_T}, n, \theta\right)$$ Eq 2-14

Using dimensional analysis Eq. (14) becomes

$$P = \sigma_0 h^2 \Pi_{1\theta}\left(\frac{E_0}{\sigma_0}, \frac{E_L}{E_T}, \frac{\sigma_L}{\sigma_T}, n, \theta\right)$$ Eq 2-15

and from Eq. (2-11)

$$C = \frac{P}{h^2} = \sigma_0 \Pi_{1\theta}\left(\frac{E_0}{\sigma_0}, \frac{E_L}{E_T}, \frac{\sigma_L}{\sigma_T}, n, \theta\right)$$ Eq 2-16

or

$$C = \frac{P}{h^2} = \sigma_0 \Pi_{1i}\left(\frac{E_0}{\sigma_0}, \frac{E_L}{E_T}, \frac{\sigma_L}{\sigma_T}, n\right); \quad i = 1, 2, 3.$$ Eq 2-17

where i =1, 2, 3 represent the cone half angles 50, 60 and 70.3 degrees, respectively.

Similarly, the unloading slope, S_m, at the maximum depth of indentation, h_m, is given as:

$$S_m = h_m \sigma_0 \Pi_{2i}\left(\frac{E_0}{\sigma_0}, \frac{E_L}{E_T}, \frac{\sigma_L}{\sigma_T}, n\right); \quad i = 1, 2, 3.$$ Eq 2-18

The plastic work ratio R_w can be represented as:

$$R_w = \frac{W_p}{W_t} = \Pi_{3i}\left(\frac{E_0}{\sigma_0}, \frac{E_L}{E_T}, \frac{\sigma_L}{\sigma_T}, n\right); \quad i = 1, 2, 3.$$ Eq 2-19

The depth ratio R_h is given by:

$$R_h = \frac{h_r}{h_m} = \Pi_{4i}\left(\frac{E_0}{\sigma_0}, \frac{E_L}{E_T}, \frac{\sigma_L}{\sigma_T}, n\right); \quad i = 1, 2, 3.$$ Eq 2-20

The actual forms of these dimensionless functions and their construction are discussed in section 2.4 and summarized in Appendix A.

2.3.2 Computational modeling

A transversely isotropic material is symmetric about an axis normal to the plane of isotropy. Hence, an axisymmetric two-dimensional finite element model can be used to capture the indentation response if the indentation direction is perpendicular to the plane of isotropy. However, if indentation is performed parallel to the plane of isotropy a three dimensional model would be required to simulate an indentation experiment. The present study involved indentations both perpendicular and parallel to the plane of isotropy and hence, used a three-dimensional model for both cases for better comparison. The general purpose finite element package of ABAQUS was used to conduct all the simulations.

A schematic of the conical indenter used is shown in Fig. 2-1c where θ = the included half angle of the indenter and h_m = the maximum indentation depth. Three indenters with cone half angles of 50, 60 and 70.3 degrees were used. A cone angle of 70.3 degrees has been shown to be equivalent to a Berkovich indenter. The indenter was modeled as a rigid body and the contact as frictionless. Also, large deformation computations were performed. The Von-Mises stress contours obtained and mesh design used for the analysis and the typical after indentation are shown in Fig. 2-3 and Fig. 2-4.

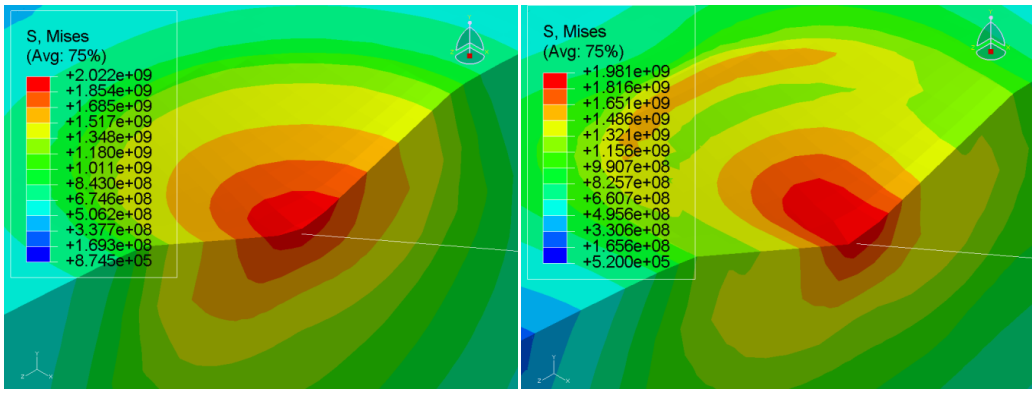

(a) (b)

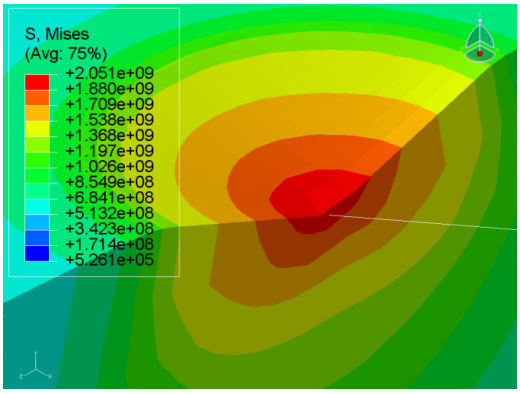

(c)

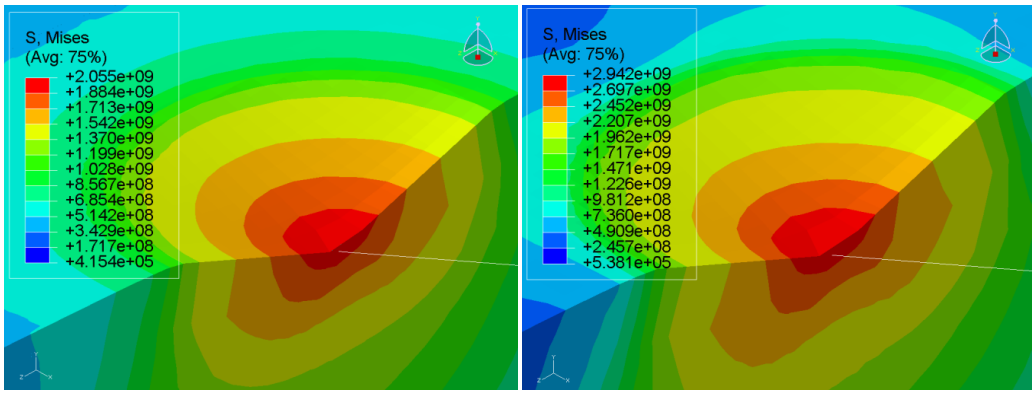

(d) (e)

Figure 2-3: A comparison of the Von-Mises stress contours for materials with different degrees of anisotropy where, (a) is a material with elastic anisotropy indented in the transverse direction, (b) is a material with plastic anisotropy indented in the transverse direction, (c) is an isotropic material, (d) is a material with elastic anisotropy indented in the longitudinal direction, (e) is a material with plastic anisotropy indented in the longitudinal direction.

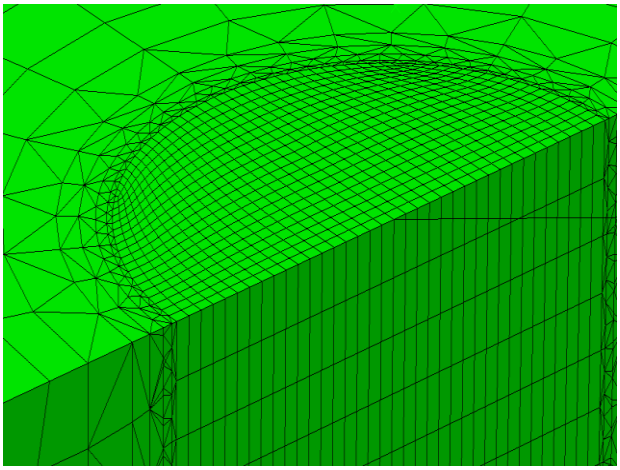

Figure 2-4: The three-dimensional finite element model invoked for characterizing the indentation response of transversely isotropic materials.

A typical model comprised of 12000 eight-noded, hex-elements, with a fine mesh near the contact region and a gradually coarser mesh further away to ensure numerical accuracy. The fine inner meshing and the coarser boundary meshing were connected by 30000 four-noded tetrahedral elements. It was ensured that at the maximum load, the minimum number of contact elements in the contact zone cross-section was no less than 225 in each finite element model. The mesh was determined to be insensitive to far field boundary conditions and was well tested for convergence.

2.4 Results and discussion

2.4.1 Computational results

In the present study 120 materials that represent a wide range of elastic and plastic behavior were identified. The values of mean Young's modulus E_0 ranged from 50 to 200 GPa, mean yield strength σ_0 from 210 to 1400 MPa, strain hardening exponent n from 0 to 0.3, and Poisson's ratio v was fixed at 0.3. Also, the ratio of E_L/E_T and σ_L/σ_T were varied from 1 to 2 for each of these cases.

Furthermore, for all the transversely isotropic materials, two types of indentations were considered:

- Longitudinal indentations - Indentations perpendicular to the plane of isotropy and,
- Transverse indentations - Indentations parallel to the plane of isotropy.

The three-dimensional finite element model described in the previous section was used to obtain the complete longitudinal and transverse loading and unloading indentation responses for all the materials. Careful analysis was conducted to determine the exact forms of the dimensionless functions that best described the relationships between the material properties and the corresponding indentation response parameters. It was found that, in general, no single function was able to accurately capture the relationship between the material properties and the indentation parameters for the whole range of materials that were chosen for the analysis. However, by subdividing the whole range of materials into six smaller groups (as indicated in Fig. 2-5), accurate dimensionless functions were obtained for each of the groups of materials.

The equations are given in the form - Π_{jkl}, where 'j' varies from 1 to 3 and signifies the indenter type - 1 for 50^0, 2 for 60^0 and 3 for 70.3^0, 'k' varies from 1 to 3 and conveys the type of dimensionless function - 1 for C, 2 for S_m, 3 for R_w, and finally 'i' represents the material group and varies from 1 to 6. Furthermore, x, y, z and n, respectively, represent the properties E_0, E_L/E_T, σ_L/σ_T and the strain hardening exponent. The complete set of dimensionless functions is provided in the appendix section. As an example:

$$\Pi_{111} = \frac{C}{\sigma_0} = \big(n^2(18.8281 + 24.4279y^2 - 35.3573yz + 34.7982z^2)(-76.246 + 26.4381Log[x] - 2.2314Log[x]^2) + (4.0803 + 0.018y^2 - 0.1495yz + 0.2848z^2)(-20.5207 + 8.2753Log[x] - 0.7002Log[x]^2) + n(40.1085 - 9.34258y^2 + 14.6262yz - 4.8869z^2)(47.4263 - 17.0119Log[x] + 1.5602Log[x]^2)\big)$$

Eq. 2.21

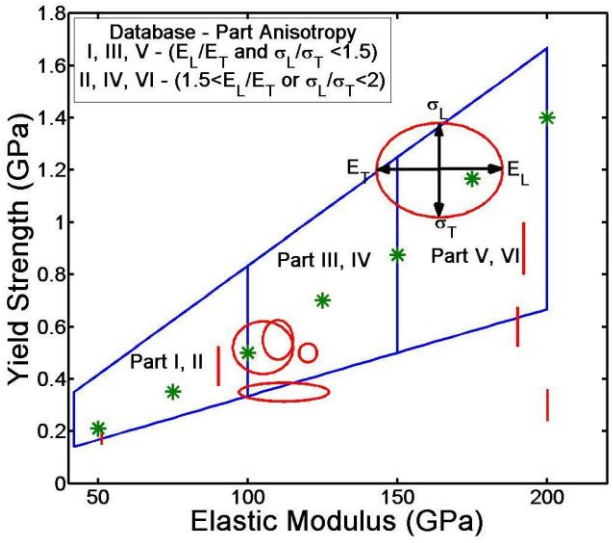

Figure 2-5: A schematic illustrating the division of the material property database into six domains for the formulation of the forward and reverse algorithms. Ten prominent transversely isotropic engineering materials are also depicted in red. The major and minor axes of the ellipse depict the elastic and plastic anisotropy exhibited by these materials respectively. The '*' indicate the position of isotropic materials chosen to construct the database.

For the indentation of isotropic materials, a representative strain at which the loading curvatures of large number of materials could be independent of strain hardening may be identified. However, in the present study, where the indentation response of transversely isotropic materials is analyzed, such a strain level could not be identified owing to the higher number of material constants upon which the loading curvature depends.

2.4.2 Forward analysis/algorithms

The dimensionless functions identified in the present study can be readily invoked to construct a forward algorithm that can predict the longitudinal and transverse indentation response parameters of any given material within the range of properties considered in the present study. To confirm the robustness of the form and curve fit of the dimensionless functions used in the forward algorithm, the indentation response parameters of 120 materials (identified in the previous section) and 10 new set of materials properties, predicted by the forward algorithm were compared to the results obtained from finite element simulations for longitudinal and transverse indentations for all three indenters (with half cone angles of 50, 60 and 70.3 degrees). A good match was found between the predictions of the forward algorithm and the finite element simulations (Table 2.2).

Table 2.2: Summary of the errors obtained in the prediction of the indentation responses of 130 transversely isotropic materials through the forward analysis developed in the present study. (a) Indentation perpendicular to the plane of isotropy and (b) indentation parallel to the plane of isotropy.

(a)

Cone half angle	% Error in C	% Error in S_m	% Error in R_w
50	0.165	0.579	0.043
60	0.301	0.308	0.046
70	0.255	0.209	0.06

(b)

Cone half angle	% Error in C	% Error in S_m	% Error in R_w
50	1.442	0.893	0.221
60	1.753	0.517	0.282
70	1.652	0.343	0.376

2.4.3 Reverse analysis/algorithms

The reverse analysis leads to the prediction of a material's elastic and plastic properties using its indentation response. In the past, robust algorithms have been designed to predict the elastic and plastic properties of isotropic materials using distinct dimensionless functions. However, for the case of transversely isotropic materials, it is not easy to formulate such algorithms owing to an increase in the number of material properties that need to be predicted. In the present study, a novel approach to predict the material properties (using both longitudinal and transverse indentations) has been proposed.

A large and dense database of 4800 materials within the domain of the original 120 materials was identified. The indentation responses of all the 4800 materials were obtained using the forward algorithm. (This database was also divided into 6 parts of 850 materials each and the corresponding set of dimensionless functions was used for the forward analysis.) The reverse analysis was then conducted as shown in Fig. 2-6. A step-wise procedure of the reverse analysis, which utilizes all 9 indentation parameters obtained from the P-h responses using the three different indenter angles, is enumerated as follows:

1. The entire database of the forward analysis of 4800 materials is captured in a fourth order tensor $\mathbf{DB}_{ijkl}$, where, i defines the part number that goes from 1 to 6, j defines the material position in the database that goes from 1 to 850 for each part, k defines the angle of the indenter for which the response in calculated which is l, 2 or 3, respectively, for 50, 60 or 70.3 degree cone angles

respectively, and l defines a particular aspect of the P-h response where 1, 2 or 3, respectively, represent C, S_m or R_w.

2. The P-h response (C, S_m, R_w) measured from indentation experiments with indenter angles of 50, 60 and 70.3 degrees is assigned to a matrix $\mathbf{Q_{kl}}$ where, k and l hold the same definitions as above.
3. $\mathbf{Q_{kl}}$ is compared with $\mathbf{DB_{ijkl}}$ for each of the parts and their 850 materials. Two material property sets, which are closest to $\mathbf{Q_{kL}}$, and their corresponding parts are determined. These two sets are assigned to matrices $\mathbf{M_{1kl}}$ and $\mathbf{M_{2kl}}$, respectively.
4. These two sets are used as seed material properties and a procedure similar to that used by Lan and Venkatesh [4] is then followed, as described below, to reach to the final result of the reverse analysis.
5. For the chosen seed properties the corresponding indentation response parameters (C_1, S_{m1}, R_{w1}, C_2, S_{m2}, R_{w2}, C_3, S_{m3}, R_{w3}) are obtained from the functional forms presented by the forward algorithms for the corresponding part to which $\mathbf{M_{kl}}$ belongs.
6. The experimentally measured set of indentation parameters $\mathbf{Q_{kl}}$ (from step 2) are compared to the indentation parameters computed in step 5. An error function that computes the total sum of the squares of errors of all the indentation response parameters is determined.
7. If the error function produces an error below a certain lower critical threshold, (chosen as 99.98% accuracy in the indentation response parameters) the set $\mathbf{M_{kl}}$ is accepted as a feasible solution to the reverse analysis.

8. If not, the error function is minimized by systematically considering a number of combinations of material properties to obtain the best solution set for the materials elastic and plastic properties.
9. If the iterative process leads to a physically non-feasible solution ($n<0$, $E_L/E_T<1$, $\sigma_L/\sigma_T<1$)[1], the process is restarted (setting $n=0$, $E_L/E_T= \sigma_L/\sigma_T=1$) till a feasible solution is obtained.
10. A condition of minimum accuracy in the indentation response parameters is set at 99.98%. The solution set which has lower error among M_{1kl} and M_{2kl}'s variations is reported as the final solution.

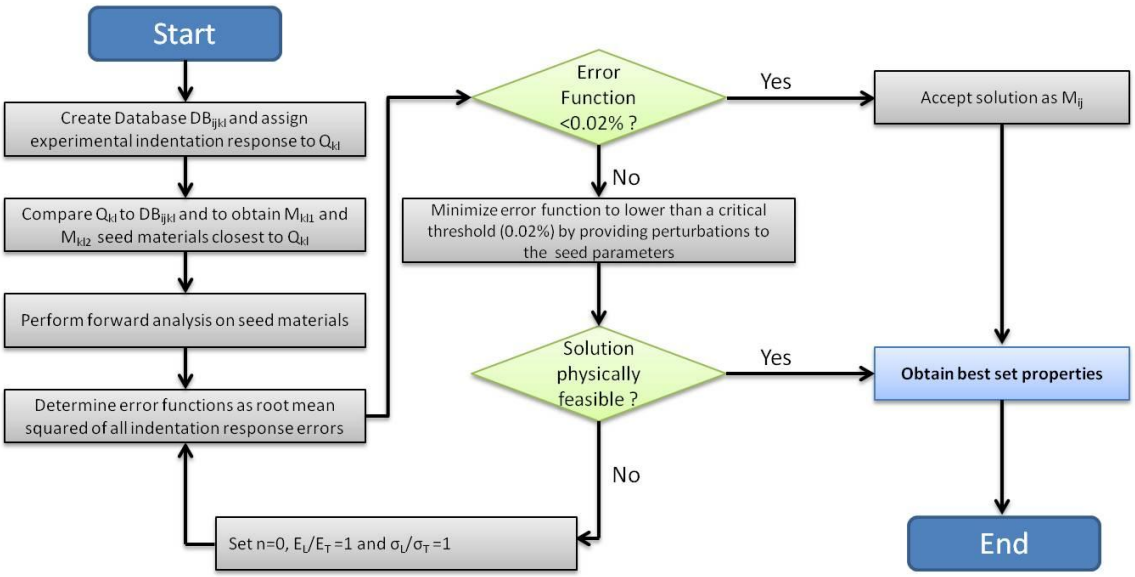

Figure 2-6: Schematic illustrating the reverse analysis/algorithm developed in the present study for determining the elastic and plastic properties of transversely isotropic materials.

In order to check and validate the reverse analysis, a total of 1400 materials were chosen and a cycle of forward and reverse analysis was conducted on all of them for

[1] Indentation is performed under the assumption that $E_L>E_T$ and $\sigma_L>\sigma_T$.

both longitudinal and transverse indentation. The results showed perfect match between the original material properties and the final material properties obtained using the reverse algorithm, thus proving the reversibility of the process.

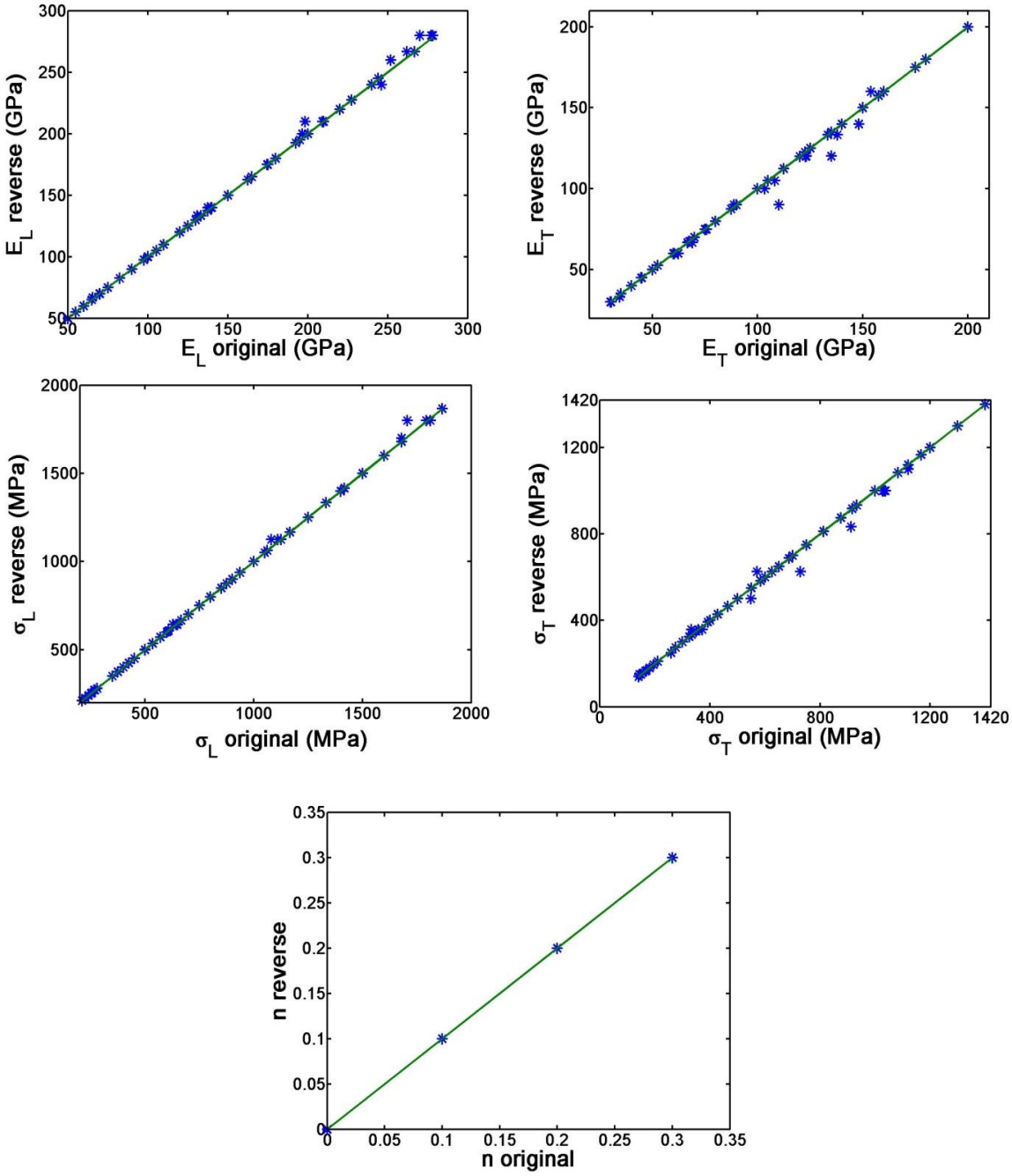

Figure 2-7: A comparison, for the initial 120 materials chosen, between actual material properties and those obtained through reverse analysis, for indentation perpendicular to the plane of isotropy.

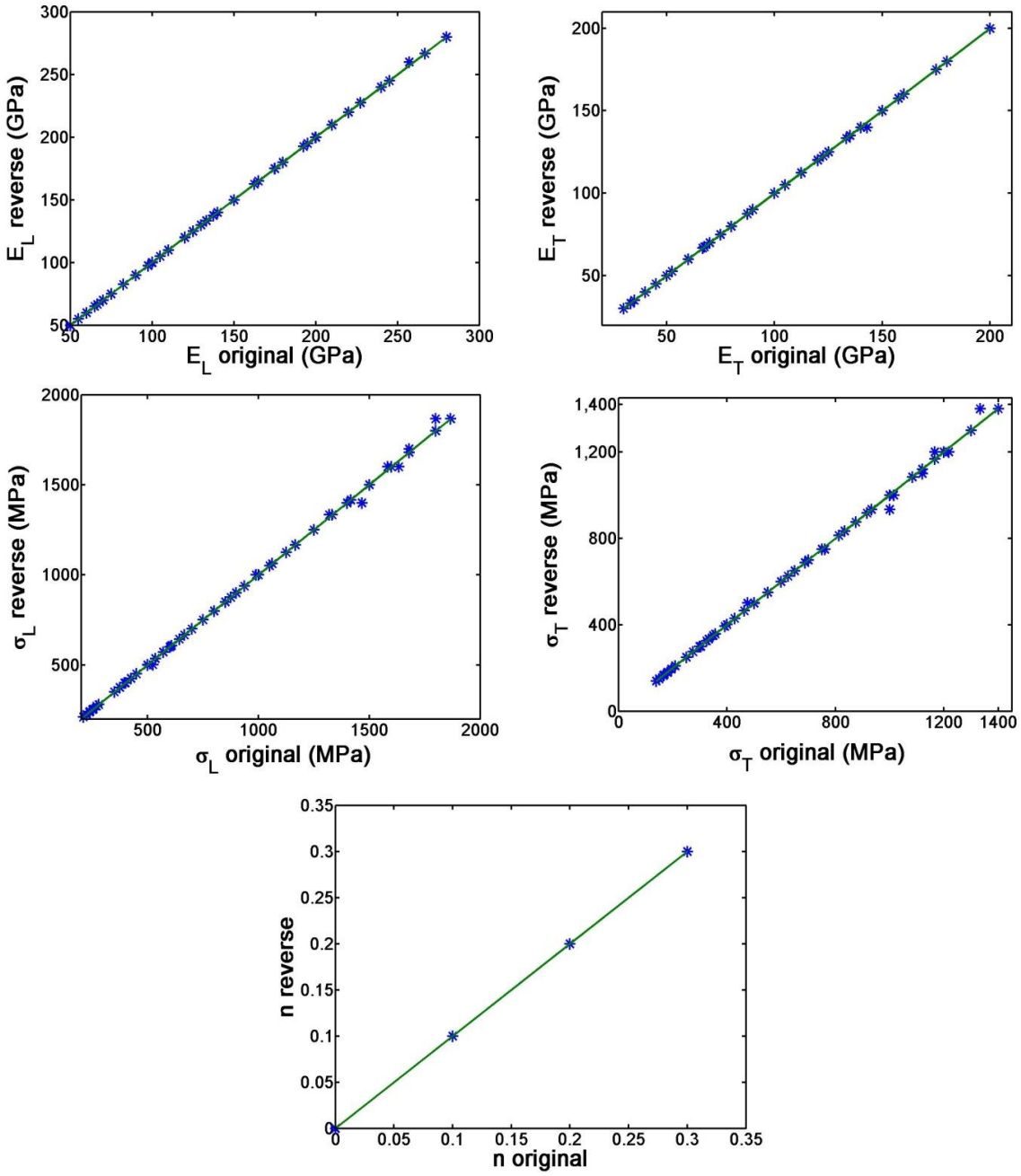

Figure 2-8: A comparison, for the initial 120 materials chosen, between actual material properties and those obtained through reverse analysis, for indentation parallel to the plane of isotropy.

In order to verify the robustness of the reverse algorithm the reverse analysis was performed on the original set of 120 materials whose P-h responses was determined through finite element computation. Figures 2-7 and 2-8 present a comparison of the true value of the elastic and plastic properties of the material with that

obtained through the reverse analysis. The reverse analysis was further validated with a set of twelve materials that was chosen from within the material property space. From the analysis it is evident that for both longitudinal and transverse indentations the reverse analysis yields reasonable results for all materials.

The analysis described so far presented a reverse algorithm that assigned equal weights to the errors in the estimation of all the indentation response parameters (i.e., C, S_m, R_w). However, this could be modified depending on the needs and objectives to obtain targeted accuracy for a certain set of material properties which could be more useful than the others or for a certain domain of material properties if the domain is already known to some extent. However, it cannot always be said that a reasonable solution can be obtained with any arbitrary weight distribution. Thus, caution and practice are necessary to identify the optimal weight of each dimensionless function's contribution to the error function.

2.4.4 Uniqueness analysis

2.4.4.1 Uniqueness of the forward analysis

In order to verify the uniqueness of the forward algorithm, 130 materials were considered. Both finite element simulations and the forward analysis algorithm were used to calculate the indentation response parameters of these materials. The forward algorithms yielded a unique set of P-h responses (C, S_m, R_w) for all the 130 cases. A maximum of 6% or 7% mismatch was found between the results of the finite element analysis and those predicted by the forward algorithms for longitudinal or transverse indentations, while the average error of the forward analysis was found to be 0.2% or

0.85%, respectively, thus proving the high accuracy and uniqueness of the forward analysis (Table 2.2).

2.4.4.2 Uniqueness of the reverse analysis

In order to verify the uniqueness of the reverse analysis, the indentation parameters obtained by the finite element simulations for 130 materials were used as input parameters for the reverse analysis. It was found that each set of the indentation parameters mapped uniquely to its corresponding set of material properties, thus demonstrating the uniqueness of the reverse algorithm.

For longitudinal indentations, 109 of the 120 sets of indentation parameters subjected to reverse analysis provided accurate and exact values of material properties. The remaining 11 provided results within a maximum error of 15% in material properties and an average error of 3%. 8 of the additional 12 cases considered for reverse analysis yielded exact results with the maximum error for the remaining 4 being under 25% and an average error that was less than 7% (Table 2.3).

For transverse indentations, 99 of the 120 cases of indentation parameters subjected to reverse analysis provided accurate and exact values of material properties. The remaining 21 provided results within a maximum error of 17% in material properties and an average error of 6%. 6 of the additional 10 cases considered for reverse analysis yielded exact results with the maximum error for the remaining 4 being under 30% and an average error that was less than 8% (Table 2.3).

Table 2.3: Summary of the errors obtained in the determination of the elastic and plastic properties of 130 transversely isotropic materials through the reverse analysis developed in the present study.

Reverse Analysis	Average % Error E_0	Std Dev	Average % Error E_L/E_T	Std Dev	Average % Error σ_0	Std Dev	Average % Error σ_L/σ_T	Std Dev	Average % Error n	Std Dev
120 Cases: Longitudinal Indent	0.21	0.76	0.86	2.84	0.24	0.83	0.61	2.29	0	0
10 Cases: Longitudinal Indent	1.50	3.47	4.60	10.68	2.13	3.83	5.36	10.23	0	0
120 Cases: Transverse Indent	0.866	1.07	4.8	5.24	0.4	2.64	4.80	9.39	0	0
10 Cases: Transverse Indent	2.50	4.36	5.60	9.74	3.13	4.37	4.36	10.78	0	0

2.4.5 Sensitivity analysis

2.4.5.1 Sensitivity of the forward analysis

A sensitivity analysis similar to that used for the indentation studies of isotropic materials [e.g.,[38]] is invoked in the present study. The original set of 120 materials was first used to check the sensitivity of the forward analysis. It was observed that a ±5% change in any one of the material properties leads to a variation of no more than ±7.5**% i**n the indentation response parameters for indentations perpendicular to the plane of isotropy and ±10**%** for indentations parallel to the plane of isotropy. This confirms the low sensitivity and robustness of the forward analysis.

2.4.5.2 Sensitivity of the reverse analysis

For both longitudinal and transverse indentations, each indentation parameter (C, S_m, R_w), was varied through ±2% (about its true value) and the corresponding variation in the material properties predicted by the reverse analysis was observed. Table 2.4 presents a comparison of the material properties predicted by the reverse analysis using the true indentation parameters and those predicted with a +2% variation in the values of C, S_m and R_w about their true values. Similarly, sensitivity studies were conducted on -2% variations in the values of C, S_m and R_w about their true values as well.

Table 2.4: Summary of the variations in the elastic and plastic properties of 130 transversely isotropic materials obtained through the reverse analysis in response to simulated variability of about ±2% in the experimentally measured indentation responses. (a) Indentation perpendicular to the plane of isotropy and (b) indentation parallel to the plane of isotropy.

(a)

Variation	% E_0	Std Dev	% E_L/E_T	Std Dev	% σ_0	Std Dev	% σ_L/σ_T	Std Dev	n	Std Dev
2% in C	0.58	1.33	4.55	6.8	0.73	1.71	6.97	5.87	0	0
-2% in C	0.74	1.42	3.52	6.62	0.814	1.51	6.655	6.29	0	0
2% in S	1	1.66	8.3	7.78	1.1	1.84	4.1	5.92	0	0
-2% in S	1.77	1.80	5.9	6.19	1.72	2.13	6.81	9.17	0	0
2% in W	0.22	0.76	0.86	2.84	0.24	0.82	0.62	2.29	0	0
-2% in W	3.45	1.93	5.75	3.06	3.4	1.99	9	5.93	0	0

(b)

Variation	% E_0	Std Dev	% E_L/E_T	Std Dev	% σ_0	Std Dev	% σ_L/σ_T	Std Dev	n	Std Dev
2% in C	1.7	2.93	10.9	8.58	3.16	6.27	14	15.49	0	0
-2% in C	2.2	3.32	14.1	13.42	4.8	8.87	12.2	16.32	0	0
2% in S	2.55	3.84	12.9	17.95	4.7	8.48	12.6	13.73	0	0
-2% in S	1.72	2.87	15	17.61	4.1	8.375	12	12.86	0	0
2% in W	5.1	3.83	22.4	15.96	8.9	10.63	20.1	15.35	0	0
-2% in W	3.4	2.86	16.7	12.56	7.4	6.95	20.7	13.65	0	0

In general, the variation in material properties obtained by the reverse analysis to ±2% in the values of C, S_m and R_w about their true values is low. For example, the maximum errors in the estimation of the elastic and plastic properties - E_L/E_T and σ_L/σ_T are, respectively, about 8% and 7%, in longitudinal indentations. However, the corresponding errors in the transverse indentations are around 22% and 20%. The material properties E_T and σ_T exhibit higher sensitivity to variations in the indentation parameters. All material properties exhibit high sensitivity to variations in S_m while they exhibit relatively low sensitivity to variations in R_w.

As these sensitivity studies were designed to capture real experimental measurement errors that tend to be around ±2%, it can be concluded that the sensitivity of the reverse algorithm is within reasonably acceptable limits from a practical perspective as well.

A comparison of the average material properties of transversely isotropic materials determined through the reverse analysis based on finite element simulations of isotropic materials and the reverse analysis developed in the present study that is based on the finite element simulations of transversely isotropic materials was also made (Table 2.5). While the average elastic properties of the transversely isotropic materials (i.e., E_o) may be determined within about 30% error using the algorithms developed earlier for isotropic materials, there could be significant errors (of the order of 80% or more for certain materials) in the determination of the average plastic properties (i.e., σ_o and n). Thus, the algorithms developed in the present study are expected to provide accurate and robust estimates for the elastic and plastic properties of transversely isotropic materials.

Table 2.5: A comparison of the average material properties of transversely isotropic materials determined through the reverse analysis based on finite element simulations of isotropic materials and the reverse analysis developed in the present study that is based on the finite element simulations of transversely isotropic materials. (a) Indentation perpendicular to the plane of isotropy and (b) indentation parallel to the plane of isotropy.

(a)

Mat.	**Actual properties**					**Present reverse algorithm predicted properties**					**Dao et. al. predicted properties**			**Error in isotropic predicted properties**		
	E (GPa)	E_L/E_T	σ (MPa)	σ_L/σ_T	n	E (GPa)	E_L/E_T	σ (MPa)	σ_L/σ_T	n	E (GPa)	σ (MPa)	n	% Error E	% Error σ	% Error n
1	100	1	500	1	0.1	100	1	500	1	0.1	105.3	485.9	0.11	5.30	2.82	10.00
2	150	1	875	1	0.1	150	1	875	1	0.1	160.1	800	0.116	6.73	8.57	16.00
3	200	1	1400	1	0.1	200	1	1400	1	0.1	214	1280	0.12	7.00	8.57	20.00
4	100	2	500	1	0.1	100	2	500	1	0.1	83.77	531.3	0.105	16.23	6.26	5.00
5	100	1	500	2	0.1	100	1	500	1.9	0.1	100.9	448.8	0.136	0.90	10.24	36.00
6	100	2	500	1	0.3	100	2	500	1	0.3	80	650	0.23	20.00	30.00	23.33
7	100	1	500	2	0.3	100	1	500	1.8	0.3	100.6	557.77	0.29	0.60	11.55	3.33
8	150	2	875	1	0.1	150	2	875	1	0.1	124.4	956.8	0.096	17.07	9.35	4.00
9	150	1	875	2	0.1	150	1	875	2	0.1	155.3	1117.4	0.107	3.53	27.70	7.00
10	150	2	875	1	0.3	150	2	875	1	0.3	120	1197	0.2	20.00	36.80	33.33
11	150	1	875	2	0.3	150	1	875	2	0.3	153	971	0.286	2.00	10.97	4.70
12	200	2	1400	1	0.1	200	2	1400	1	0.1	165	1553.2	0.091	17.50	10.94	9.00
13	200	1	1400	2	0.1	200	1	1400	1.7	0.1	220	1250	0.16	10.00	10.71	60.00
14	200	2	1400	1	0.3	200	2	1400	1	0.3	159	2097.2	0.2	20.50	49.80	33.33
15	200	1	1400	2	0.3	200	1	1400	1.9	0.3	205.7	1586	0.27	2.85	13.29	10.00

(b)

Mat.	Actual properties					Present reverse algorithm predicted properties					Dao et. al. predicted properties			Error in isotropic predicted properties		
	E (GPa)	E_L/E_T	σ (MPa)	σ_L/σ_T	n	E (GPa)	E_L/E_T	σ (MPa)	σ_L/σ_T	n	E (GPa)	σ (MPa)	n	% Error E	% Error σ	% Error n
1	100	1	500	1	0.1	100	1	500	1	0.1	106	486	0.1	6.00	2.80	20.00
2	150	1	875	1	0.1	150	1	875	1	0.1	151	880	0.1	0.87	0.57	20.00
3	200	1	1400	1	0.1	200	1	1400	1	0.1	210	1300	0.1	5.00	7.14	10.00
4	100	2	500	1	0.1	100	2	500	1	0.1	118	340	0.2	18.25	32.00	100.00
5	100	1	500	2	0.1	100	1	500	2	0.1	105	605	0.1	5.00	21.00	27.00
6	100	2	500	1	0.3	100	2	500	1	0.3	114	450	0.3	14.00	10.00	3.33
7	100	1	500	2	0.3	100	1	500	2	0.3	104	917	0.2	4.00	83.40	26.67
8	150	2	875	1	0.1	150	2	875	1	0.1	176	600	0.2	17.33	31.43	100.00
9	150	1	875	2	0.1	150	1	875	2	0.1	155	1110	0.1	3.33	26.86	0.00
10	150	2	875	1	0.3	150	1.9	875	1	0.3	172	804	0.3	14.67	8.11	6.67
11	150	1	875	2	0.3	150	1	875	2	0.3	155	805	0.2	3.67	8.00	30.00
12	200	2	1400	1	0.1	200	2	1400	1	0.1	235	947	0.2	17.50	32.36	100.00
13	200	1	1400	2	0.1	200	1	1400	2	0.1	206	1917	0.1	3.00	36.93	30.00
14	200	2	1400	1	0.3	200	1.9	1400	1	0.3	230	1300	0.3	15.00	7.14	8.33
15	200	1	1400	2	0.3	200	1	1400	2	0.3	205	1700	0.2	2.50	21.43	33.33

2.5 Application of the forward and reverse indentation analyses to engineering materials

Forward and reverse analysis was carried out for three isotropic materials, Al 6061 T651, Al 7075 T6511 and Copper, whose dual indentation (70.3 and 60 degree cone angle) experimental results has been reported in literature [34, 46]. In spite of there being data for only two indentation angles the results of the forward and reverse analysis agree closely with the experimental data as shown in Fig. 2-9. This shows that the algorithms developed can be used even without having a complete data set of P-h curves. However, a complete data set of all three indenter angles provides a much higher confidence measure for the obtained results.

Also, three transversely isotropic materials known from literature [45], (i.e., Al 2030 T7, Al 15% SiC and Ti-15V3Cr-3Al-3Sn) were considered for the forward and reverse analysis. First, the longitudinal indentation 'experiments' of these three materials with two indenter cone angles were simulated using three-dimensional finite element simulations and their corresponding 'pseduo-experimental' indentation responses (i.e., P-h curves) were obtained (Fig. 2-10). Subsequently, these indentation responses were used as input for the reverse analysis to predict the elastic and plastic properties (Fig. 2-11). It is demonstrated that the forward algorithm predicts the indentation responses and the reverse algorithm predicts the elastic and plastic properties of these transversely isotropic materials with good accuracy.

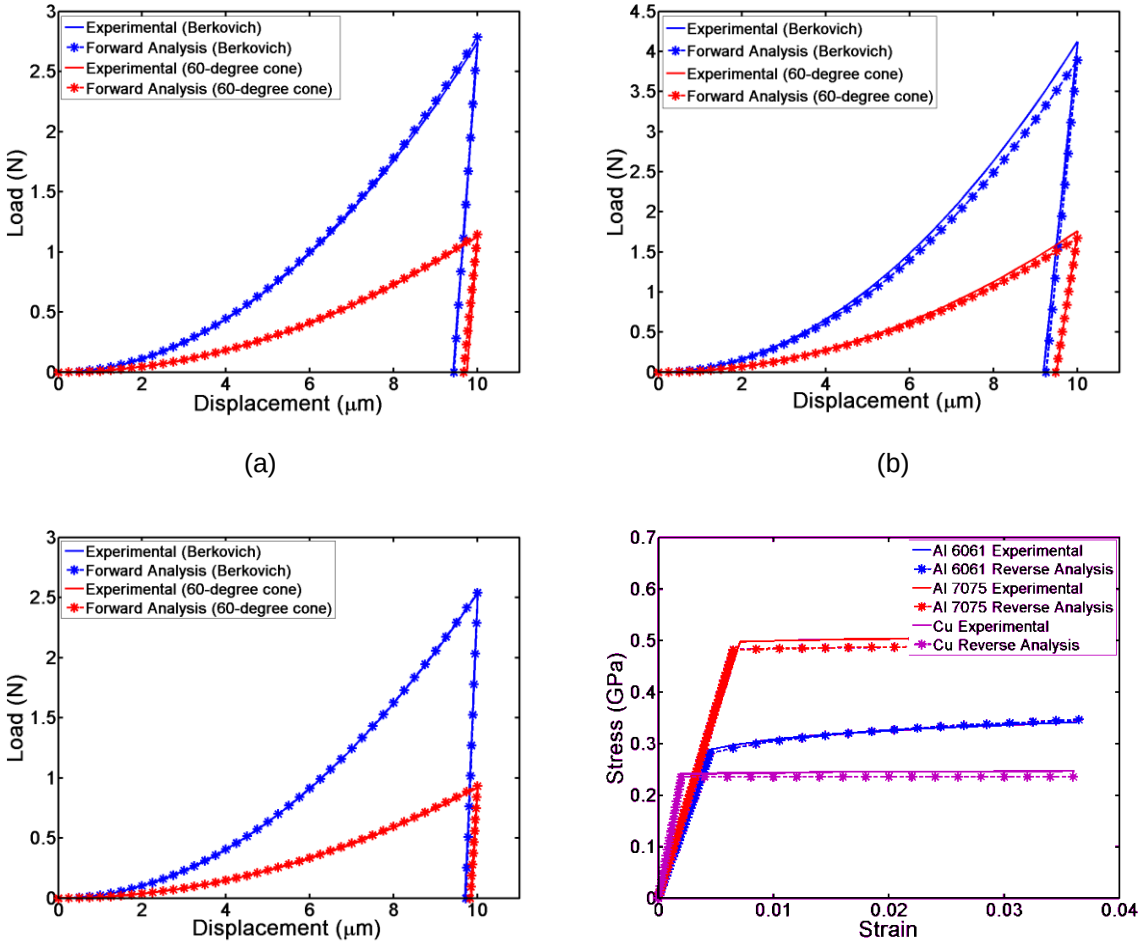

Figure 2-9: A comparison between forward analysis and experimentally obtained data for isotropic materials: (a) Al 6061 T651, (b) Al 7075 T6511. (c) Cu, (d) reverse analysis results compared with actual material properties.

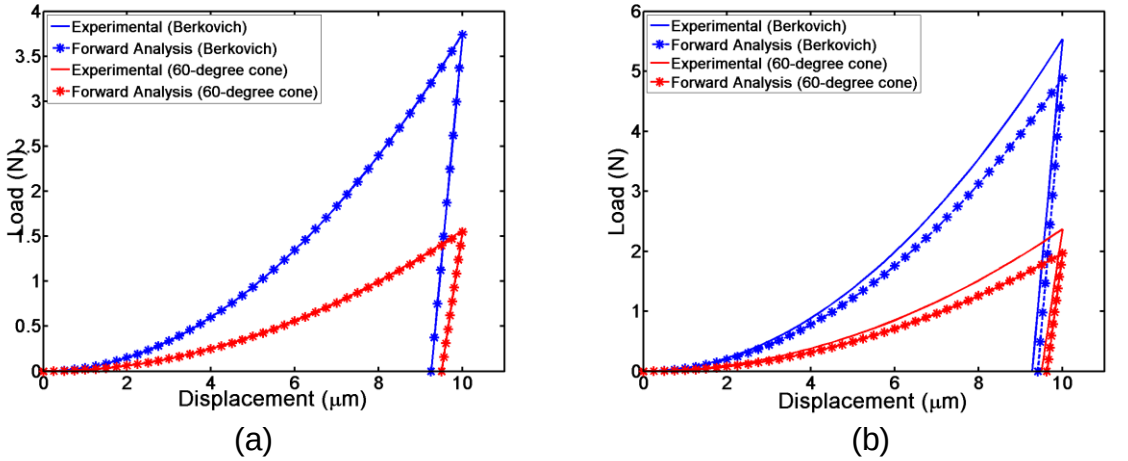

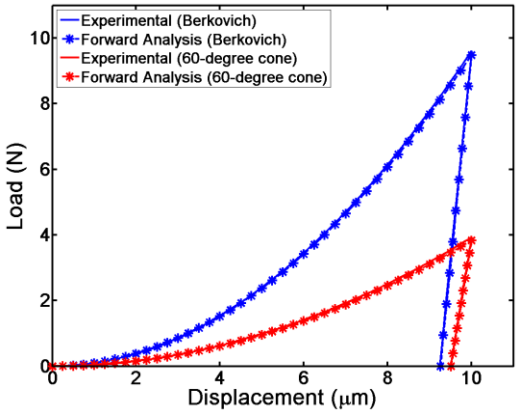

(c)

Figure 2-10: A comparison between forward analysis and experimentally obtained data for transversely isotropic materials: (a) Al 2030 T7, (b) Al-15%SiC, (c) Ti-15V3Cr-3Al-3Sn.

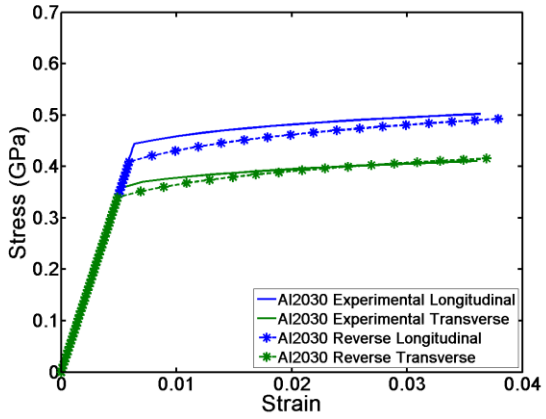

(a)

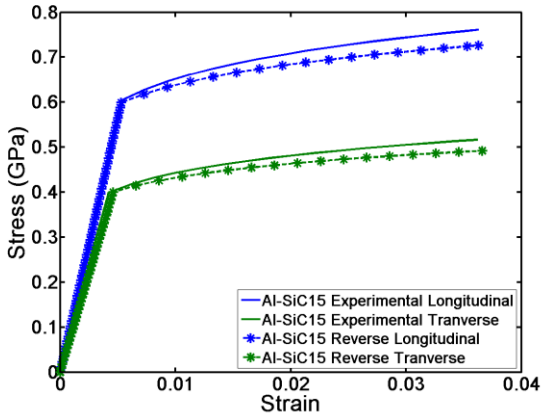

(b)

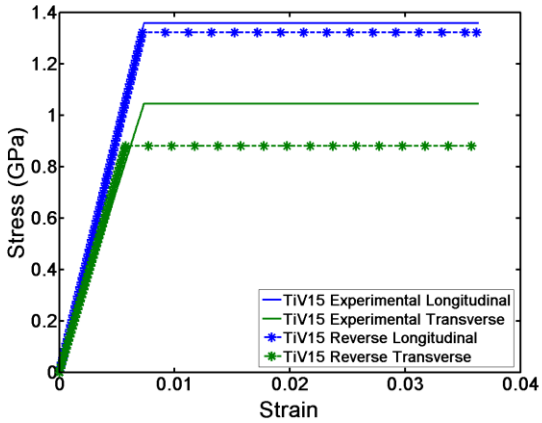

(c)

Figure 2-11: A comparison between reverse analysis and data obtained from literature for transversely isotropic materials: (a) Al 2030 T7, (b) Al-15%SiC, (c) Ti-15V3Cr-3Al-3Sn.

2.6 Conclusions

Prior studies have largely focused on developing the forward and reverse indentation analysis of isotropic materials. As there are several engineering ‘bulk’ and ‘thin film’ materials which are transversely isotropic in nature and exhibit varying degrees of elastic and plastic anisotropy, there is a compelling need to understand the indentation behavior of such transversely isotropic materials. Hence, the principal objective of the present study was to obtain a comprehensive understanding of the indentation response of transversely isotropic materials. The main conclusions from the present study are highlighted as follows:

(i) Using a combination of dimensional analysis and large deformation finite element simulations of triple indentations of 120 materials, a framework for capturing the indentation response of transversely isotropic materials was developed.

(ii) By constructing a dense database of over 4800 combinations of material properties within the bounds of the original set of 120 materials, forward algorithms that predicted the indentation response of materials and the reverse algorithms that helped estimate the material elastic and plastic properties from measured indentation responses were formulated for both longitudinal and transverse indentations.

(iii) Issues of accuracy, reversibility, uniqueness, and sensitivity within the context of the indentation of transversely isotropic materials were addressed carefully. Using 1400 combinations of material properties, it was demonstrated that

there was perfect reversibility between the material properties and their indentation responses as predicted by the forward and reverse algorithms.

(iv) A maximum of 6% and 7% mismatch was found between the results of the finite element analysis and those predicted by the forward algorithms respectively for longitudinal and transverse indentations, while the average error of the forward analysis was found to be 0.2% or 0.85%, respectively, thus demonstrating the high accuracy and uniqueness of the forward analysis.

(v) For longitudinal indentations, 109 of the 120 sets of indentation parameters subjected to reverse analysis provided accurate and exact values of the material properties. The remaining 11 provided results within a maximum error of 15% in material properties and an average error of 3%. For transverse indentations, 99 of the 120 cases of indentation parameters subjected to reverse analysis provided accurate and exact values of the material properties. The remaining 21 provided results within a maximum error of 17% in material properties and an average error of 6%.

A sensitivity analysis using 120 cases with a ±2% variation in the material properties in the forward algorithm and ±2% variation in the indentation responses in the reverse algorithms demonstrated the robustness of the algorithms developed in the present study, with the longitudinal indentations providing relatively less sensitivity to variability in indentation responses as compared to the transverse indentations.

3 Indentation hardness in transversely isotropic materials

3.1 Introduction

Over the past two decades the investigation of the elastic, plastic and hardness properties using instrumented indentation techniques has steadily gained the interest and focus of many studies e.g., [2, 4-6, 16, 18, 31, 34, 35, 38, 39, 42, 47-63] The motivation behind developing techniques to predict hardness of materials spawns from its simplicity and versatility in applications which require property determination of small volume materials like thin films and surface coatings.

However, much of the prior studies have focused on studying the indentation response and hardness characteristics of isotropic materials. As most thin film and several bulk materials exhibit varying degree of anisotropy in both the elastic and plastic domain, it is imperative to understand the indentation behavior and hardness response of such anisotropic materials.

In the previous chapter, the indentation behavior of transversely isotropic materials was analyzed and a framework was developed to connect the material elastic and plastic properties with their indentation responses through the indentation forward and reverse algorithms. In the present study, a comprehensive understanding of the hardness characteristics of transversely isotropic materials is developed.

The principal objectives of the present study are:

(i) To formulate a method to predict the indentation hardness of transversely isotropic materials with a knowledge of the elastic and plastic properties of the indented materials.

(ii) To develop a method to predict the indentation hardness of transversely isotropic materials with a knowledge of the indentation force-depth response of the indented materials without explicitly measuring the area of contact.

(iii) To develop an understanding of the variation of hardness with the elastic and plastic properties of a wide range of transversely isotropic materials.

(iv) To identify relationships between the indentation hardness of transversely isotropic materials and the yield stress and the Tabor's representative stress[64].

The present chapter is organized as follows. A brief description of the fundamentals of indentation and indentation hardness is presented in section 3.2. A framework based on dimensional analysis and computational modeling for understanding the indentation response of transversely isotropic materials is formulated in section 3.3. The results of the indentation simulations and the algorithms developed for predicting the hardness of transversely isotropic materials are presented in section 3.4. The relationship of hardness to material properties are examined in section 3.5. Principal conclusions are highlighted in section 3.6.

3.2 Indentation hardness

Instrumented indentation involves indenting a substrate material with a (flat, sharp or spherical) indenter and observing the corresponding force (P) - depth (h) relationship

during the loading and unloading cycles. As indentation theory has been taken up in detail in the previous chapter, only those equations pertaining to hardness shall be discussed here. The notations used here are the same as those used in the previous work.

Indentation hardness of a material is defined as the ratio of load to projected area of contact.

$$H = \frac{P_m}{A_m} \qquad \text{Eq 3-1}$$

where, A_m is the true projected area of contact at maximum load P_m.

The other pertinent parameters obtained from sharp indentation are:

$$P = Ch^2 \qquad \text{Eq 3-2}$$

$$S_m = \left(\frac{dP_u}{dh} \right) \Bigg|_{h_m} \qquad \text{Eq 3-3}$$

$$R_W = \frac{W_P}{W_T} \qquad \text{Eq 3-4}$$

where, C is the loading curvature, S_m is the slope of the unloading curve at maximum depth, and R_w is the plastic work ratio.

In the case of transversely isotropic materials, indentation can be performed either perpendicular or parallel to the plane of isotropy. These two cases are referred to as longitudinal and transverse indentations, respectively, in this study.

In general, the P-h response and the area of contact (i.e., the true projected area of contact after accounting for pile up or sink in) of a transversely isotropic material (e.g., with σ_L/σ_T =2; σ_L = 0.28 GPa and σ_T = 0.14 GPa) varies considerably from its isotropic counterpart for which the elastic and plastic properties are obtained as a simple average of the properties of the transversely isotropic material (e.g., σ_0 = 0.21 GPa) (Fig. 3-1, 3-2). It can be observed in Fig. 3-2, the indentation imprint for transverse indentation shows a varying degree of pile-up/sink-in owing to the lack of symmetry of material properties in the transverse plane. The projected area of contact in this case is an ellipse and the value of A_m is also calculated then as the area of this ellipse.

Overall, the indentation hardness of transversely isotropic materials is expected to depend on the direction of indentation with respect to the plane of isotropy.

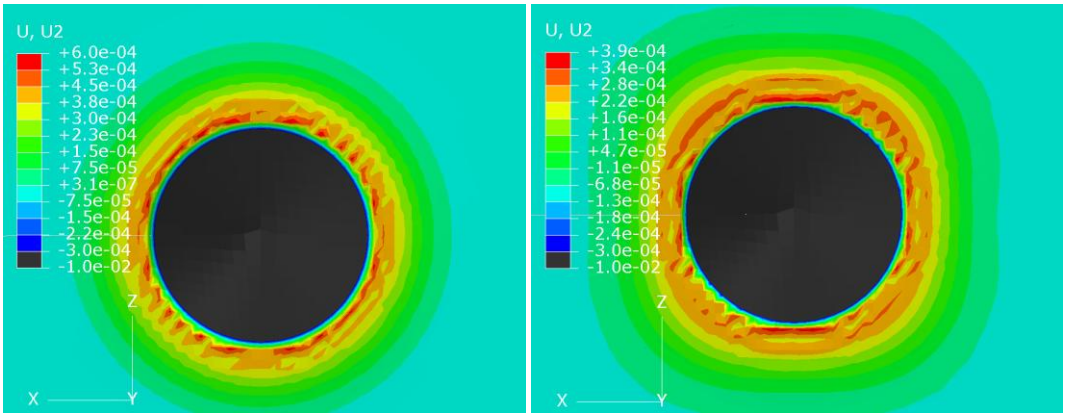

(a) (b)

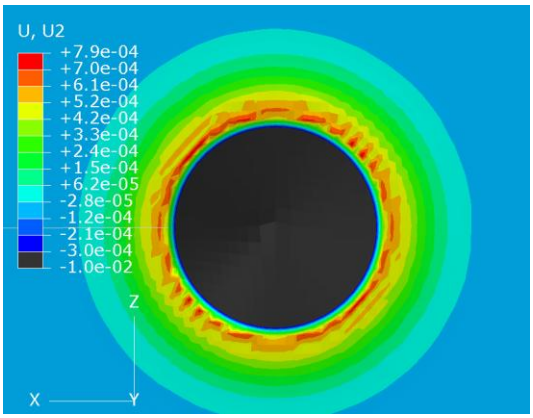

(c)

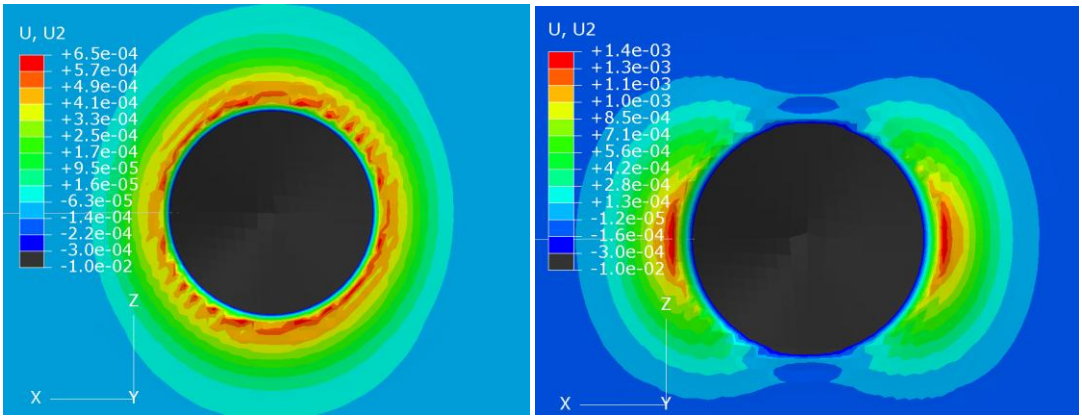

(d) (e)

Figure 3-1: A comparison of the vertical displacement contours displaying the pile-up/sink-in for materials with different degrees of anisotropy where, (a) material with elastic anisotropy indented in the longitudinal direction, (b) material with plastic anisotropy indented in the longitudinal direction, (c) isotropic material, (d) material with elastic anisotropy indented in the transverse direction, (e) material with plastic anisotropy indented in the transverse direction.

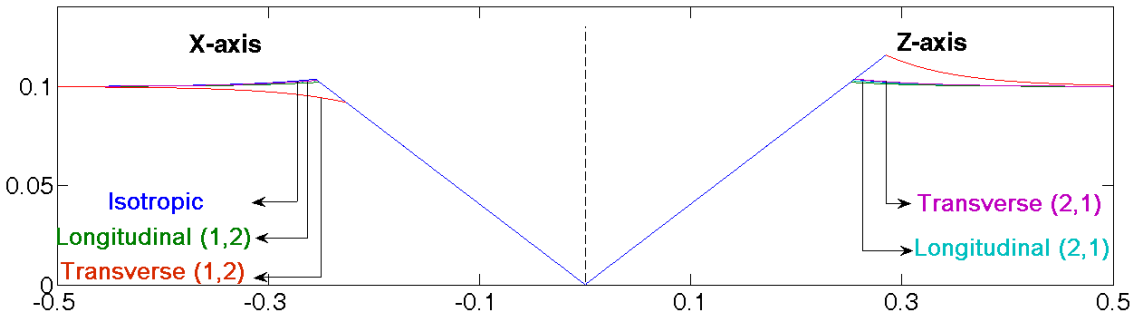

Figure 3-2: A comparison of indentation profiles, for the two in-plane directions x and z, for materials with different degree of isotropy. Here, (x,y) depict the anisotropy in the elastic and plastic regime.

3.3 Framework for the indentation analysis of transversely isotropic materials

In the present study, a combination of dimensional analysis and finite element simulations is invoked to establish the relationships between the elastic and plastic properties of transversely isotropic materials and hardness for longitudinal and transverse indentation.

3.3.1 Dimensional analysis

In prior studies, dimensional analysis has been invoked to identify closed form universal functions that capture the indentation behavior of isotropic materials. In the present chapter, as described below, dimensional analysis is invoked to develop closed form universal functions to capture the indentation behavior with respect to hardness and true projected contact area of transversely isotropic materials.

For a sharp indenter with a cone half angle of θ, the load P required to indent a power law hardening transversely isotropic material can be written as follows. The parameters used here hold the same definitions as those used in chapter 2.

$$P = P\left(h, E_0, \sigma, \frac{E_L}{E_T}, \frac{\sigma_L}{\sigma_T}, n, \theta\right) \qquad \text{Eq 3-5}$$

Using dimensional analysis Eq. (3-5) becomes

$$P = \sigma_0 h^2 \Pi_{1\theta}\left(\frac{E_0}{\sigma_0}, \frac{E_L}{E_T}, \frac{\sigma_L}{\sigma_T}, n, \theta\right) \qquad \text{Eq 3-6}$$

The area of contact A_m can be written as:

$$A_m = A_m\left(h, \frac{E_0}{\sigma_0}, \frac{E_L}{E_T}, \frac{\sigma_L}{\sigma_T}, n, \theta\right) \quad \text{Eq 3-7}$$

And also as,

$$A_m = h^2 \Pi_{4\theta}\left(\frac{E_0}{\sigma_0}, \frac{E_L}{E_T}, \frac{\sigma_L}{\sigma_T}, n, \theta\right) \quad \text{Eq 3-8}$$

Now dividing equation 3-6 by equation 3-8 we get for hardness H_m:

$$H_m = \frac{P}{A_m} = \sigma_0 \Pi_5\left(\frac{E_0}{\sigma_0}, \frac{E_L}{E_T}, \frac{\sigma_L}{\sigma_T}, n\right) \quad \text{Eq 3-9}$$

For θ=70.3 degrees.

As the present discussion considers two different indentation orientations, and focuses on the area of contact and indentation hardness, equations 3-8 and 3-9 can be changed each into two distinct equations as:

$$A_m = h^2 \Pi_{4i}\left(\frac{E_0}{\sigma_0}, \frac{E_L}{E_T}, \frac{\sigma_L}{\sigma_T}, n\right); \text{ i =1, 2.} \quad \text{Eq 3-10}$$

$$H_m = \frac{P}{A_m} = \sigma_0 \Pi_{5i}\left(\frac{E_0}{\sigma_0}, \frac{E_L}{E_T}, \frac{\sigma_L}{\sigma_T}, n\right); \text{ i =1, 2.} \quad \text{Eq 3-11}$$

Where, i =1, 2 represents the direction of indentation for longitudinal and transverse indentation respectively.

The actual forms of these dimensionless functions and their construction are discussed in the next section and summarized in the appendix section.

3.3.2 Computational modeling

As described in the companion article, three-dimensional finite element models were developed, in ABAQUS, to simulate the indentation of a large number of transversely isotropic materials which exhibit a wide range of elastic and plastic anisotropy. A rigid, frictionless conical indenter with a cone half angle of 70.3 degrees was used for the simulations which have been shown to be equivalent to indentations with a Berkovich indenter. The indentation load-depth response characteristics and the area of contact under maximum load for both longitudinal and transverse indentations were obtained.

Careful analysis was conducted to determine the exact forms of the dimensionless functions that best described the relationships between the material elastic and properties, the corresponding indentation response parameters and the material hardness.

The range of materials chosen was split into six groups as shown in Fig. 3-3. Ten prominent transversely isotropic engineering materials are also depicted in red. The major and minor axes of the ellipse depict the elastic and plastic anisotropy exhibited by these materials respectively. By subdividing the whole range of materials considered in the analysis into six smaller groups, accurate dimensionless functions that relate the hardness of the transversely isotropic materials with the material properties were obtained for each of the groups of materials. For example, the detailed form of one of the expressions is given as follows:

$$\Pi_{154} = \frac{H}{\sigma_0} = \begin{pmatrix} n^2\,(20.42 + 5.46\,y^2 - 18.28yz + 6.34z^2)(-229.69 + 87.4\mathrm{Log}[x] - 8.25\,\mathrm{Log}[x]^2) + \\ n\,(1.9 - 5\,y^2 + 14.46\,y\,z - 3.97\,z^2)(-107.43 + 40.91\,\mathrm{Log}[x] - 3.87\mathrm{Log}[x]^2) + \\ (5.42 - 0.12y^2 + 0.14yz + 0.36z^2)\,(12.42 - 4.6\ \mathrm{Log}[x] + 4.5\mathrm{Log}[x]^2) \end{pmatrix} \quad (15)$$

The equations are presented as Π_{jkl}, where j varies from 1 to 2 and signifies the indenter orientation - 1 for longitudinal indentation and 2 for transverse indentation; k varies from 4 to 5 and conveys the type of dimensionless function - 4 for A_m and 5 for H_m; and l represents the group number and varies from 1 to 6. X, Y and Z represent the properties E_0, E_L/E_T and σ_L/σ_T respectively, and n represents the strain hardening exponent.

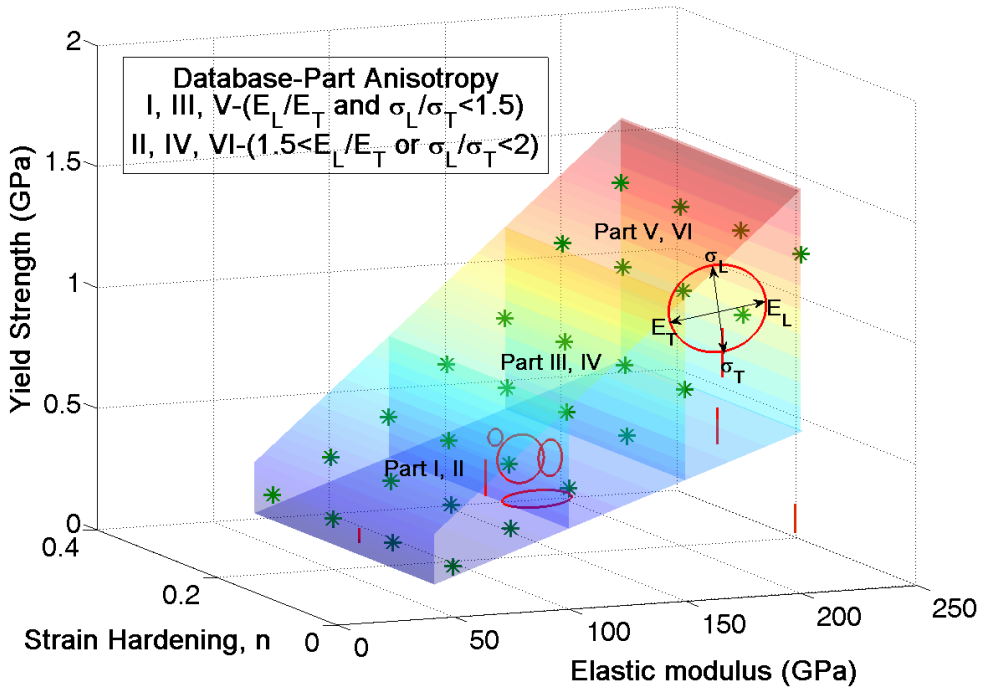

Figure 3-3: A schematic illustrating the material property database for the formulation of the forward and reverse algorithms. (a) Depicts the distribution of commonly occurring anisotropic materials with respect to the database chosen. The '*' indicate the position of isotropic materials chosen to construct the database. (b) Depicts the division of the database into six domains for the formulation of the forward and reverse algorithms.

3.4 Results

In the present study, two methods to predict the hardness of transversely isotropic materials have been identified.

3.4.1 Hardness prediction from known material properties

In the first method, the hardness of the transversely isotropic materials can be predicted from known elastic and plastic properties of the indented substrate materials for longitudinal and transverse indentations. For both classes of indentation, the process involves two main steps:

- Determining the part of the database within which the material under consideration is bounded.
- Applying the corresponding dimensionless function to obtain the values of the contact area and the indentation hardness for the two indenter orientations.

The dimensionless functions presented here were validated by testing them on the 120 initial materials chosen to create the database as well as 10 different materials with properties scattered within the database. The values for the contact areas and the indentation hardness obtained through the algorithm proposed here were then compared with the corresponding true values observed from the finite element simulations conducted. An excellent match between the two was observed, thus proving the validity of the algorithm. Fig. 3-4 provides a comparison of the actual value of the hardness of the material to that obtained through the analysis conducted.

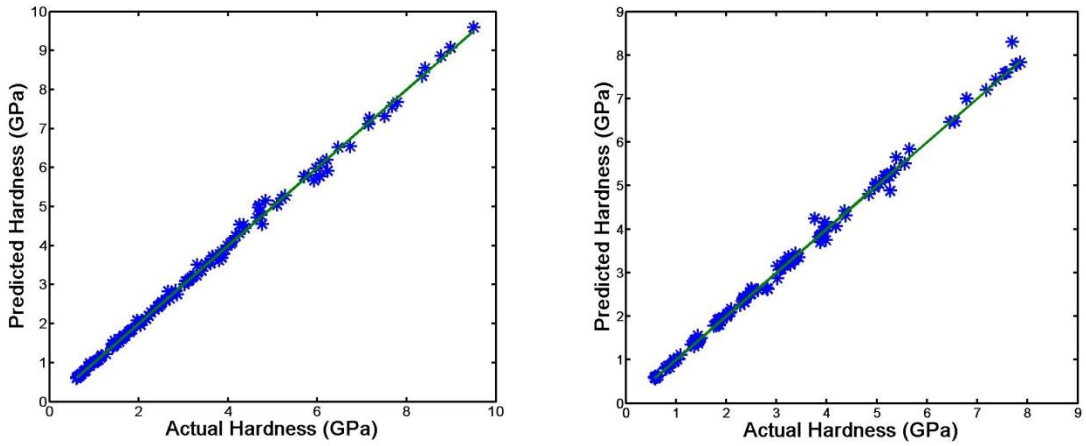

(a) (b)

Figure 3-4: A comparison between actual hardness and that obtained through analysis from known material properties, for 130 chosen materials, for (a) indentation perpendicular to the plane of isotropy and (b) for indentation parallel to the plane of isotropy.

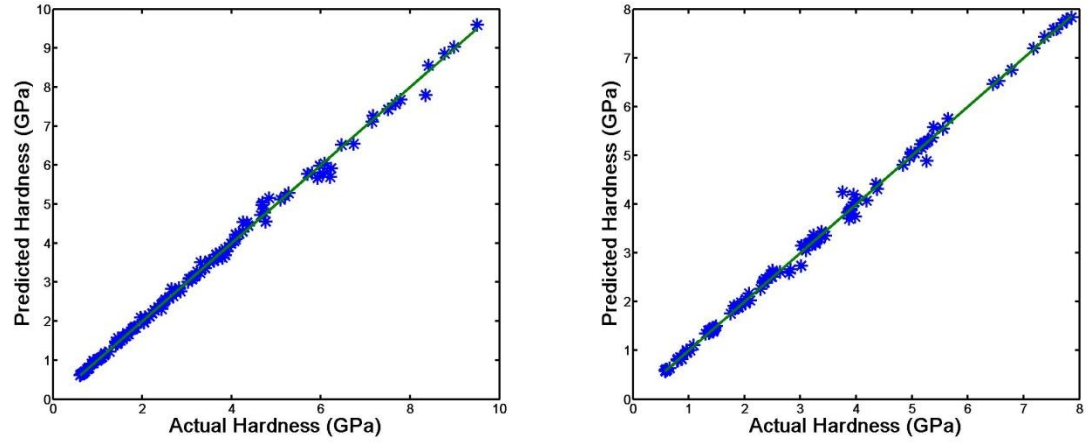

(a) (b)

Figure 3-5: A comparison between actual hardness and that obtained through analysis from known indentation curve properties, for 130 chosen materials, for (a) indentation perpendicular to the plane of isotropy and (b) for indentation parallel to the plane of isotropy.

3.4.2 Hardness prediction from known indentation response

In the second method, the hardness of the transversely isotropic materials can be predicted from the indentation response of the indented material. In this method, the reverse algorithm presented in the previous chapter is first invoked to determine the properties of the indented materials from the measured indentation response.

Subsequently, the hardness and area of contact between the indenter and substrate is determined in a manner similar to that described in section 3.4.1. Thus, from known indentation response of a transversely isotropic the hardness of the material is then predicted without the need to actually measure the area of contact. The accuracy of the hardness predictions depends on the accuracy of the reverse analysis used to predict the materials properties, which has been demonstrated to be very good in the previous chapter. Fig. 3-5 shows a comparison of actual hardness values to that obtained by using the material properties obtained through reverse analysis.

3.5 Discussion

The variation of hardness with the elastic and plastic properties of transversely isotropic materials and the relationships between the hardness and the yield stress and Tabor's representative stress were carefully studied.

3.5.1 Variation of hardness with elastic and plastic anisotropy

Fig. 3.6-3.9 present the variation of hardness with elastic and plastic properties of transversely isotropic materials from which the following observations are made (which are common to both longitudinal and transverse indentation hardness).

(i) Hardness increases with an increase in the strain hardening exponent, the average yield stress and the average elastic modulus.

(ii) Multiple materials with different combination of properties can exhibit identical hardness values.

(iii) Hardness tends to be higher for materials with plastic anisotropy and lower for materials with elastic anisotropy.

(iv) The change in hardness due to plastic anisotropy is higher than that due to an equivalent elastic anisotropy.

(v) The rate of change of hardness with elastic anisotropy is greater at higher strain hardening values.

(vi) At low plastic anisotropy and low strain hardening, there is little variation in the transverse hardness with elastic anisotropy. At high plastic anisotropy there is a more distinct reduction in transverse hardness with increase in elastic anisotropy.

(vii) Transversely isotropic materials with identical average material properties can have elastic and plastic anisotropies in combinations which yield identical hardness values. However, the probability of both the longitudinal and transverse hardness being identical for different materials is small.

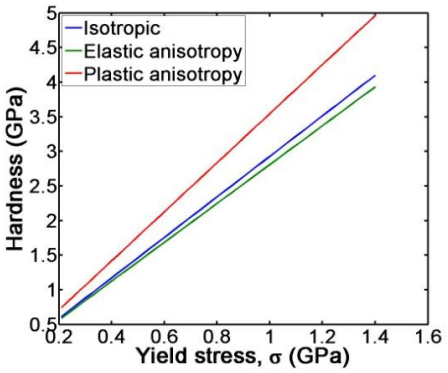

(a)

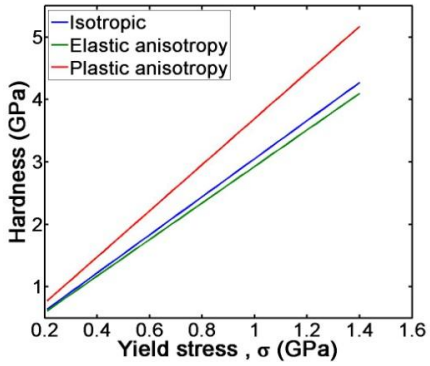

(b)

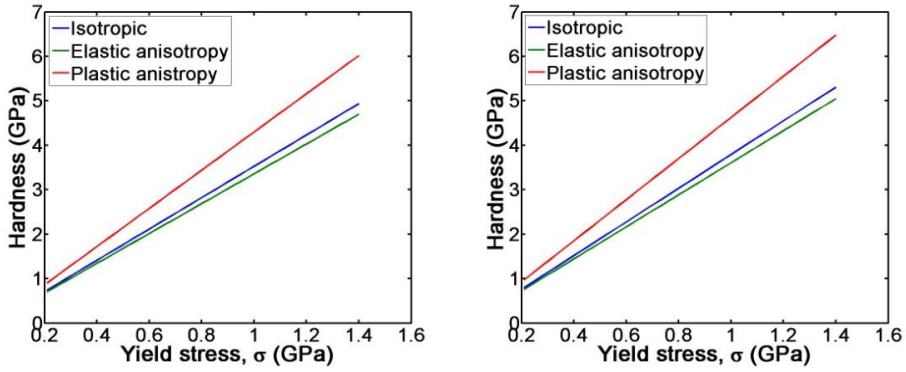

(c)

(d)

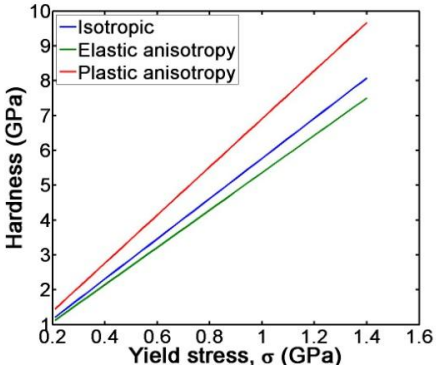

(e)

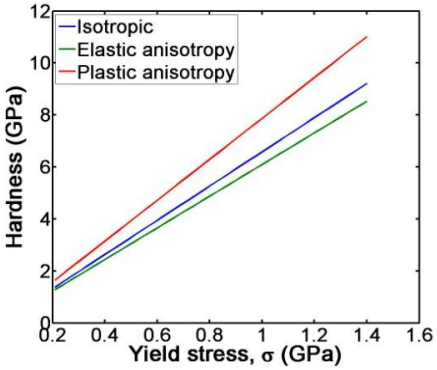

(f)

Figure 3-6:(a), (c), (e) for E_0/σ_0=160 and n=0, 0.1, 0.3 respectively and (b), (d), (f) for E_0/σ_0=220 and n=0, 0.1, 0.3 for longitudinal indentation.

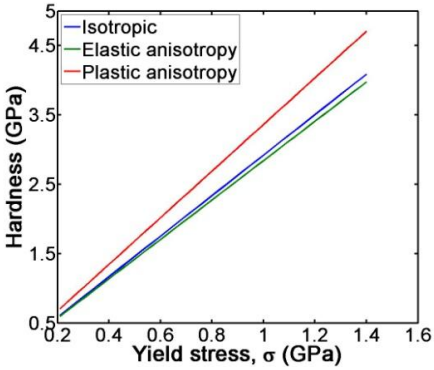

(a)

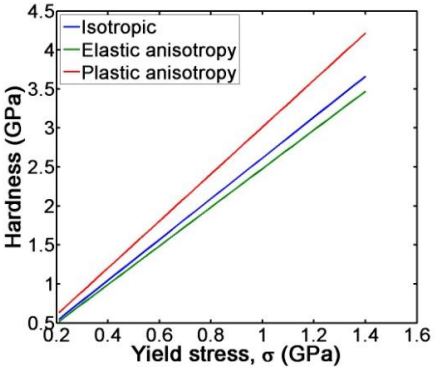

(b)

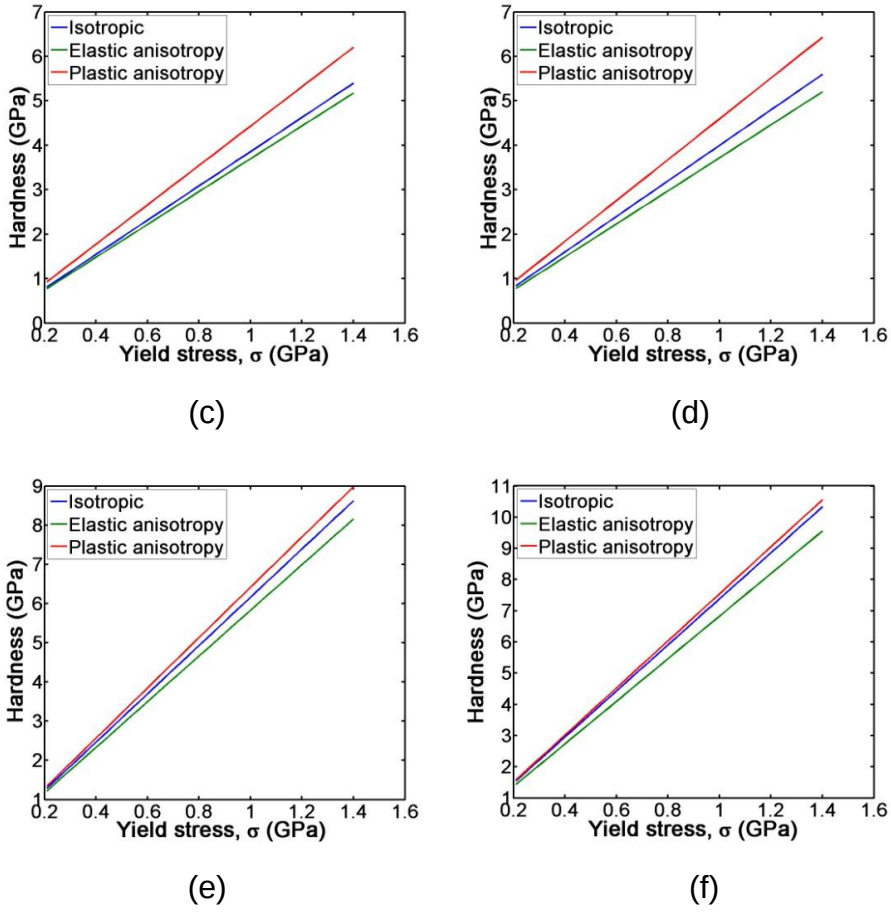

Figure 3-7: (a), (c), (e) for E_0/σ_0=160 and n=0, 0.1, 0.3 respectively and (b), (d), (f) for E_0/σ_0=220 and n=0, 0.1, 0.3 respectively for transverse indentation.

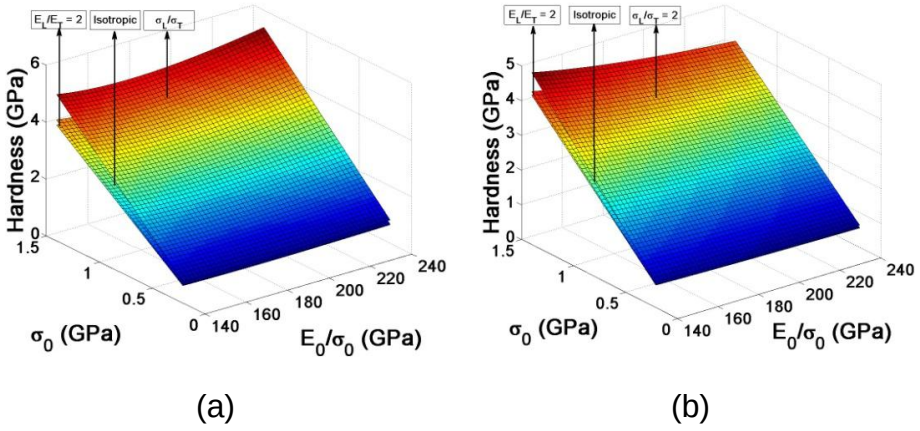

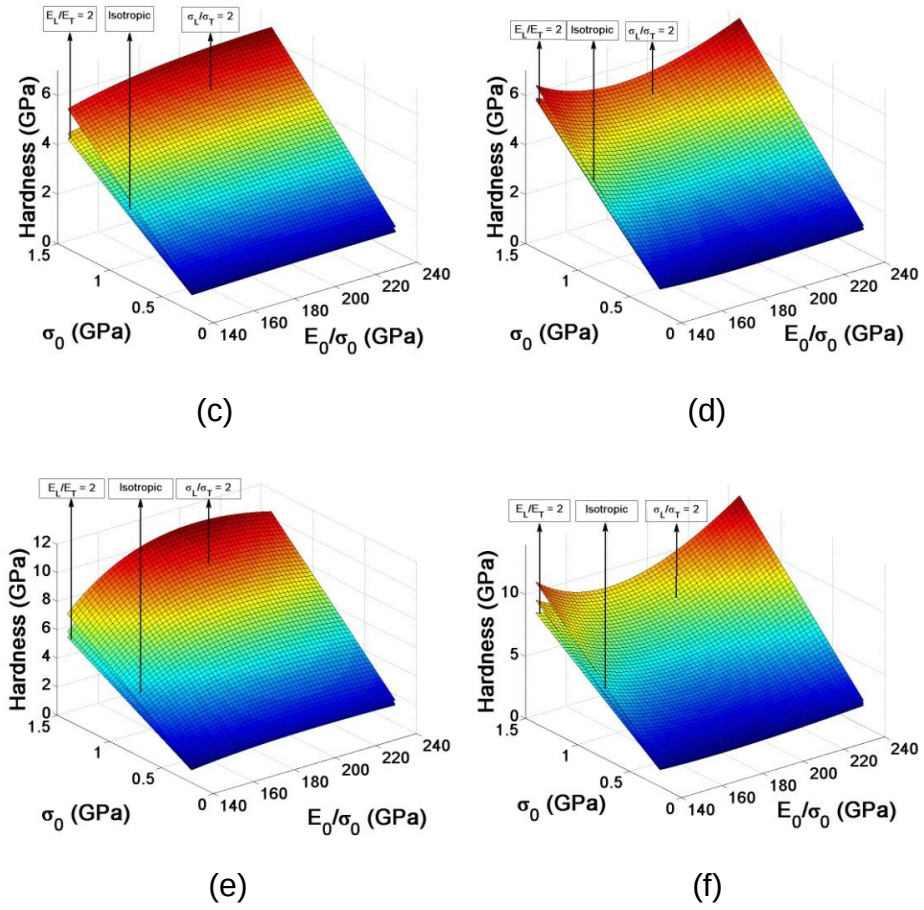

Figure 3-8: (a), (c), (e) for n=0, 0.1, 0.3 respectively for longitudinal indentation and (b), (d), (f) for n=0, 0.1, 0.3 respectively for transverse indentation.

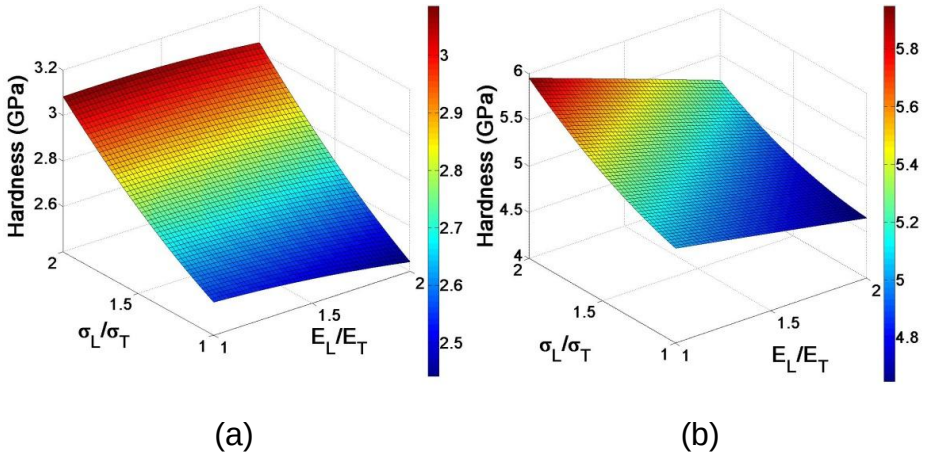

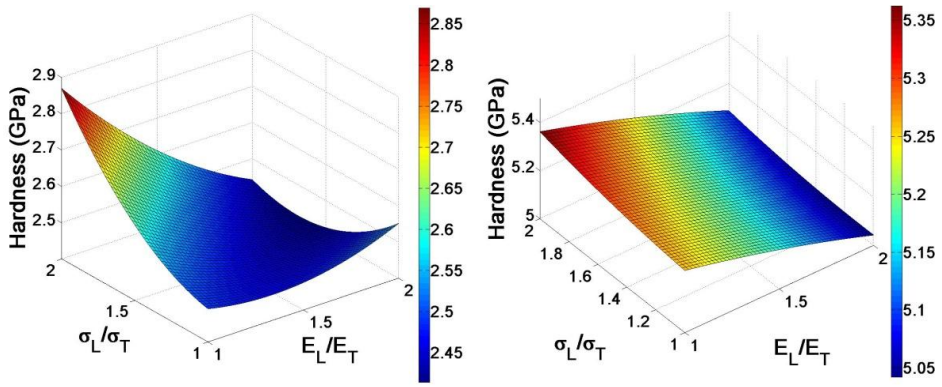

(c) (d)

Figure 3-9: Variation of indentation hardness with varying degree of elastic and plastic transverse isotropy for a material with average yield stress of 0.875 GPa and average Young's modulus of 150 GPa for, (a), longitudinal indentation with no strain hardening, (b), longitudinal indentation of a material with strain hardening coefficient = 0.3, (c), transverse indentation of a material with no strain hardening, and (d), transverse indentation of a material with strain hardening coefficient = 0.3.

3.5.2 Relationship of hardness with yield stress and representative stress

Within the context of the range of materials considered in the present study, the relationships between the hardness of transversely isotropic materials in the longitudinal and transverse directions, to the average yield stress and the Tabor's representative stress are examined. Fig. 3-10 shows contour plots of the variation of $\left(\frac{H}{\sigma_0}\right)$ with strain hardening and $\frac{E_0}{\sigma_0}$.

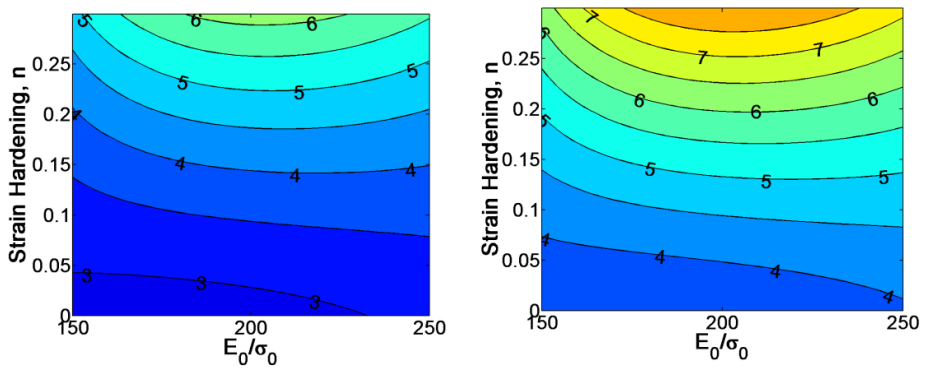

(a) (b)

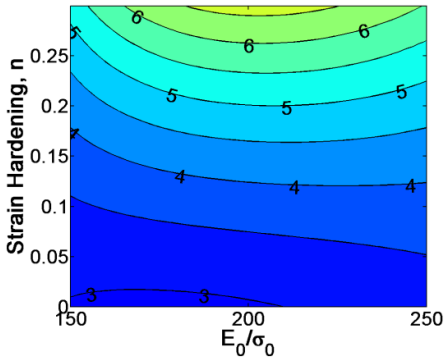

(c)

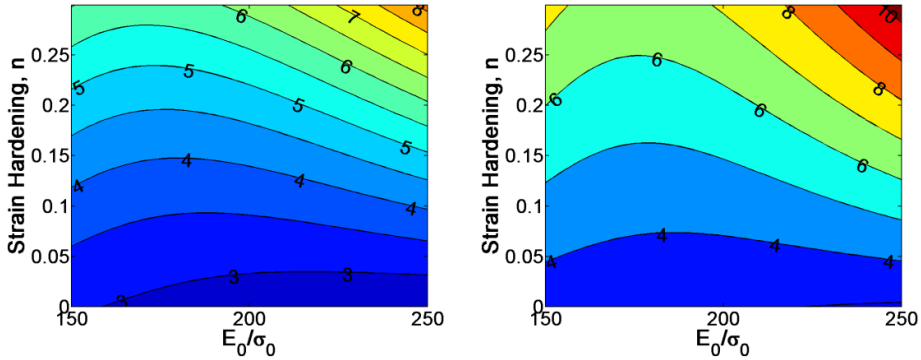

(d) (e)

Figure 3-10: Variation of the ratio of hardness over average yield stress σ_0, with varying strain hardening and E_0/σ_0. Where, (a) material with elastic anisotropy indented in the longitudinal direction, (b) material with plastic anisotropy indented in the longitudinal direction, (c) isotropic material, (d) material with elastic anisotropy indented in the transverse direction, (e) material with plastic anisotropy indented transverse in the direction.

Earlier work by Tabor (on isotropic materials) suggests that hardness can be approximately related to the representative stress as $\left(\frac{H}{\sigma_t}\right)=3$. Here, σ_t is the tabor representative stress and is defined as the stress at strain $\varepsilon_t \approx \frac{0.22}{\left(1-\nu^2\right)\tan\theta}$. For the case of conical indentation with a cone half angle of 70.3 degrees, the value of representative strain is approximated to 8%. In order to investigate these characteristics for the case of transversely isotropic materials, the ratio of longitudinal and transverse

hardness to average representative yield stress, for isotropic, elastically anisotropic, and plastically anisotropic materials is studied. Fig. 3-11 presents contour plots of the variation of hardness over average tabor representative stress with varying strain hardening and $\frac{E_0}{\sigma_0}$. The average Tabor representative stress was calculated as the average of the longitudinal and transverse stresses at 8% strain. The ratios $\left(\frac{H}{\sigma_0}\right)$ and $\left(\frac{H}{\sigma_t}\right)$ are referred to as R_0 and R_t, respectively, in this discussion.

From these studies the following observations are made:

(i) For materials with no strain hardening, the ratio R_0 is greater for materials with plastic anisotropy than the isotropic case and lesser for materials with elastic anisotropy for both longitudinal and transverse indentations.

(ii) For materials with no strain hardening, the ratio R_0 can vary from 2.5 to 3.5 depending on the properties of materials and degree of anisotropy.

(iii) For materials with strain hardening, R_0 can be as high as 10.

(iv) R_t can take values varying from 2.2 to 4 for the range considered, depending on the degree of anisotropy and the materials properties. While, R_t takes values considerably closer to 3 for all strain hardening than R_0, the variation in R_t is still too large for it to be approximated to a single value.

(v) R_t is greater for materials with plastic anisotropy than the isotropic case and lesser for materials with elastic anisotropy for both longitudinal and transverse indentation.

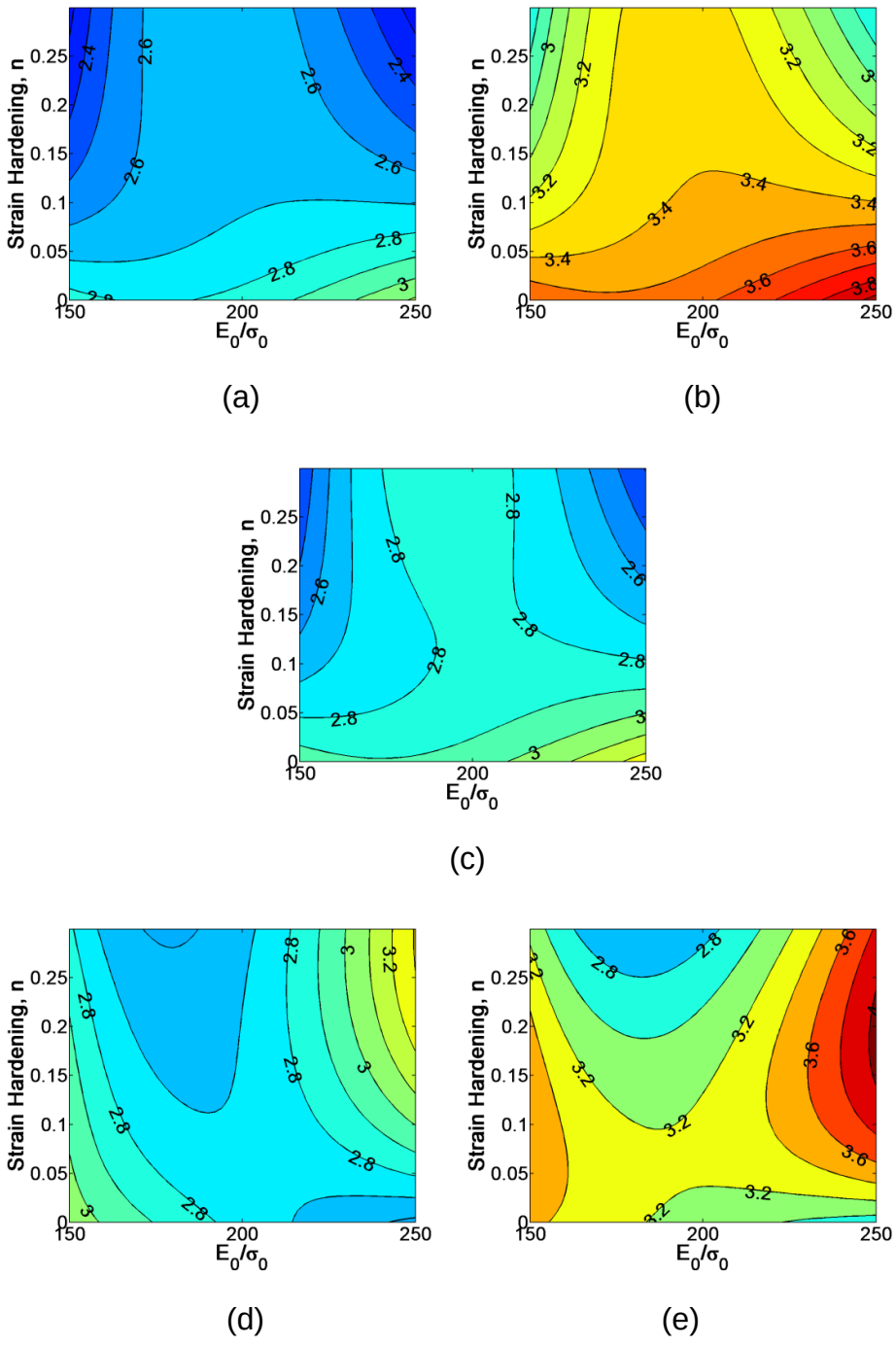

Figure 3-11: Variation of the ratio of hardness over representative stress from σ_L and σ_T averaged, as defined by Tabor et. al. with varying strain hardening and E_0/σ_0. Where, (a) material with elastic anisotropy indented in the longitudinal direction, (b) material with plastic anisotropy indented in the longitudinal direction, (c) isotropic material, (d) material with elastic anisotropy indented in the transverse direction, (e) material with plastic anisotropy indented transverse in the direction.

3.6 Conclusion

Much of the prior studies in the field of hardness have focused on developing an understanding of the hardness characteristics of isotropic materials. However, several engineering materials in the bulk and thin film form exhibit varying degrees of elastic and plastic anisotropy and a comprehensive understanding of the hardness behavior of such transversely isotropic materials is not yet available. Hence, the present study was focused on developing a framework for predicting and understanding the hardness characteristics of transversely isotropic materials. The principal conclusions from the present study are given below.

(i) Hardness increases with an increase in the strain hardening exponent, the average yield stress and the average elastic modulus.

(ii) Multiple materials with different combination of elastic and plastic properties can exhibit identical hardness values.

(iii) Hardness tends to be higher for materials with plastic anisotropy and lower for materials with elastic anisotropy. The change in hardness due to plastic anisotropy is higher than that due to an equivalent elastic anisotropy. The rate of change of hardness with elastic anisotropy is greater at higher strain hardening values.

(iv) For materials with no strain hardening, the hardness to average yield stress ratio (R_0) is greater for materials with plastic anisotropy than the isotropic case and lesser for materials with elastic anisotropy for both longitudinal and transverse indentations.

(v) For materials with no strain hardening, the ratio R_0 can vary from 2.5 to 3.5 depending on the materials properties and degree of anisotropy. For materials with strain hardening, R_0 can be as high as 10.

(vi) The hardness to Tabor's representative stress ratio (R_t) can take values varying from 2.2 to 4, depending on the degree of anisotropy and the materials properties. R_t is greater for materials with plastic anisotropy than the isotropic case and lesser for materials with elastic anisotropy for both longitudinal and transverse indentation.

4 Indentation fatigue behavior of transversely isotropic materials

4.1 Introduction

Cyclic loading and fatigue behavior of metals has considerable significance in engineering applications. A metal subject to cyclic fatigue loading displays crack initiation and growth with increase in number of cycles. Paris law defines the crack propagation in a material as a power law of the range of the stress intensity factor $\Delta K = K_{max} - K_{min}$. Recent studies [65, 66] have shown that the crack growth depends on both the intrinsic mechanism of crack advance ahead of the crack tip and the extrinsic mechanism of crack tip shielding behind the tip. These studies have proposed that the crack growth is a power law function of K_{max} as well as of ΔK.

$$\frac{da}{dN} = CK_{\max}{}^{m}\ \Delta K^{n} \qquad \text{Eq 4-1}$$

Where, ‘a’ is the crack length and m, n and C are empirical constants that depend on the materials properties, loading rate, microstructure, and environment, etc.

Studies have been made in the past exploring the utility of instrumented indentation for cyclic fatigue loading to determine the fatigue properties of materials [9, 11, 12, 67-73]. Instrumented indentation provides distinct advantages over other techniques owing to the advantage of being able to test smaller and smaller samples

and also to determine localized properties of the material as opposed to a bulk property prediction. Owing to the growing application of micro and nano scale structures and thin films, it has become imperative to be able to test materials for their fatigue life on very small scales. Indentation fatigue testing presents a simple solution to this problem. Studies using instrumented indentation have shown that when subject to cyclic indentation fatigue loading, the indenter can continuously sink into the specimen, with each cycle, under the same maximum load. It has also been demonstrated that indentation fatigue depth propagation is similar to fatigue crack propagation when the material is subject to over- and underloading conditions. A quantitative analysis was undertaken by Xu et. al [10] to develop a fatigue depth propagation law for indentation with a flat cylindrical indenter. The work by Xu et. al provides a law for indentation fatigue depth propagation. Their study however, works under the assumption of isotropic material properties and does not accommodate any anisotropy that may be present in the material.

The present study attempts to shed some light on the change in the cyclic indentation behavior as a result of transverse isotropy in the plastic domain of metals occurring during its fabrication process like rolling, extruding etc.

This chapter is organized as follows. Indentation fatigue behavior and the need for studying the effect of plastic anisotropy on indentation fatigue is explained in section 4.2. Transversely isotropic material indentation and the variation of indentation fatigue response with plastic anisotropy are discussed in section 4.3. Section 4.4, makes observations on the extrapolation of the indentation fatigue law proposed by Xu et al. to

account for the degree of anisotropy in the metal. A few conclusions and possible future avenues are discussed in section 4.5.

4.2 Indentation fatigue response

As mentioned in the previous section, under cyclic fatigue indentation the indenter is found to continuously sink into the specimen with each cycle. This phenomenon can be attributed to the dissipation of energy in the plastic zone under the indenter. The effect is best noticed in flat indentations due to its wide plastic zone. The rate of sinking in of the indenter has been found to be dependent on the maximum load as well as the load amplitude given. The process of sinking in is also dynamic and dependent on the rate of loading and unloading. Fig. 4-1 shows a simplistic view of flat indentation on a substrate.

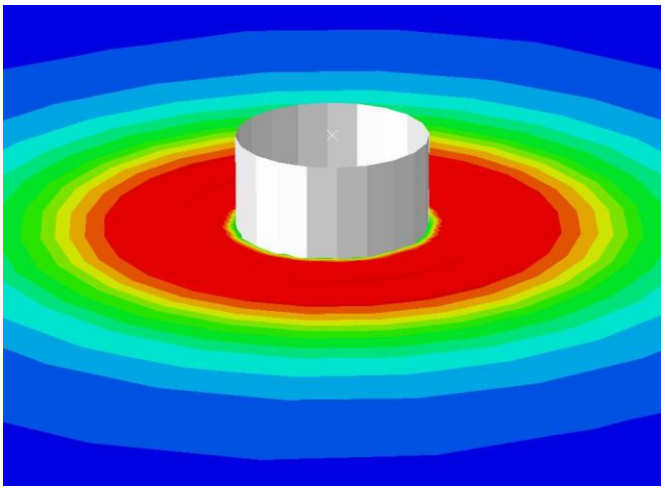

Figure 4-1: Indentation of a substrate by a flat indenter.

Following the argument of Xu et. al, the similarity in the stress singularity in a circumferential crack on a cylindrical sample under mode I loading and the rim of contact between a cylindrical indenter and the substrate, can be utilized to obtain a maximum stress intensity and a stress intensity range during indentation fatigue as:

$$K_{\max} = \frac{P_{\max}}{2a\sqrt{\pi a}}; \qquad \text{Eq 4-2}$$

$$\Delta K = \frac{\Delta P}{2a\sqrt{\pi a}} \qquad \text{Eq 4-3}$$

Where, ‘a’ is the radius of the cylindrical indenter and P_{max} and ΔP are the maximum load and the load range respectively. Using this, Xu et. al went on to formulate a steady state depth propagation law for instrumented indentation. They proposed that depth propagation can be described quantitatively as:

$$\frac{dh}{dN} = C_i K_{\max}{}^{n_i} \Delta K^{m_i} \qquad \text{Eq 4-4}$$

Where C_i, m_i, and n_i are constants of indentation fatigue, which depend on material/microstructure and testing environment. The law is then validated using simulations and experimental evidence.

In this study we attempt to access the variation in the parameters C_i, m_i, and n_i with the degree of plastic anisotropy. Fig. 4-2 shows a comparison for indentation depth with number of cycles, between the isotropic and transversely isotropic ductile copper alloy. As can be observed there is a considerable disparity brought about by the plastic anisotropy in the material and needs to be accounted for when dealing with metals which exhibit transverse isotropy.

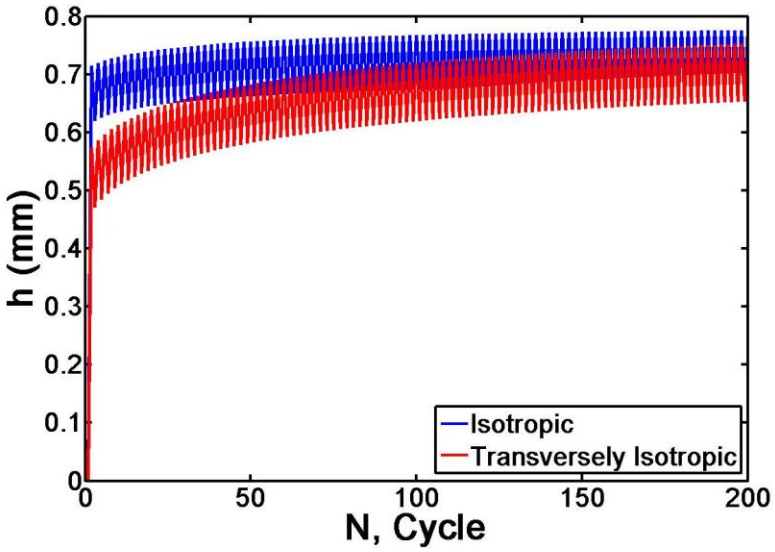

Figure 4-2: A comparison of the variation of indentation depth with number of cycles for indentation on a transversely isotropic material and the corresponding isotropic material with the same average properties.

4.3 Cyclic indentation of transversely isotropic materials

Consider a polycrystalline copper alloy with equiaxed microstructure. The microstructure causes the alloy to exhibit isotropy. However, when the same alloy is subject to plastic deformation processes such as rolling, the material undergoes changes in its microstructure and often exhibits transverse isotropy in its plastic domain. Transverse isotropy exists when a material has one set of properties along one plane and a different set of properties perpendicular to this plane. Transverse isotropy in the plastic domain implies the metal has different yield strengths parallel and perpendicular to the plane of isotropy. Lamellar microstructure in metals causes them to have different yield strengths parallel and perpendicular to the grain orientation and hence transverse isotropy. Within the context of indentation, transversely isotropic materials have been shown to exhibit responses varying significantly from their isotropic counterparts with the same average material properties. Also, indentation can be performed either parallel or perpendicular to the plane of isotropy obtaining distinct responses. Our study focuses

on indentation parallel to the plane of isotropy. The transverse anisotropy is quantified here as the ratio of the longitudinal to transverse yield strength σ_L/σ_T and is varied from 1 to 2 as most metals after deformation exhibit transverse isotropy within this range.

Instrumented indentation is modeled using the commercially available software Abaqus. A 3D model is constructed with 80000 hexagonal elements for the material and the indenter modeled as a rigid flat cylindrical punch of 3mm radius.

Simulations were carried for multiple materials varying the maximum load, load range and the degree of anisotropy. For the purpose of illustration we discuss the results obtained for a ductile copper alloy with Young's modulus of 119.9 GPa, Poisson's ratio of 0.35, average initial yield stress of 73.50 MPa and linear hardening rate of 0.369 GPa. The plastic anisotropy was varied as $1<\sigma_L/\sigma_T<2$.

4.4 Results and discussion

Fig.4-3 (a, b) show a comparison of the variation of the indentation depth rate with K_{max} and ΔK respectively, for isotropic and transversely isotropic copper alloy. For the isotropic case the results obtained are very close to that reported by Xu et. al for the same material properties. This validates the simulation and modeling undertaken. Further we can observe a clear difference in the values of the parameters n_i and m_i, (slope of the lines in Fig. 4-3a and 4-3b respectively) for the isotropic and transversely isotropic cases. Table 4.1 tabulates the values of these parameters. Results similar to those shown were observed for all the materials tested. Thus it can be observed that with increasing transverse anisotropy the parameters also show an increase in value. This implies that the material shows greater sinking in rates per cycle as the anisotropy

increases for indentation parallel to the plane of isotropy. Here, it is postulated that an additional parameter could be added to account for the anisotropy of the material. However, the amount of data obtained and the possible influence of other parameters such as the rate of loading and unloading prevent any concrete conclusions on whether it is possible to obtain a single parameter to account for the degree of a materials isotropy.

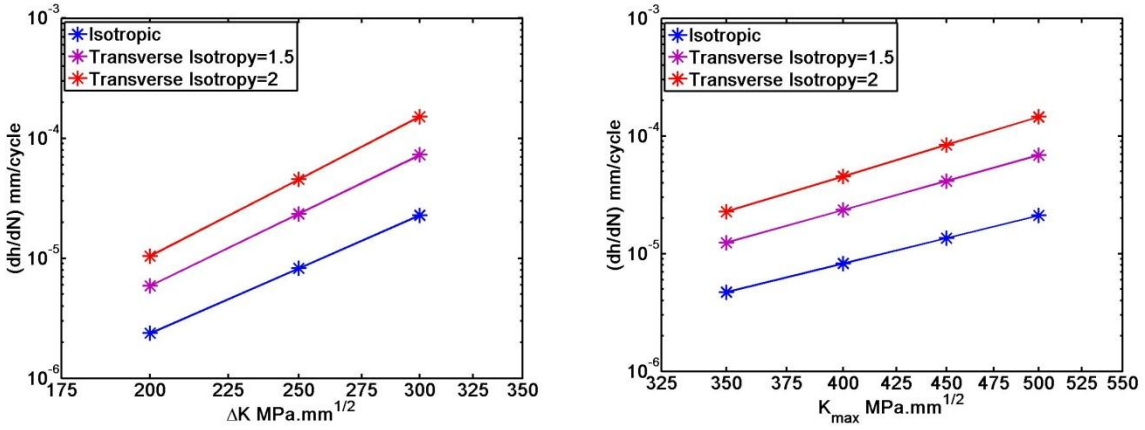

(a) (b)

Figure 4-3: Variation of indentation depth rate per cycle for isotropic and transversely isotropic materials with (a) varying ΔK and (b) K_{max} values for ductile copper.

Table 4.1: The table shows the variation of the indentation fatigue law parameters n_i and m_i with varying anisotropy.

Material	**n_i**	**m_i**
Isotropic	4.3	5.6
Transverse Isotropy = 1.5	4.8	6.2
Transverse Isotropy = 2	5.2	6.6

4.5 Conclusion and future work

The present study is a first step towards understanding the fatigue behavior of anisotropic materials under indentation loading. We build on prior work done on the flat indentation of isotropic materials under cyclic loading. The study makes observations on the change in material behavior under fatigue with its anisotropy. This work only serves as a start and hopes for much further study to be undertaken in the field. In the future a thorough and comprehensive study of the influence of anisotropy on indentation fatigue can be undertaken. Also, indentation response while indenting perpendicular to the plane of isotropy may be studied as well. It is hoped that studies will help unearth the mechanism behind the influence of microstructure as well as material properties on the depth propagation rate in an indentation fatigue experiment.

5 Investigation of equibiaxial residual stress using indentation analysis

5.1 Introduction

Investigation of Residual stress is a topic of considerable interest in engineering applications. The residual stress existing in a component considerably influences its properties such as fatigue, fracture, corrosion resistance. Residual stresses in components occur in a wide variety of situations, a few examples are: (i) welded or brazed components, (ii) surface coatings, thick and thin films deposited on substrates, (iii) components with reinforcements (iv) components subjected to deformation during forming. A wide variety of techniques have evolved over the years to determine the amount of residual stress existing in a component [74, 75]. For eg. XRD, strain/curvature measurements, hole drilling, layer removal, optical fluorescence, chemical etching, etc. However, the use of these techniques is limited in certain situations owing to the problems associated with accuracy of measurement, spatial resolution, ease of measurement, applicability to a broad range of materials and geometries, feasibility for use as a quality control device in mass production or during service, and flexibility for scaling up from small to large components.

Indentation as a means to measure residual stress in a material was suggested by Suresh et. al [76] owing to its distinct advantages of being simple, versatile, virtually non

destructive, applicable to local as well as volume averaged stress determination, especially useful in determining stresses in thin films and surface coatings. It also offers the possibility of determination of residual stresses without prior knowledge of the material's properties. Subsequently, multiple studies have been carried out using indentation analysis to predict the residual stresses in materials [53, 77-86]. Also, instrumented indentation has emerged as a very popular tool for the determination of material properties from indentation curve parameters. Combining these two it was then speculated that material properties as well as the degree of residual stress could be predicted from known indentation response parameters. J. Yan et. al [87] devised an algorithm to predict two unknown material parameters from known indentation response and two known material parameters for isotropic materials with strain hardening. Chen et. al [88] used sharp indentation to develop a method to predict the properties and residual stress of elastic perfectly plastic materials from known indentation response parameters. However, their method involves normalized indentation work which might not always be an independent parameter obtained from an indentation experiment.

Prior studies on the determination of residual stress using indentation have focused residual stresses in isotropic specimen. However, a wide range of materials which are especially convenient to test using indentation techniques are transversely isotropic in nature. Many bulk as well as thin film materials are almost invariably transversely isotropic in nature especially in the plastic regime. To the best of our knowledge there has been little research on the indentation response behavior of anisotropic materials with residual stress.

The present study initially follows a procedure similar to that used by Chen et. al but uses the ratio of plastic work done to total work done by the indenter as the third independent indentation parameter to obtain algorithms to predict residual stress as well as material properties for elastic perfectly plastic isotropic materials. The study then moves on from there using a similar argument to develop algorithms to predict residual stress and transversely isotropic material parameters from indentation response, given prior knowledge of the materials elastic behavior.

The objectives of the present study are:

(i) To develop robust forward-reverse algorithms to accurately and uniquely predict the residual stress and material properties from known indentation response parameters for isotropic elasto-plastic materials.

(ii) To develop robust forward-reverse algorithms to accurately and uniquely predict the residual stress and material properties from known indentation response parameters and elastic parameters for elasto-plastic materials that exhibit transverse isotropy in the plastic regime.

(iii) To assess the sensitivity of the obtained algorithms in both cases.

The analysis on isotropic materials shall be henceforth referred to as case I, and that on transversely isotropic materials as case II.

The document is organized as follows. Theoretical background information on transverse isotropy in the plastic regime, equi-biaxial state of stress and the fundamentals of indentation are presented in section 5.2. A framework based on dimensional analysis and computational modeling is formulated in section 5.3. The results of the indentation simulations, the forward-reverse indentation algorithms, and

the sensitivity issues associated with the forward and reverse analyses are discussed in section 5.4. Principal conclusions are highlighted in section 5.5.

5.2 Transverse isotropy, equibiaxial residual stress and indentation

5.2.1 Transverse isotropy in the plastic regime

As discussed in chapter two, plastic transverse isotropy can be defined with the help of Hills criterion for yielding. Using the same approximations and definitions as described in chapter two, and restricting the present analysis to materials with no strain hardening, plastic transverse isotropy can be defined using two parameters, σ_y the average yield stress and σ_L/σ_T the ratio of longitudinal to transverse yield stress.

5.2.2 Equibiaxial residual stress

Within the context of this study, for both case I and case II, materials are considered to be elastic perfectly plastic with an equibiaxial residual stress $\sigma_{rx}= \sigma_{ry}$ and $\sigma_{rz}=0$. The residual stress is assumed to have been brought about by subjecting the material to mechanical and/or thermal loading which include: (i) non-uniform cooling down; (ii) deposition of a surface coating or a thin film on a substrate (iii) shot peening; (iv) laser shock peening; (v) bending or normal loading; (vi) mechanical working.

It is assumed that these processes give rise to equibiaxial stresses in the material. Since the material is assumed to have no strain hardening the yield stress σ_y (average yield stress in the case of materials with plastic transverse isotropy) does not change whether the material has undergone plastic deformation or not. Also, the Von Mises effective stress σ_e due to the equibiaxial stress can be written as:

$$\sigma_e = \frac{1}{\sqrt{2}}\sqrt{\left(\sigma_{rx} - \sigma_{ry}\right)^2 + \left(\sigma_{ry} - \sigma_{rz}\right)^2 + \left(\sigma_{rz} - \sigma_{rx}\right)^2} \quad \text{Eq 5-1}$$

It can be seen that this gives $\sigma_e = \sigma_{rx} = \sigma_{ry}$.

Also, the residual strain can be expressed as:

$$\varepsilon_{rx} = \varepsilon_{ry} = \frac{\sigma_e}{E}(1-\nu)$$

Thus for an elastic-perfectly plastic isotropic material with equibiaxial residual stress there are three independent parameters under consideration namely, E, σ_y and σ_r where, σ_r is the residual stress in the material. Also, for materials with transverse isotropy an additional independent parameter σ_L/σ_T is required to define the degree of anisotropy in the plastic regime. As mentioned previously, the objective of this study is to devise a method to predict these independent parameters using instrumented indentation. To be able to predict these parameters uniquely it is necessary to obtain mutually exclusive relations between material properties and indentation response from an indentation experiment.

5.2.3 Indentation theory

As explained in previous chapters, the loading response for a power law hardening material is governed by Kicks Law:

$$P = Ch^m \quad \text{Eq 5-2}$$

Where, C is the loading curvature and is constant for a given material and indenter. Values of m, the exponent depends on the indenter. This law is applicable to materials

with no strain hardening as well since they are a subset of materials which obey power law hardening. The maximum indentation depth h_m occurs at the maximum load of P_m.

The initial unloading slope at maximum depth is defined as,

$$S_m = \left(\frac{dP_u}{dh} \right)\Big|_{h_m} \qquad \text{Eq 5-3}$$

where P_u is the unloading force and h_m the maximum depth. The area under the loading curve is the total work done (W_T) and the area under the unloading curve represents the recovered elastic work done by the system (W_E). The plastic work done is given as $W_P = W_T - W_E$ and the plastic to total work ratio (R_w) is given as:

$$R_w = \left(\frac{\int_0^{h_m} P dh - \int_{h_r}^{h_m} P_u dh}{\int_0^{h_m} P\, dh} \right)$$

or

$$R_w = \frac{W_P}{W_T} \qquad \text{Eq 5-4}$$

Here, it is postulated that the three parameters C, S_m, and R_w are mutually exclusive for elastic-perfectly plastic materials. In the past Chen et. al have used the total work done by the indenter as the third independent indentation response parameter. It can be seen for materials whose indentation loading obeys Kick's law, the

total work done by the indenter is a function of the loading parameter and hence cannot be assumed to be an independent parameter obtained from an indentation experiment. Hence, the third independent parameter is taken as the ratio of the plastic to total work done by the indenter.

For the case of materials with plastic transverse isotropy (case II), longitudinal indentation is carried as it is assumed that the transverse plane harbors the equibiaxial residual stress. Also, since four material parameters are required to define the transversely isotropic material with residual stress and indentation only yields three independent parameters, the analysis assumes prior knowledge of the Young's modulus of the material.

5.3 Framework for the indentation analysis

5.3.1 Dimensional analysis

In the case of isotropic materials and longitudinal indentation of transversely isotropic materials, owing to the existing symmetry, indentation can be performed using an axisymmetric model. However, the present study is performed with the motive of extending the work to anisotropic materials as well as to materials without residual stress symmetry and hence uses a 3-D model to simulate indentation.

The first goal of this work is to establish robust relationships between indentation response parameters and materials properties including the residual stress in the material for both case I and II. From this point onwards the two cases of isotropic and transversely isotropic materials are considered sequentially within each section to avoid confusion.

5.3.1.1 Case I

Dimensional analysis is used to obtain functional forms for relations between isotropic material properties and indentation response. Once general forms of these equations are obtained, to determine their exact form, a study with 110 computational models with material properties varying over a wide range is conducted. The values of Young's modulus E ranges from 50 to 200 GPa, yield strength σ_y from 100 to 2000 MPa, and the residual stress to yield strength ratio σ_r/σ_y varying from -0.9 to 0.9. The range of materials and residual stress considered is depicted in Fig. 5-1. The exact form of the relations is then established by curve fitting the simulation data to the functions forms.

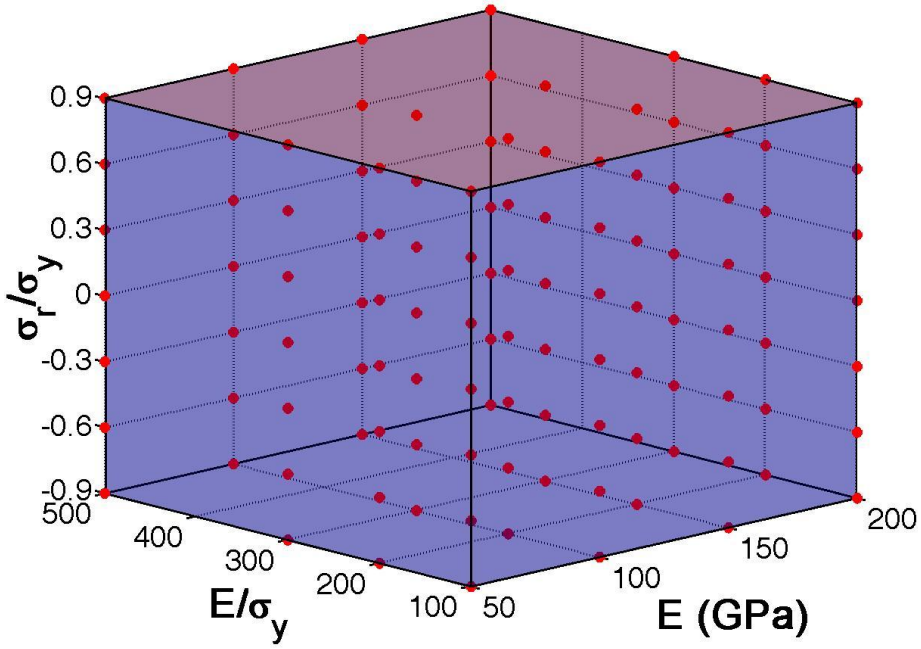

Figure 5-1: A schematic illustrating the material property database considered and the range of residual stress considered for the formulation of the forward and reverse algorithms in case I.

As described below, dimensional analysis is invoked to develop closed form universal functions to capture the indentation behavior of isotropic elastic-plastic materials with residual stress.

For a sharp indenter with a half cone angle of θ, the load required to indent an elastic-perfectly plastic material with residual stress can be written as:

$$P = P\left(h, E, \sigma_y, \sigma_r, \theta\right) \qquad \text{Eq 5-5}$$

Where, h is the depth of indentation.

Using dimensional analysis Eq. (5-5) becomes

$$P = \sigma_y h^2 \Pi_{1\theta}\left(\frac{E}{\sigma_y}, \frac{\sigma_r}{\sigma_y}, \theta\right) \qquad \text{Eq 5-6}$$

For a cone half angle of 70.3 degrees the function for load P becomes

$$P = \sigma_y h^2 \Pi_1\left(\frac{E}{\sigma_y}, \frac{\sigma_r}{\sigma_y}\right) \qquad \text{Eq 5-7}$$

or

$$C = \frac{P}{h^2} = \sigma_y \Pi_1\left(\frac{E}{\sigma_y}, \frac{\sigma_r}{\sigma_y}\right)$$

Similarly the unloading slope at maximum depth and the plastic to total work ratio can be written as dimensionless equations:

$$S_m = h_m \sigma_y \Pi_2 \left(\frac{E}{\sigma_y}, \frac{\sigma_r}{\sigma_y} \right) \quad \text{Eq 5-8}$$

$$R_W = \frac{W_P}{W_T} = \Pi_3 \left(\frac{E}{\sigma_y}, \frac{\sigma_r}{\sigma_y} \right) \quad \text{Eq 5-9}$$

The actual forms of these dimensionless functions and their construction are discussed in section 5.3.2.

5.3.1.2 Case II

Dimensional analysis is carried out in a manner very similar to that of case I, for the case of materials with plastic transverse isotropy, to obtain functional forms of relations between material properties and indentation response. Once general forms of these equations are obtained, to determine their exact form, a study with 85 computational models with material properties and degree of anisotropy varying over a wide range is conducted. The values of yield strength, σ_y ranges from 100 to 2000 MPa, the anisotropy in the plastic regime, σ_L/σ_T ranges from 1 to 2 and the residual stress to yield strength ratio σ_r/σ_y varying from -0.9 to 0.9. The Young's modulus is assumed to be known and hence is kept constant here. The range of materials and residual stress considered is depicted in Fig. 5-2. The exact form of the relations is then established by curve fitting the simulation data to the functions forms.

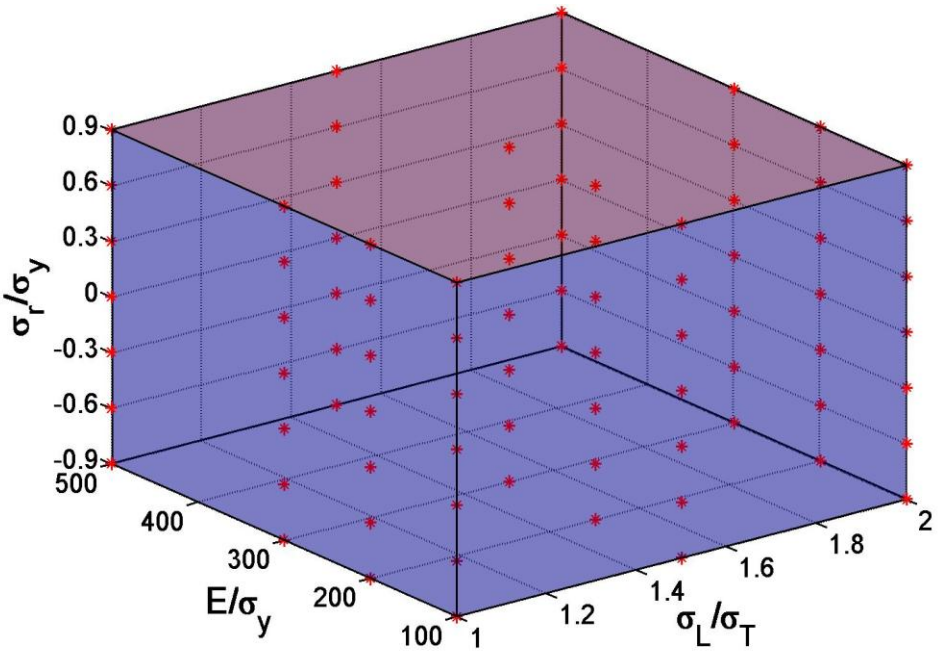

Figure 5-2: A schematic illustrating the material property database considered and the range of residual stress considered for the formulation of the forward and reverse algorithms for case II.

Following the dimensional analysis for case I, dimensionless equations obtained for case II can be listed as follows:

$$C = \sigma_y \Pi_1 \left(\frac{E}{\sigma_y}, \frac{\sigma_r}{\sigma_y}, \frac{\sigma_L}{\sigma_T} \right) \quad \text{Eq 5-10}$$

$$S_m = h_m \sigma_y \Pi_2 \left(\frac{E}{\sigma_y}, \frac{\sigma_r}{\sigma_y}, \frac{\sigma_L}{\sigma_T} \right) \quad \text{Eq 5-11}$$

$$R_W = \frac{W_P}{W_T} = \Pi_3 \left(\frac{E}{\sigma_y}, \frac{\sigma_r}{\sigma_y}, \frac{\sigma_L}{\sigma_T} \right) \quad \text{Eq 5-12}$$

As stated earlier, this analysis begins with the assumption of known values of Young's modulus hence the equations 5-10 and 5-11 can be changed as

$$\frac{C}{E} = \frac{\sigma_y}{E}\Pi_1\left(\frac{E}{\sigma_y}, \frac{\sigma_r}{\sigma_y}, \frac{\sigma_L}{\sigma_T}\right) \qquad \text{Eq 5-13}$$

$$\frac{S_m}{E} = h_m \frac{\sigma_y}{E}\Pi_2\left(\frac{E}{\sigma_y}, \frac{\sigma_r}{\sigma_y}, \frac{\sigma_L}{\sigma_T}\right) \qquad \text{Eq 5-14}$$

Thus for known E the indentation response parameters can be expressed as a function of the three remaining unknown material parameters namely, yield stress, residual stress and degree of anisotropy. Equations 5-12, 5-13, and 5-14 can now be used as three independent equations to determine the plastic properties and residual stress in materials.

5.3.2 Computational modeling

The computational modeling, for both case I and II, of the experiment involves two main stages.

(i) Subjecting the material to an equibiaxial stress σ_r and holding the material at that stress to simulate a state of residual stress.

(ii) Performing indentation on the material using a sharp indenter and obtaining the indentation parameters.

A 3-D model similar to that described in the first two chapters is used for the computations. The general purpose finite element package of ABAQUS is used to conduct all the simulations. Computational analysis is performed for all materials (110 in case I and 85 in case II) to obtain the complete loading and unloading indentation response for all the materials with varying residual stress. Careful analysis is conducted

to determine the exact forms of the dimensionless functions that best describe the relationships between the material properties and the corresponding indentation response parameters. Excellent curve fits are obtained for the variation of the indentation parameters as a function of the materials properties and residual stress for the assumed functional forms. The detailed form of the expressions, for case I, is given as follows:

$$\Pi_{11} = \frac{C}{\sigma_y} = \left(\begin{array}{l} 43.38 - 24.49\,y - 2.07\,y^2 + x\,(0.33 + 0.04`y - 0.075y^2) + \\ x^2\,(-0.0008 - 0.000014y + 0.0003y^2) \end{array} \right) \quad \text{Eq 5-15}$$

$$\Pi_{12} = \frac{S_m}{\sigma_y h_m} = \left(\begin{array}{l} -117.2 + 53.6\,y + 96.7\,y^2 + x\,(8.25 - 1.79\,y - 1.64y^2) + \\ x^2\,(0.0014 + 0.0038y + 0.0047y^2) \end{array} \right) \quad \text{Eq 5-16}$$

$$\Pi_{13} = R_w = \left(\left(0.7 + 0.08y + 0.033y^2 + x\,(0.0018 - 0.0006y - 0.0002y^2) \right) \right) \quad \text{Eq 5-17}$$

where, x and y represent the properties E/σ_y and σ_r/σ_y respectively.

The detailed form of the equations obtained for case II is provided in Appendix C.

5.4 Results and discussion

5.4.1 Analysis of the functions

The analysis here involves an investigation on the accuracy of the functions in predicting the indentation parameters. Once again, the analysis is split into the two cases considered.

5.4.1.1 Case I

The dimensionless functions presented are validated by testing them on the 110 initial materials chosen to create the database as well as 12 different materials with properties scattered within the database. The values for the indentation response parameters obtained through the forward analysis are then compared with the true values observed from the simulation experiments conducted. An excellent match between the two is observed thus proving the validity of the equations. The error between the two is shown for each parameter in Table 5.1.

Table 5.1: Average and standard deviation of the error percentage in the indentation response parameters predicted by the forward analysis for case I.

Parameter	Average % Error	Std Dev
C	0.36	0.54
S_m	0.35	0.41
R_w	0.03	0.02

The influence of residual stress on the indentation response parameters is then studied in detail. Fig. 5-3a shows the variation of loading parameter normalized with respect to the yield stress with varying residual stress. Similarly, Fig. 5-3(b, c) show the variation of the other two indentation parameters with residual stress. The following conclusions may be drawn from the trends shown in the figures:

- The normalized loading parameter C/σ_y increases with increasing compressive residual stress and decreases with increasing tensile residual stress.

- Normalized slope at maximum depth $S_m/h_m*\sigma_y$ displays lower sensitivity to changes in residual stress. It however displays a slight decrease in value as stress goes from compressive to tensile.
- R_w for higher E/σ_y is almost constant in the compressive residual stress region and increases with increasing tensile residual stress.

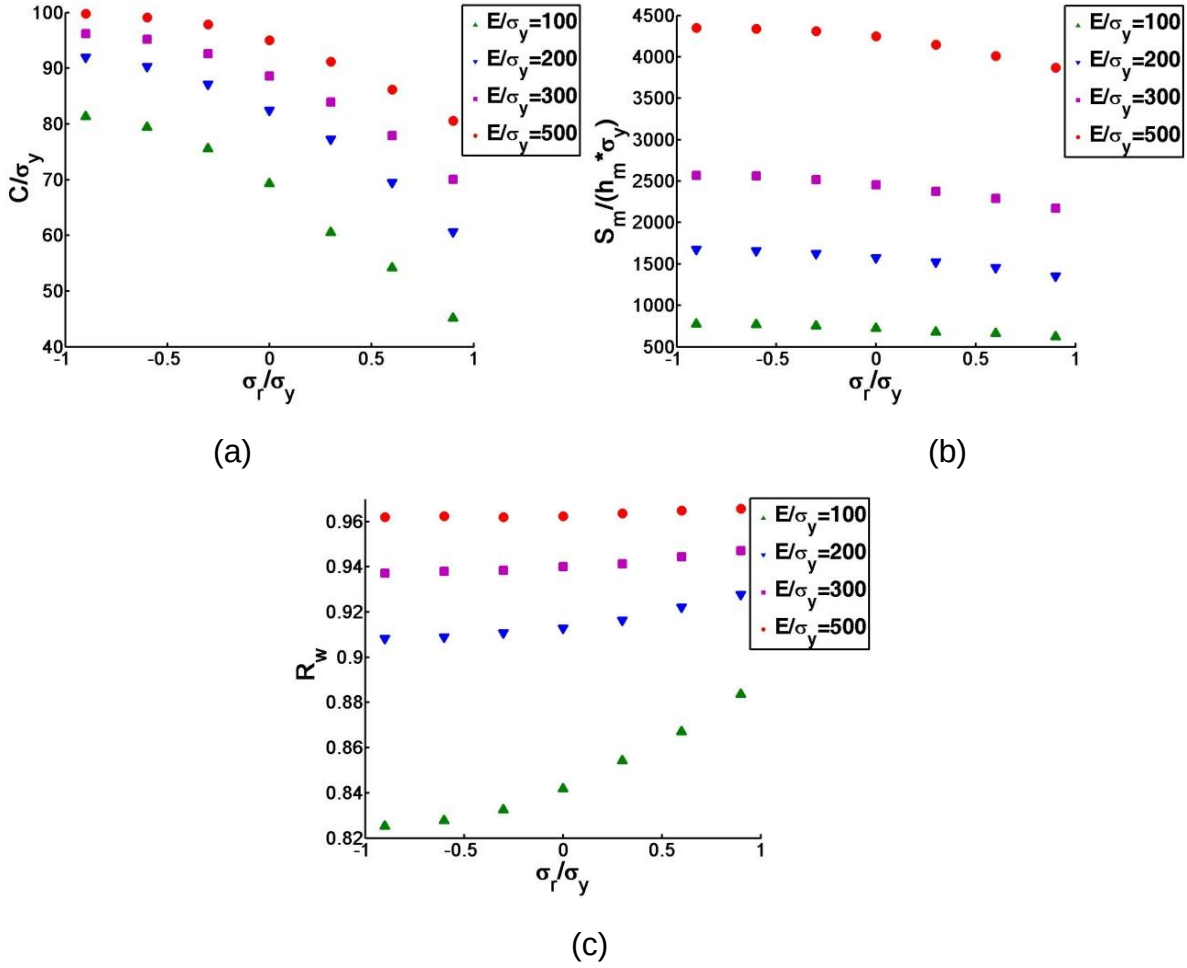

Figure 5-3: The variation of loading parameters normalized with respect to the yield stress with varying residual stress. (a) Loading curve parameter C normalized (b) Slope of unloading curve at maximum depth normalized, (c) Plastic to total work ratio.

5.4.1.2 Case II

The functions obtained for case II are validated in a manner similar to that in case I, 85 materials chosen are subjected to dimensionless functions. Once again, an excellent

match between the predicted and actual values for the indentation response is observed. (Table 5.2)

Table 5.2: Average and standard deviation of the error percentage in the indentation response parameters predicted by the forward analysis for case II.

Parameter	Average % Error	Std Dev
C	0.34	0.39
S_m	0.42	0.38
R_w	0.06	0.05

The influence of degree of anisotropy for different residual stress values on the indentation response is then studied systematically. Fig. 5-4 shows the variation of the indentation response normalized to elastic modulus with varying degree of anisotropy for materials with no residual stress, tensile residual stress and compress residual stress.

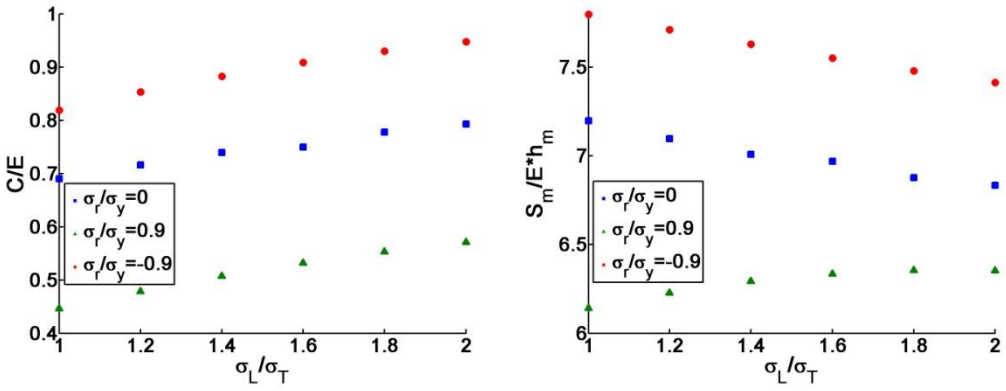

(a) (b)

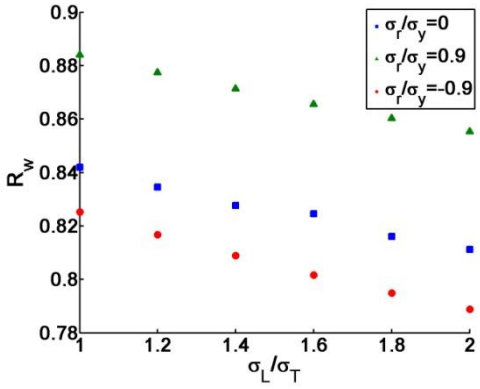

(c)

Figure 5-4**:** The variation of indentation parameters normalized with respect to the elastic modulus with varying anisotropy. (a) Loading curve parameter C normalized (b) Slope of unloading curve at maximum depth normalized, (c) Plastic to total work ratio.

The trends shown in the above figures lead to interesting observations:

- The normalized loading parameter C/E increases with increasing anisotropy and also the rate of increase of the parameter can be observed to be independent of residual stress.
- The variation of normalized slope at maximum depth $S_m/h_m*\sigma_y$ with anisotropy displays varying trends with varying residual stress; it decreases for materials with tensile residual stress and increases for materials with compressive residual stress. The slope at maximum depth decreases with increasing anisotropy for materials with no residual stress.
- R_w decreases with increasing anisotropy and the rate of decline is independent of residual stress.

5.4.2 Reverse analysis

Once the accuracy of the forward analysis (predicting indentation response from known material parameters) is established, the reverse analysis, for case I and II,

predicting material properties and residual stress from known indentation response parameters is attempted.

A simple error minimization algorithm very similar to that used in chapter 2 is devised to estimate the residual stress and material parameters from known indentation response. The algorithm followed for both cases is almost identical hence only that for materials with transverse isotropy is elucidated here. Using the forward analysis equations an extensive database of indentation response of 3660 materials within the data range is constructed. A step wise procedure of the reverse analysis is enumerated here. Also, a schematic form of the algorithm is shown in Fig. 5-5.

- The entire forward analysis database of 3660 materials is put in a tensor $\mathbf{DB_{ij}}$, where, i defines the material position in the database and goes from 1 to 3660 and j defines the P-h response and is 1, 2 or 3 for C, S_m or R_w respectively.
- The P-h response (C, S_m, R_w) measured from an indentation experiment is assigned to a matrix $\mathbf{Q_{ij}}$ where, i and j hold the same definitions as above.
- $\mathbf{Q_{ij}}$ is compared with $\mathbf{DB_{ij}}$ for each of the 3660 materials. Two material property sets, which are closest to $\mathbf{Q_{ij}}$ are determined. These two sets are assigned to matrices $\mathbf{M_{1ij}}$ and $\mathbf{M_{2ij}}$ respectively.
- These two sets are used as seed material properties and a procedure similar to that used by H. Lan and T. A. Venkatesh [4] is then followed to reach at the final result of the reverse analysis.

- For the chosen seed properties the corresponding indentation response parameters (C, S_m, R_w) are obtained from the functional forms presented by the forward algorithms.
- The experimentally measured set of indentation parameters $\mathbf{Q_{ij}}$ (from step 2) are compared to the indentation parameters computed in step 5. An error function that computes the root mean square of errors of all the indentation response parameters is determined.
- If the error function produces an error below a certain lower critical threshold, (chosen as 99.8% accuracy in indentation response parameters) the set $\mathbf{M_{ij}}$ is accepted as a feasible solution to the reverse analysis.
- If not, the error function is minimized by systematically considering a number of combinations of material properties around $\mathbf{M_{ij}}$ to obtain the best solution set for the material's elastic and plastic properties.
- If the iterative process leads to a physically non-feasible solution ($\sigma_L/\sigma_T<1$), the process is restarted after assigning the seed properties as the closest feasible solution till a feasible solution is obtained.
- A condition of minimum accuracy in the indentation response parameters is set at 99.8%. The solution set which has lower error among $\mathbf{M_{1ij}}$ and $\mathbf{M_{2ij}}$'s variations is reported as the final solution.

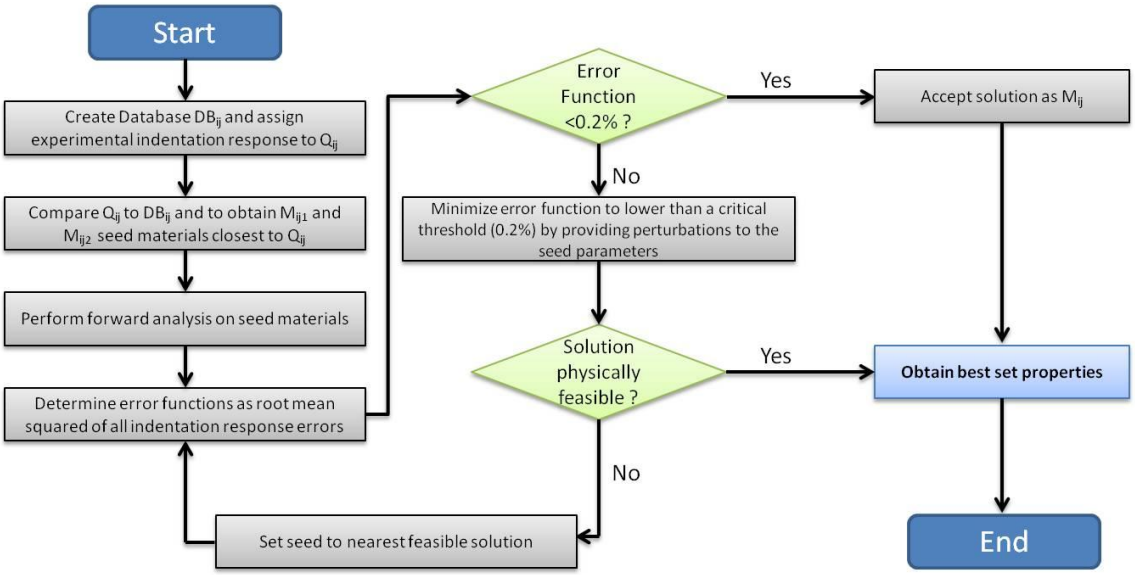

Figure 5-5: Schematic illustrating the algorithm followed by the reverse analysis for material property identification.

To initially validate the reverse analysis and also to test the code for possible bugs, a reversibility test is carried out using the 3660 materials database. Initial known material properties are subject to forward analysis to obtain indentation response parameters and these response parameters are then subject to the reverse analysis to obtain material properties. All 3660 cases considered converged back to the original material properties proving the validity of the analysis algorithm.

Once the algorithm is validated for both cases, the accuracy of the analysis for each case is undertaken.

5.4.2.1 Case I

Reverse analysis is performed on the 110 materials whose P-h response is determined through finite element computation. The results obtained are shown in the form of graphs (Fig. 5-6). A comparison between actual material properties and residual stress and those predicted by the reverse analysis is displayed. It can be observed that

the reverse analysis predicted properties accurately converge with the actual properties for all three material properties E, E/σ_y, σ_r/σ_y. Also, it is observed that the algorithm predicts tensile residual with almost unerring accuracy and shows a small error in the calibration of compressive residual stress. This is attributed to a better curve fit relation obtained for the behavior of tensile residual stress materials under indentation.

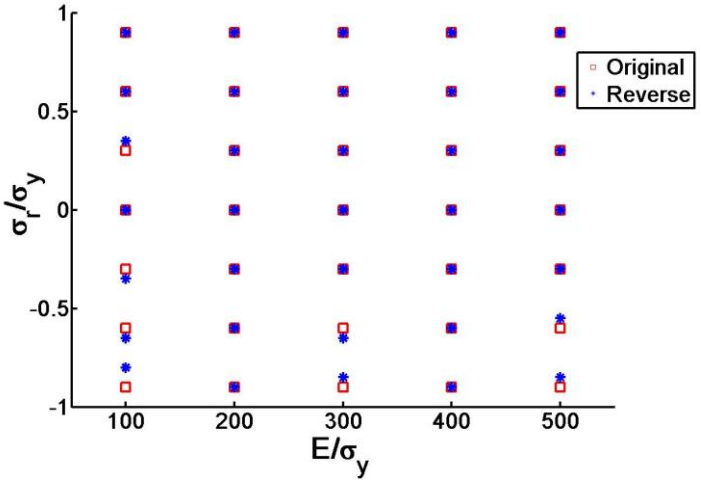

(a)

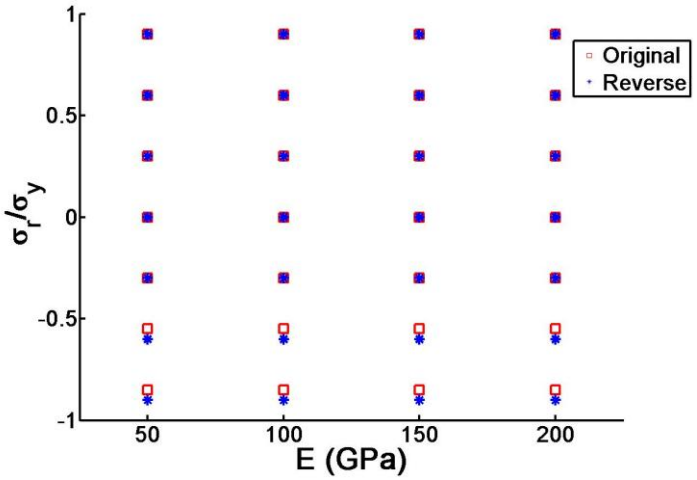

(b)

Figure 5-6: A comparison between actual material properties and residual stress, and that obtained through analysis from known indentation curve properties, for case I, for (a) residual stress σ_r/σ_y and E/σ_y (b) residual stress σ_r/σ_y and E.

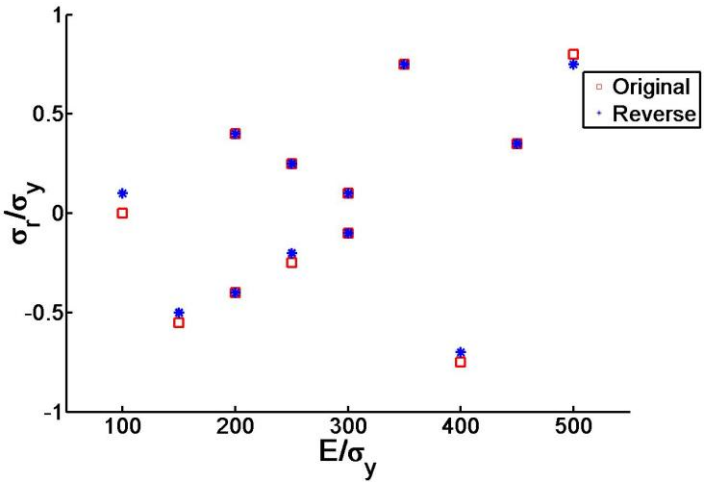

Figure 5-7: A comparison between actual material properties and residual stress, and that obtained through analysis from known indentation curve properties, for 12 additional randomly chosen materials, for residual stress σ_r/σ_y and E/σ_y.

To further verify the results obtained by the reverse analysis, another twelve separate and arbitrary materials with varied residual stress are chosen lying within the database domain. The indentation response of these materials is obtained using finite element simulations. These response parameters are then subject to the reverse analysis and the results compared with the actual material properties and residual stress. The reverse analysis results for these are shown in the plots (Fig. 5-7). Once again a very good match is obtained. Table 5.3 shows the average error and standard deviation in predicting each material property for case I.

Table 5.3: Average and standard deviation of the error percentage in the material properties and residual stress predicted by the reverse analysis for case I.

Parameter	Average % Error	Std Dev
E/σ_y	0.1	0.1
σ_y	0.1	0.1
σ_r/σ_y	3	0.5

5.4.2.2 Case II

The accuracy of the reverse analysis in predicting the transversely isotropic properties as well as the materials residual stress is thoroughly investigated. The indentation response of materials with varying degree of anisotropy and residual stress is fed into the reverse analysis algorithm and the predicted properties are compared with the actual properties of the material and the actual existing residual stress. Fig. 5-8 shows a sample of the results obtained. It can be seen that the actual properties and predicted properties match well.

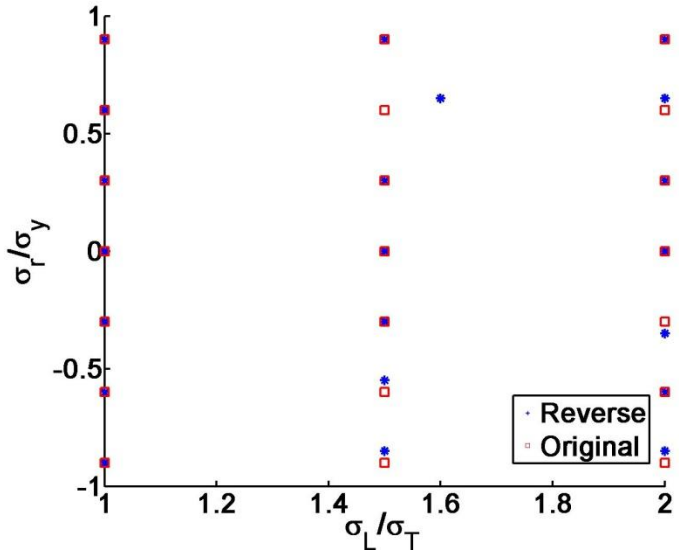

Figure 5-8: A comparison between actual anisotropy and residual stress, and that obtained through reverse analysis from known indentation curve properties for case II.

Table 5.4 shows the average error and standard deviation in the prediction of material parameters for case II.

Table 5.4: Average and standard deviation of the error percentage in the material properties and residual stress predicted by the reverse analysis for case II.

Parameter	Average % Error	Std Dev
E/σ_y	1	0.8
σ_L/σ_T	3.6	2.1
σ_r/σ_y	2.9	2.5

5.4.3 Sensitivity analysis

5.4.3.1 Sensitivity of the forward analysis

A sensitivity analysis similar to that used for the indentation studies of isotropic materials with no residual stress is invoked in the present study for both cases. It is observed that a ±5% change in any one of the material properties or residual stress leads to a variation of no more than ±7.5**% i**n the indentation response parameters for both cases. This ensures low sensitivity of the equations to slight changes in input parameters.

5.4.3.2 Sensitivity of the reverse analysis

An analysis is carried out to verify the sensitivity of the reverse algorithms used in both cases, to changes in the indentation parameters, provided as input from experiments. Each indentation parameter (C, S_m, R_w), is varied through ±2% (about its true value) and the corresponding variation in the residual stress and material properties predicted by the reverse analyses is observed. Fig. 5-9 depicts the results of the reverse analysis compared with the actual material properties for the isotropic case. Due to the nature of the reverse algorithm and its tendency to attempt to converge to results below a critical error function threshold, the sensitivity of the results to experimental errors in indentation parameter measurement is very low. Table 5.5 and

5.6 present a quantitative comparison of the material properties predicted by the reverse analysis using the true indentation parameters and those predicted with a variation in the values of C, S_m and R_w about their true values, for both the isotropic materials and transversely isotropic materials considered. Similarly, sensitivity studies are conducted on -2% variations in the values of C, S_m and R_w about their true values as well.

Table 5.5: Average and standard deviation of the error percentage in the material properties and residual stress predicted by the reverse analysis with variation in the input indentation response parameters for case I.

Variation	**% σ_y**	**Std Dev**	**% E/σ_y**	**Std Dev**	**% σ_r/σ_y**	**Std Dev**
2% in C	0.5	1.33	0.6	3.1	3.57	3.87
-2% in C	0.94	0.42	0.814	1.11	2.15	2.29
2% in S	2.71	0.66	4.1	2.4	6.1	1.82
-2% in S	3.77	1.83	1.72	2.13	6.81	4.17
2% in W	0.22	0.16	0.24	0.82	0.62	2.29
-2% in W	0.45	0.93	1.4	0.99	4.01	1.93

Table 5.6: Average and standard deviation of the error percentage in the material properties and residual stress predicted by the reverse analysis with variation in the input indentation response parameters for case II.

Variation	**% E/σ_y**	**Std Dev**	**% σ_L/σ_T**	**Std Dev**	**% σ_r/σ_y**	**Std Dev**
2% in C	2.5	1.53	2.46	2.03	5.57	2.82
-2% in C	2.34	0.72	2.8	1.87	4.15	2.78
2% in S	3.63	0.96	4.62	1.5	7.1	2.95
-2% in S	3.47	1.23	1.95	2.03	5.94	4.51
2% in W	0.32	0.23	0.64	0.62	0.92	1.24
-2% in W	0.54	0.43	1.8	0.69	3.52	0.98

In general, the variation in material properties obtained by the reverse analysis to ±2% in the values of C, S_m and R_w about their true values is low. For example, the maximum errors in the estimation of the plastic, elastic and residual stress properties – σ_y, E/σ_y and σ_r/σ_y are, about 5% and 7% and 15% respectively. The residual stress determination exhibits higher sensitivity to variations in the indentation parameters. All material properties exhibit high sensitivity to variations in S_m while they exhibit relatively low sensitivity to variations in R_w.

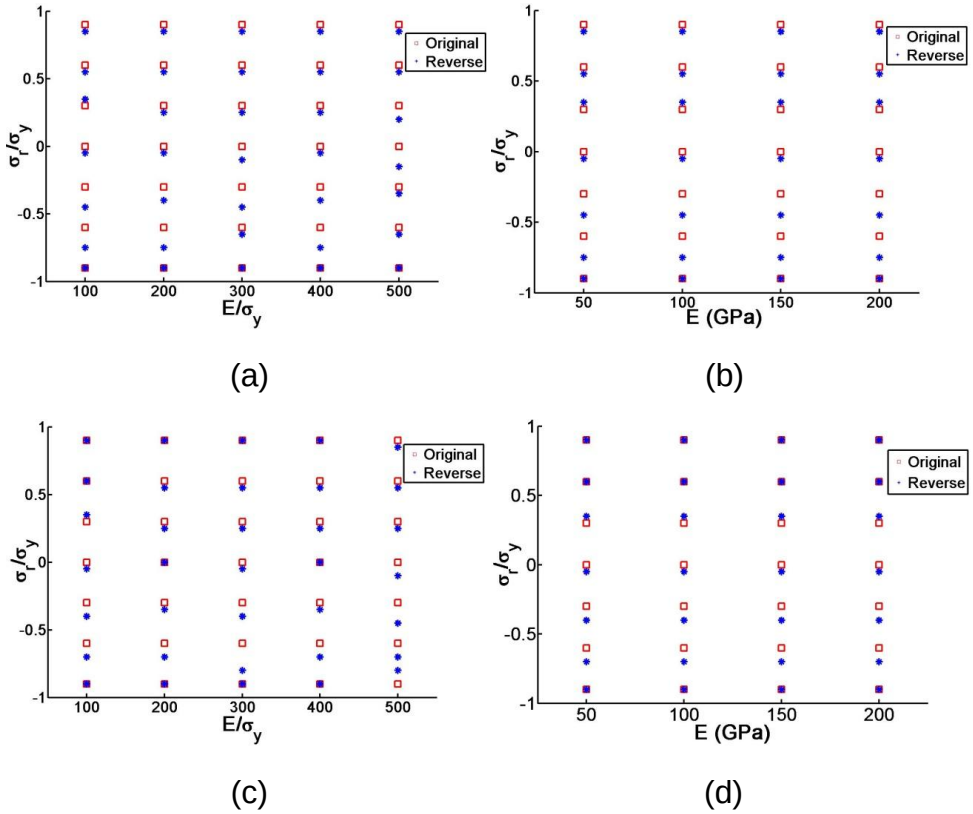

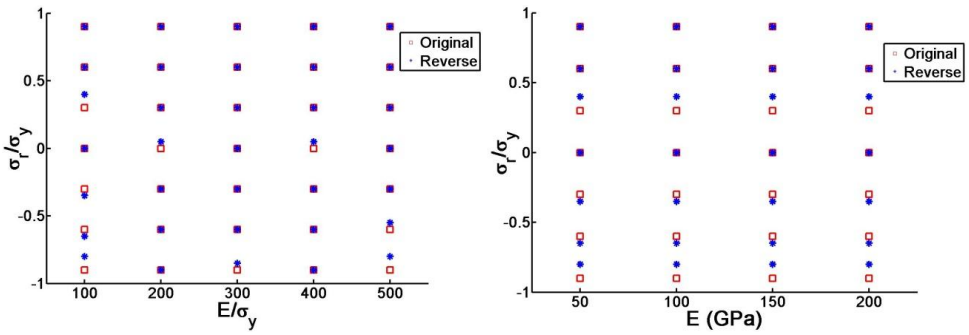

(e) (f)

Figure 5-9: Sensitivity analysis for the reverse analysis, the figure shows the variation of reverse analysis results for a two percent variation in the indentation response parameters for case I. (a), (b) 2 percent variation in C, (c), (d) 2 percent variation in S_m (e), (f) 2 percent variation in R_w.

5.5 Conclusions and future work

The study utilizes indentation response parameters to successfully predict material properties and existent biaxial residual. Two distinct cases are considered here (i) Isotropic elastic perfectly plastic materials (ii) elastic perfectly plastic materials with transverse isotropy in the plastic regime. For the analysis of transversely isotropic materials it is assumed that the elastic modulus of the material is known from prior studies on the material. For both the cases considered dimensional analysis is performed to determine the functional forms of relations between material properties and indentation response. Curve fitting over a large database of materials is performed to obtain the exact form of the relations. A simple error function minimization algorithm is developed to then predict material properties from indentation response parameters. The solutions obtained are checked for their accuracy, uniqueness and sensitivity.

6 Concluding remarks

The key contributions of this thesis, as a result of computational and analytical approaches are the following.

1. Comprehensive parametric studies for indentation of transversely isotropic materials for transverse and longitudinal indentation is undertaken to develop robust forward and reverse algorithms. The forward algorithm predicts the indentation response from known transversely isotropic material properties. The reverse algorithm extracts transversely isotropic material properties from three sharp indentation response experiments with cone half angles of 50, 60 and 70.3 degrees. The obtained forward-reverse algorithms are extensively tested for accuracy and uniqueness. The sensitivity of the algorithms to experimental errors in the measurement of indentation response is studied in detail.
2. A comprehensive study is performed on the true projected area of contact during indentation of a transversely isotropic material with a sharp indenter of cone half angle 70.3 degrees. Algorithms are developed to successfully predict the true projected contact area from known material properties for both transverse and longitudinal indentation. Utilizing previously devised forward-reverse algorithms, prediction of indentation hardness, from known indentation loading and unloading data is achieved without any need for prior knowledge of the material's properties, or of measurement of the contact area. A detailed study is undertaken

to study the variation of hardness with empirical constituent properties of transversely isotropic materials.

3. Indentation fatigue behavior of transversely isotropic materials is studied. Cyclic indentation is carried out on transversely isotropic materials as well as their isotropic counterparts. Observations are made on the change in material behavior under fatigue with its anisotropy. Variations in the parameters of a fatigue law proposed in literature are studied.
4. Using computational analysis, functions correlating indentation response from a single berkovich indenter to the equibiaxial residual stress and material properties of elastic perfectly plastic materials, with isotropic or plastic transversely isotropic properties, are developed. Algorithms are devised to predict the materials properties and existing residual stress from a single sharp indentation experiment and vice versa. The algorithm is then checked for its accuracy, uniqueness of results and sensitivity of the predicted residual stress and material properties to error in experimental measurement of indentation response.

7 Suggestions for future work

As technology advances and novel materials as well as novel devices spawn, it has become ever challenging to characterize the properties of materials. Depth sensing instrumented indentation as an experimental tool to study mechanical properties of small volume materials provides a simple and elegant solution to many problems. This thesis has laid the foundation for the investigation of transversely isotropic materials using indentation. A few directions in which the study can be moved forward from here are suggested here.

- The forward-reverse algorithms devised here for transverse and longitudinal indentation can be combined to devise an algorithm which ensures very low sensitivity and high accuracy of the reverse analysis.
- An in-depth analysis on the indentation fatigue response of transversely isotropic materials and a fatigue law similar to that proposed for isotropic materials can be attempted.
- Prediction of residual stress for materials with hardening behavior and extension of this to materials with anisotropy in elastic as well as plastic regimes can be envisioned.
- Using dynamic modeling of the indentation experiment high strain rate behavior of materials can be studied.

This thesis has presented a comprehensive analysis of sharp indentation response of elasto-plastic transversely isotropic materials. Both static and dynamic indentation analyses have been explored. The mechanical properties, hardness, residual stress and fatigue response of transversely isotropic materials are systematically studied and valuable advancements into development of indentation as a characterization tool are achieved. The directions in which this work can be furthered, as mentioned above are described sequentially here.

This second and third chapter of this thesis is dedicated to the study of transversely isotropic materials and provides characterization techniques using indentation in the transverse or the longitudinal direction. It has been shown here that the two indentation orientations yield distinct P-h responses. The two indentation responses can be used together thereby validating each other and also providing greater confidence in the obtained results. Also, the analysis can be furthered to materials with higher degree of anisotropy such as orthotropic materials by utilizing the response parameters obtained from multiple indenter orientations as parameters for the reverse analysis.

The fourth chapter explores the field of indentation fatigue response of transversely isotropic materials. The work needs to be extended to a thorough study of the fatigue behavior of transversely isotropic materials and to the determination of the mechanics behind the fatigue response under dynamic loading. It is shown in this work that anisotropy has a significant influence in the fatigue response thus warranting the need for a law relating anisotropy to the materials response to cyclic indentation.

Residual stress in materials influences the materials properties and performance considerably. The fifth chapter of this thesis provides a technique for predicting plastic properties and residual stress of transversely isotropic materials from indentation response parameters. The technique assumes prior knowledge of the elastic modulus of the material and also utilizes a single indentation experiment. This work can be furthered by the utilization of multiple indentations with different cone angles and indentation orientations to be able to predict the residual stress as well as materials properties for anisotropic materials. A thorough analysis leading to a deep understanding of the dynamics behind the variation in indentation response of anisotropic materials with residual stress can be made. Also, the present work only deals with equibiaxial residual stresses. The analysis can be extended to more complicated distribution of residual stresses as well.

As a final suggestion into future work using dynamic indentation as used for fatigue studies, a highly promising area for indentation analysis lies in the study of high strain rate behavior of materials including metallic materials, metallic glasses, composites thin films and ceramics.

In the area of high strain rate studies, while methods such as Hopkinsons's split bar are well developed, the indentation method offers unmatched versatility, simplicity and elegance. For attaining high strain rates the indenter needs to be moved into the sample or the sample moved onto the indenter at high velocities. The necessary tools for thrusting the indenter or the sample and also to measure the associated force-displacements and other parameters are yet to be fully developed. To begin with, along the lines of this thesis, computational analysis and development of suitable algorithms

can be attempted to elucidate the high strain rate response of materials. Dynamic analysis packages such as LS-Dyna can be utilized to execute the computational analysis. A comprehensive analysis using dimensional analysis and optimization algorithms as utilized by the present thesis can be formulated.

Thus to conclude, the present work successfully utilizes indentation response to predict the material parameters, hardness, residual stress and fatigue characteristics of transversely isotropic materials. Indentation characterization and our ever increasing ability of computational analysis and simulation can, in the future be used to further delve into materials and their properties under static, dynamic or impact loading.

References

[1] Delobelle P, Fribourg-Blanc E, Remiens D. Thin Solid Films 2006;515:1385.

[2] Fischer-Cripps AC. Vacuum 2000;58:569.

[3] Giannakopoulos AE, Suresh S. Scripta Mater 1999;40:1191.

[4] Lan HZ, Venkatesh TA. Acta Mater 2007;55:2025.

[5] Venkatesh TA, Van Vliet KJ, Giannakopoulos AE, Suresh S. Scripta Mater 2000;42:833.

[6] Oliver WC, Pharr GM. J Mater Res 1992;7:1564.

[7] Tabor D. J I Met 1951;79:1.

[8] Chen YF, Sung PH, Wu CD, Fang TH. Mater Lett 2012;71:84.

[9] Kiener D, Motz C, Grosinger W, Weygand D, Pippan R. Scripta Mater 2010;63:500.

[10] Xu BX, Yue ZF, Chen X. Scripta Mater 2009;60:854.

[11] Xu BX, Yue ZF, Wang J. Mech Mater 2007;39:1066.

[12] Yang FQ, Peng LL, Okazaki K. J Mater Sci 2007;42:4513.

[13] Bhattacharya AK, Nix WD. Int J Solids Struct 1988;24:881.

[14] Bhattacharya AK, Nix WD. Int J Solids Struct 1991;27:1047.

[15] Chen YM, Ruff AW, Dally JW. J Mater Res 1994;9:1314.

[16] Giannakopoulos AE, Larsson PL, Vestergaard R. Int J Solids Struct 1994;31:2679.

[17] Bolshakov A, Oliver WC, Pharr GM. J Mater Res 1996;11:760.

[18] Larsson PL, Giannakopoulos AE, Soderlund E, Rowcliffe DJ, Vestergaard R. Int J Solids Struct 1996;33:221.

[19] Cheng YT, Cheng CM. Appl Phys Lett 1998;73:614.

[20] Dao M, Chollacoop N, Van Vliet KJ, Venkatesh TA, Suresh S. Acta Mater 2001;49:3899.

[21] Ogasawara N, Chiba N, Chen X. J Mater Res 2005;20:2225.

[22] Tho KK, Swaddiwudhipong S, Liu ZS, Zeng K. Mat Sci Eng a-Struct 2005;390:202.

[23] Giannakopoulos AE. J Appl Mech-T Asme 2000;67:409.

[24] Giannakopoulos AE, Suresh S. Acta Mater 1999;47:2153.

[25] Cheng G, Venkatesh TA. Phil Mag Lett, vol. In press, 2012.

[26] Borodich FM, Keer LM, Korach CS. Nanotechnology 2003;14:803.

[27] Giannakopoulos AE, Suresh S. Int J Solids Struct 1997;34:2357.

[28] Cheng YT, Cheng CM. Phil Mag Lett 1998;78:115.

[29] Cheng YT, Cheng CM. Phil Mag Lett 1998;77:39.

[30] Xu ZH, Agren J. Philos Mag 2004;84:2367.

[31] Chollacoop N, Ramamurty U. Mat Sci Eng a-Struct 2006;423:41.

[32] Swaddiwudhipong S, Hua J, Harsono E, Liu ZS, Ooi NSB. Model Simul Mater Sc 2006;14:1347.

[33] Swaddiwudhipong S, Hua J, Tho KK, Liu ZS. Model Simul Mater Sc 2006;14:71.

[34] Chollacoop N, Dao M, Suresh S. Acta Mater 2003;51:3713.

[35] Bucaille JL, Stauss S, Felder E, Michler J. Acta Mater 2003;51:1663.

[36] Tho KK, Swaddiwudhipong S, Liu ZS, Zeng K, Hua J. J Mater Res 2004;19:2498.

[37] Swaddiwudhipong S, Tho KK, Liu ZS, Zeng K. Int J Solids Struct 2005;42:69.

[38] Lan H, Venkatesh TA. Philos Mag 2007;87:4671.

[39] Lan HZ, Venkatesh TA. J Mater Res 2007;22:1043.

[40] Luo J, Lin J. Int J Solids Struct 2007;44:5803.

[41] Heinrich C, Waas AM, Wineman AS. Int J Solids Struct 2009;46:364.

[42] Cheng YT, Cheng CM. Mat Sci Eng R 2004;44:91.

[43] Cheng YT, Cheng CM. J Appl Phys 1998;84:1284.

[44] Nakamura T, Gu Y. Mech Mater 2007;39:340.

[45] ASM. ASM Handbook. Properties and selection Vol I, II, 1990.

[46] Chollacoop N, Ramamurty U. Scripta Mater 2005;53:247.

[47] Backes B, Durst K, Goken M. Philos Mag 2006;86:5541.

[48] Bao YW, Wang W, Zhou YC. Acta Mater 2004;52:5397.

[49] Bucaille JL, Stauss S, Schwaller P, Michler J. Thin Solid Films 2004;447:239.

[50] Chen KS, Chen TC, Ou KS. Thin Solid Films 2008;516:1931.

[51] Chen WM, Li M, Zhang T, Cheng YT, Cheng CM. Mat Sci Eng a-Struct 2007;445:323.

[52] Kese K, Li ZC. Scripta Mater 2006;55:699.

[53] Larsson PL. J Test Eval 2004;32:310.

[54] Lee JH, Lee H, Kim DH. J Mater Res 2008;23:2528.

[55] Lichinchi M, Lenardi C, Haupt J, Vitali R. Thin Solid Films 1998;333:278.

[56] Lim YY, Chaudhri MM. Philos Mag A 1999;79:2979.

[57] Marx V, Balke H. Acta Mater 1997;45:3791.

[58] Ogasawara N, Chiba N, Chen X. Scripta Mater 2006;54:65.

[59] Oliver WC. J Mater Res 2001;16:3202.

[60] Oliver WC, Pharr GM. Mrs Bull 2010;35:897.

[61] Pharr GM, Bolshakov A. J Mater Res 2002;17:2660.

[62] Wang JT, Hodgson PD, Yang CH. J Mater Res 2012;27:313.

[63] Xu ZH, Rowcliffe D. Philos Mag A 2002;82:1893.

[64] Tabor D. J I Met 1951;79:1.

[65] Liu SY, Chen IW. J Am Ceram Soc 1991;74:1197.

[66] Dauskardt RH, James MR, Porter JR, Ritchie RO. J Am Ceram Soc 1992;75:759.

[67] Prakash RV. T Indian I Metals 2010;63:173.

[68] Skrzypczak M, Guerret-Piecourt C, Bec S, Loubet JL, Guerret O. J Eur Ceram Soc 2009;29:1021.

[69] Casellas D, Nagl MM, Velez M, Llanes L, Anglada M. Bol Soc Esp Ceram V 1999;38:101.

[70] Ritter JE, Lardner TJ, Grayeski W, Prakash GC, Lawrence J. J Adhesion 1997;63:265.

[71] Choi SR, Salem JA. J Mater Sci Lett 1995;14:1286.

[72] Takakura E, Horibe S. Mater T Jim 1991;32:495.

[73] Horibe S. J Mater Sci Lett 1988;7:725.

[74] Noyan IC, Cohen JB. Mater Sci Eng 1985;75:179.

[75] Ma Q, Clarke DR. Acta Metall Mater 1993;41:1817.

[76] Suresh S, Giannakopoulos AE. Acta Mater 1998;46:5755.

[77] Ma ZS, Zhou YC, Long SG, Lu CS. Sci China Phys Mech 2012;55:1032.

[78] Huber N, Heerens J. Acta Mater 2008;56:6205.

[79] Qasmi M, Delobelle P, Richard F, Bosseboeuf A. Surf Coat Tech 2006;200:4185.

[80] Xu ZH, Li XD. Acta Mater 2005;53:1913.

[81] Gibmeier J, Hartmann S, Scholtes B. Residual Stresses Vii, Proceedings 2005;490-491:454.

[82] Lee YH, Kwon D. Acta Mater 2004;52:1555.

[83] Lee YH, Kwon D, Jang JI, Kim WS. Advances in Nondestructive Evaluation, Pt 1-3 2004;270-273:35.

[84] Larsson PL. Mater Design 2011;32:1427.

[85] Peyrot I, Bouchard PO, Ghisleni R, Michler J. J Mater Res 2009;24:936.

[86] Rydin A, Larsson PL. Tribol Lett 2012;47:31.

[87] Yan J, Chen X, Karlsson AM. J Eng Mater-T Asme 2007;129:200.

[88] Chen X, Yan J, Karlsson AM. Mat Sci Eng a-Struct 2006;416:139.

Appendix A: Equations for forward-reverse analysis

Three sets of dimensionless functions (Π_1, Π_2, Π_3) for the three indenter angles (50, 60 and 70.3°) are listed in detail here. Each function as described earlier is divided into 6 parts. Thus there exist a total of 54 equations (6 parts for each dimensionless function, 3 dimensionless functions for each indenter and 3 indenters), for each indentation direction. However all six parts of each dimensionless function have the same form and only differ from each other in their parameters. The equations are listed as Π_{jkl}. Here j goes from 1 to 3 and signifies the indenter type, 1 for 50°, 2 for 60° and 3 for 70.3°, k goes from 1 to 3 and conveys the type of dimensionless function, 1 for C, 2 for S_m, 3 for R_w, finally l represents the part number and goes from 1 to 6.

x, y, z represent E_0, E_L/E_T, σ_L/σ_T respectively. Here, the equations for longitudinal indentation have been displayed.

$$\Pi_{111} = \frac{C}{\sigma_0} = \big(n^2(18.8281 + 24.4279y^2 - 35.3573yz + 34.7982z^2)(-76.246 + 26.4381Log[x] - 2.2314Log[x]^2) + (4.0803 + 0.018y^2 - 0.1495yz + 0.2848z^2)(-20.5207 + 8.2753Log[x] - 0.7002Log[x]^2) + n(40.1085 - 9.34258y^2 + 14.6262yz - 4.8869z^2)(47.4263 - 17.0119Log[x] + 1.5602Log[x]^2)\big)$$

A.1

$$\Pi_{112} = \frac{C}{\sigma_0} = (n^2(48.0936 - 4.9179y^2 + 7.4351yz + 3.568z^2)(-271.1021 + 99.4352Log[x] - 9.0629Log[x]^2) + (2.4807 - 0.0227 - 0.01532yz + 0.1211z^2)(-8.962 + 4.591Log[x] - 0.3308Log[x]^2) + n(58.9021 - 2.3482y^2 + 5.0544yz + 3.3939z^2)(57.1259 - 21.1083Log[x] + 1.971Log[x]^2))$$

A.2

$$\Pi_{113} = \frac{C}{\sigma_0} = (n^2(72.8816 - 6.7693y^2 + 14.765yz + 10.9465)(-41.3448 + 15.0602Log[x] - 1.3439Log[x]^2) + (9.221 - 0.02284y^2 - 0.2792yz + 0.5641z^2)(-27.5961 + 10.9358Log[x] - 1.0223Log[x]^2) + n(30.882 - 1.7113y^2 + 3.171yz + 2.87478z^2)(52.9008 - 20.0138Log[x] + 1.9332Log[x]^2))$$

A.3

$$\Pi_{114} = \frac{C}{\sigma_0} = (n^2(38.897 - 3.5647y^2 + 7.2828yz + 2.9085z^2)(-161.5310 + 60.69971273432222Log[x] - 5.6491Log[x]^2) + (4.4162 - 0.05579y^2 + 0.0201yz + 0.1898z^2)(-9.3535 + 4.3882Log[x] - 0.3737Log[x]^2) + n(11.921 - 0.6206y^2 + 0.8945yz + 0.7737z^2)(114.2737 - 43.5738Log[x] + 4.2665Log[x]^2))$$

A.4

$$\Pi_{115} = \frac{C}{\sigma_0} = (n^2(2.4233 - 0.35046y^2 + 1.2517yz + 0.3243z^2)(-229.0153 + 83.03545Log[x] - 6.9858Log[x]^2) + (0.5211 - 0.004834y^2 - 0.00163yz + 0.02687z^2)(20.6025 - 0.2131Log[x] + 0.3215Log[x]^2) + n(0.8183 - 0.04156y^2 + 0.02219yz + 0.09156z^2)(-11.7873 - 2.2013Log[x] + 2.5624Log[x]^2))$$

A.5

$$\Pi_{116} = \frac{C}{\sigma_0} = (n^2(35.7987 - 1.6298y^2 + 6.3678yz + 3.7218z^2)(-179.628 + 70.4389Log[x] - 6.8604Log[x]^2) + (3.5688 - 0.0526y^2 + 0.03846yz + 0.13986z^2)(-7.326769 + 4.02244Log[x] - 0.3493Log[x]^2) + n(22.0893 - 1.6545y^2 + 2.0288yz + 1.2761z^2)(71.9282 - 28.69462Log[x] + 2.924Log[x]^2))$$

A.6

$$\Pi_{121} = \frac{S_m}{\sigma_0} = (1/100)((-6.28176 + 0.986x)(2.1214 + 1.015y - 0.305y^2) + n(-10.278 + 0.2189x)(-4.7473 - 1.31738y + 0.613) + n^2(-10.0788 + 0.0766x)(4.594 + 1.9755y + 0.7322y^2))$$

A.7

$$\Pi_{122} = \frac{S_m}{\sigma_0} = (1/100)((-8.6171 + 0.7559x)(3.2114 + 0.771y - 0.1957y^2) + n(-42.31 + 0.5247x)(-3.1093 - 0.559y + 0.7412y^2) + n^2(68.4312 - 1.0165x)(2.507 - 5.464y + 2.5317y^2))$$

A.8

$$\Pi_{123} = \frac{S_m}{\sigma_0} = (1/100)((-13.2843 + 0.9627x)(2.6946 + 0.3888y - 0.0674y^2) + n^2(149.492 - 0.71104x)(-6.639 - 2.0105y + 0.02154y^2) + n(-136.623 + 0.895x)(-3.6382 - 0.8381y + 0.803y^2))$$

A.9

$$\Pi_{124} = \frac{S_m}{\sigma_0} = (1/100)(n(274.616 - 1.1475x)(-3.668 + 3.279y - 1.0836y^2) + (-5.9358 + 0.7751x)(3.032 + 0.7540211125428131y - 0.1872y^2) + n^2(-189.949 + 1.1705x)(-4.3448 - 4.1801y + 1.559y^2))$$

A.10

$$\Pi_{125} = \frac{S_m}{\sigma_0} = (1/100)(n^2(240.277 - 1.2007x)(-1.6015 - 1.3097y - 0.89y^2) + (-5.13 + 0.947x)(2.237 + 0.887y - 0.24y^2) + n(-99.1023 + 0.7398x)(-2.7494 - 0.6281y + 0.5718y^2))$$

A.11

$$\Pi_{126} = \frac{S_m}{\sigma_0} = (1/100)(n(-207.441 + 1.4794x)(-4.7457 + 5.015236766301786y - 1.5366y^2) + (-4.0996 + 0.7635x)(2.999 + 0.7567y - 0.1762y^2) + n^2(272.385 - 1.1739x)(0.7792 - 5.1011y + 1.356y^2))$$

A.12

$$\Pi_{131} = R_w = n^3(0.3345 + 0.01469y + 0.1654z)(5.3007 - 1.1826Log[x]) + (0.175 + 0.00085y - 0.000689z)(4.6192 + 0.1639Log[x]) + n^2(-0.3224 + 0.416y - 0.4833z)(-46.0036 + 17.476Log[x] - 1.651Log[x]^2) + n(-0.43 + 0.0086y - 0.0648z)(18.001 - 6.3117Log[x] + 0.56Log[x]^2)$$

A.13

$$\Pi_{132} = R_w = n^2(-0.041 + 0.025y - 0.00836y^2 + 0.207z - 0.01042yz - 0.04z^2)(-28.032 + 9.136Log[x] - 0.803Log[x]^2) + (0.0269 + 0.0003y - 0.000081y^2 - 0.0000486z + 0.000032yz - 0.000034z^2)(15.3374 + 6.3165Log[x] - 0.474Log[x]^2) + n(0.0296 - 0.0119y + 0.003y^2 - 0.00845z + 0.00081yz + 0.003z^2)(-50.72 + 10.52Log[x] - 0.447Log[x]^2)$$

A.14

$$\Pi_{133} = R_w = n^3(0.132 - 0.039y + 0.08z)(6.323 - 1.957Log[x]) + (0.168 + 0.001y - 0.00062z)(4.508 + 0.224Log[x]) + n(-0.267 + 0.0154y - 0.0676z)(21.219 - 7.593Log[x] + 0.693Log[x]^2) + n^2(-0.0002 - 0.006178y + 0.0102z)(-29.619 - 6.653Log[x] + 2.214Log[x]^2)$$

A.15

$$\Pi_{134} = R_w = (0.0476 + 0.00057y - 0.00016y^2 - 0.00017z + 0.000055yz - 0.000037z^2)(6.0252 + 4.623Log[x] - 0.3628Log[x]^2) + n^2(0.6715 - 0.2138y + 0.0518y^2 - 1.7926z + 0.0827yz + 0.3758z^2)(25.966 - 9.72Log[x] + 0.92Log[x]^2) + n(0.343 - 0.1238y + 0.02885y^2 - 0.1163z + 0.00799yz + 0.0416z^2)(26.781 - 11.0108Log[x] + 1.0983Log[x]^2)$$

A.16

$$\Pi_{135} = R_w = n^3(0.222 + 0.00864y + 0.0667z)(2.856 - 0.98Log[x]) + (0.17 + 0.00097y - 0.00024z)(4.233 + 0.264Log[x]) + n^2(-0.264 + 0.46y - 0.53z)(-57.098 + 22.878Log[x] - 2.287Log[x]^2) + n(-0.5 + 0.0995y - 0.258z)(11.494 - 4.283Log[x] + 0.4072Log[x]^2)$$

A.17

$$\Pi_{136} = R_w = n^3(0.239 + 0.0052y + 1.071z)(7.66 - 1.617Log[x]) + n(-0.387 + 0.235y - 0.0612y^2 + 0.043z - 0.0045yz - 0.0167z^2)(3.5137 - 0.485Log[\mathrm{x}]) + (0.171 + 0.0006y - 0.000133y^2 + 0.00046z + 0.00017yz - 0.00061z^2)(4.202 + 0.2657Log[x]) + n^2(-24.061 + 15.408y - 4.0741y^2 + 17.0733z - 1.1663yz - 4.2966z^2)(69.15 - 28.096Log[x] + 2.85Log[x]^2)$$

A.18

$$\Pi_{211} = \frac{C}{\sigma_0} = (n^2(69.026 - 71.23y^2 + 183.221yz - 98.883z^2)(-149.85 + 53.731Log[x] - 4.768Log[x]^2) + (3.687 - 0.0263y^2 - 0.0309yz + 0.282)(18.9 - 4.445Log[x] + 0.46Log[x]^2) + n(44.723 + 12.743y^2 - 35.5014yz + 29.373z^2)(63.228 - 23.454Log[x] + 2.228Log[x]^2))$$

A.19

$$\Pi_{212} = \frac{C}{\sigma_0} = (n(-106.38 + 25.1359y^2 - 49.103yz + 18.388z^2)(-242.875 + 90.31Log[x] - 8.42Log[x]^2)$$
$$+ n^2(373.562 + 305.986y^2 - 628.35yz + 479.3779z^2)(-152.72 + 56.6225Log[x]$$
$$- 5.242Log[x]^2) + (5.167 - 0.0889y^2 + 0.0605yz + 0.241z^2)(-9.279 + 4.81Log[x]$$
$$- 0.3623Log[x]^2))$$

A.20

$$\Pi_{213} = \frac{C}{\sigma_0} = (n^2(15.087 - 23.752y^2 + 59.974yz - 36.613z^2)(-971.32 + 372.415Log[x] - 35.484Log[x]^2)$$
$$+ (16.98 - 0.2016y^2 - 0.075yz + 1.00236z^2)(-28.421 + 11.208Log[x] - 1.0376Log[x]^2)$$
$$+ n(36.287 + 21.998 - 57.43yz + 45.866z^2)(124.9 - 48.44Log[x] + 4.751Log[x]^2))$$

A.21

$$\Pi_{214} = \frac{C}{\sigma_0} = (n^2(291.476 + 1203.446y^2 - 2317.403yz + 1647.89z^2)(-161.82 + 61.984Log[x]$$
$$- 5.933Log[x]^2) + (7.746 - 0.1278y^2 + 0.0825yz + 0.358z^2)(28.933 - 10.177Log[x]$$
$$+ 1.0334Log[x]^2) + n(653.21 - 177.107y^2 + 333.304yz$$
$$- 133.42547256604485z^2)(83.322 - 31.966Log[x] + 3.07Log[x]^2))$$

A.22

$$\Pi_{215} = \frac{C}{\sigma_0} = (n^2(146.069 - 496.61y^2 + 1244.125yz - 451.744z^2)(-198.5 + 77.882Log[x] - 7.634Log[x]^2)$$
$$+ (8.064 - 0.43 + 0.726yz + 0.188z^2)(-20.209 + 8.65Log[x] - 0.779Log[x]^2)$$
$$+ n(101.936 + 24.418y^2 - 63.716yz + 41.79174556101204z^2)(114.66 - 44.811Log[x]$$
$$+ 4.4046Log[\mathrm{x}]^2))$$

A.23

$$\Pi_{216} = \frac{C}{\sigma_0} = (n(56.93 - 4.756y^2 + 5.11yz + 3.65z^2)(-61.8 + 24.127Log[x] - 2.306Log[x]^2) + (9.04 - 0.18y^2 + 0.189yz + 0.397z^2)(-16.746 + 7.437Log[x] - 0.687Log[x]^2) + n^2(23.7 - 1.114y^2 + 9.836yz + 0.022z^2)(140.42 - 56.71Log[x] + 5.78Log[x]^2))$$

A.24

$$\Pi_{221} = \frac{S_m}{\sigma_0} = (1/100)((-6.237 + 1.1067x)(2.679 + 1.782y - 0.494y^2) + n^2(-542.199 + 2.245x)(0.8665 - 10.02y + 4.67y^2) + n(298.21 - 0.5x)(7.7 - 16.82y + 6.791y^2))$$

A.25

$$\Pi_{222} = \frac{S_m}{\sigma_0} = (1/100)((-5.892 + 0.718x)(4.663 + 2.0193y - 0.5092y^2 + 0.0144) + n(-10.285 + 2.209x)(-5.837 + 10.168y - 6.649y^2 + 1.4y^3) + n^2(63.536 - 2.3597x)(-19.774 + 40.417y - 26.8667y^2 + 5.738y^3))$$

A.26

$$\Pi_{223} = \frac{S_m}{\sigma_0} = (1/100)((-6.019 + 1.07x)(2.7547 + 1.856y - 0.509y^2) + n^2(404.779 - 2.773x)(-0.534 - 0.582y - 0.425y^2) + n(-28.27 + 0.479x)(-3.814 - 2.45y + 0.3y^2))$$

A.27

$$\Pi_{224} = \frac{S_m}{\sigma_0} = (1/100)(n^2(-205.396 + 3.0125x)(-4.095 + 7.435y - 2.786y^2) + (-8.785 + 0.929x)(3.606 + 1.623y - 0.397y^2) + n(-38.935 + 1.298x)(0.553 - 3.9138y + 1.489y^2))$$

A.28

$$\Pi_{225} = \frac{S_m}{\sigma_0} = (1/100)(n^2(-282.898 + 1.838x)(6.393 + 2.0011y - 0.0153y^2) + (-19.602 + 1.1056x)(3.773 + 0.5565y - 0.01517y^2) + n(-138.06 + 1.14x)(-5.952308455233735 - 1.482y + 0.698y^2))$$

A.29

$$\Pi_{226} = \frac{S_m}{\sigma_0} = (1/100)(n(-125.253 + 1.0518x)(-7.243 + 3.148y - 0.963y^2) + (-15.5 + 0.9157x)(4.011 + 1.4437y - 0.321y^2) + n^2(378.621 - 2.1673x)(2.472 - 7.8161y + 2.0587y^2))$$

A.30

$$\Pi_{231} = R_w = (0.2288 + 0.0018y - 0.0019z)(3.191 + 0.179Log[x]) + n^3(0.403 - 0.224y + 0.963z)(-7.58 + 1.333Log[x]) + n^2(-0.3638 + 0.0488y - 0.173z)(-54.093 + 18.237Log[x] - 1.515Log[x]^2) + n(1.204 - 0.254y + 0.228z)(-11.606 + 4.03Log[x] - 0.353Log[x]^2)$$

A.31

$$\Pi_{232} = R_w = n^2(0.125 - 0.186y + 0.0447y^2 - 0.7856z + 0.0648yz + 0.1608z^2)(-30.327 + 11.1445Log[x] - 1.007Log[x]^2) + (0.055 + 0.0008y - 0.0002y^2 - 0.00043z + 0.000122yz - 0.00005z^2)(5.025 + 3.696Log[x] - 0.2675Log[x]^2) + n(-1.113 + 0.61y - 0.141y^2 + 0.026z - 0.0267yz - 0.0573z^2)(13.765 - 4.7733Log[x] + 0.419Log[x]^2)$$

A.32

$$\Pi_{233} = R_w = n^3(-0.0188 + 0.0062y - 0.00916z)(68.965 - 7.12Log[x]) + (0.1287 + 0.0014y - 0.000986z)(5.21 + 0.403Log[x]) + n^2(-0.563 - 0.296y + 0.178z)(-127.347 + 48.4217Log[x] - 4.602Log[x]^2) + n(-1.657 + 0.3041y - 0.683z)(15.7677 - 5.92Log[x] + 0.559Log[x]^2)$$

A.33

$$\Pi_{234} = R_w = (0.0227 + 0.00052y - 0.000126y^2 - 0.000084z + 0.00003yz - 0.000044z^2)(11.13 + 9.255Log[x] - 0.681Log[x]^2) + n^2(-0.318 + 0.693y - 0.15y^2 + 2.5383z - 0.21yz - 0.502z^2)(32.822 - 12.49Log[x] + 1.1834Log[x]^2) + n(-0.496 + 0.273y - 0.0616y^2 - 0.0779z - 0.00279yz - 0.0118z^2)(67.884 - 25.24Log[x] + 2.36Log[x]^2)$$

A.34

$$\Pi_{235} = R_w = n^3(0.417 - 0.9y + 0.757z)(2.991 - 2.4851Log[x]) + (0.136 + 0.0018y + 0.001y^2 + 0.02z - 0.0022yz - 0.00756z^2)(4.13 + 0.4155Log[x]) + n^2(-0.957 + 2.48y - 2.1z)(-99.66 + 39.1Log[x] - 3.886Log[x]^2) + n(-0.21 + 0.25y - 0.2783z)(10.317 - 3.076Log[x] + 0.2476Log[x]^2)$$

A.35

$$\Pi_{236} = R_w = n(-0.27 + 0.198y - 0.0549y^2 - 0.13z + 0.0201yz + 0.0146z^2)(-20.738 + 9.379Log[x] - 1.0084Log[x]^2) + n^2(-0.011 + 0.14y - 0.0513y^2 + 0.0746z + 0.023yz - 0.00755z^2)(-21.6761 + 9.0156Log[x] - 0.9885Log[x]^2) + (0.095 + 0.00216y - 0.000495y^2 - 0.000665z + 0.0001yz - 0.00015z^2)(-3.767 + 4.68Log[x] - 0.399Log[x]^2)$$

A.36

$$\Pi_{311} = \frac{C}{\sigma_0} = (n(897.427 + 24.265y^2 - 147.8yz + 114.269z^2)(-49.35 + 18.237Log[x] - 1.678Log[x]^2) + (8.346 - 0.202y^2 + 0.223yz + 0.589z^2)(27.73 - 8.122Log[x] + 0.87Log[x]^2) + n^2(-37.62 - 523.78y^2 + 1638.94yz - 251.66z^2)(89.1 - 33.158Log[x] + 3.088Log[x]^2))$$

A.37

$$\Pi_{312} = \frac{C}{\sigma_0} = (n(356.005 - 22.099y^2 + 36.973yz + 12.99z^2)(-59.95 + 22.157Log[x] - 2.03Log[x]^2)$$
$$+ (6.995 - 0.2226y^2 + 0.2383yz + 0.295z^2)(-14.462 + 7.439Log[x] - 0.4848Log[x]^2)$$
$$+ n^2(254.79 - 36.35y^2 + 89.718yz + 7.1484z^2)(137.87 - 51.7Log[x] + 4.86Log[x]^2))$$

A.38

$$\Pi_{313} = \frac{C}{\sigma_0} = ((49.057 - 1.275y^2 + 1.0645yz + 3.2024z^2)(-38.84 + 15.124Log[x] - 1.415Log[x]^2)$$
$$+ n(90.47 - 15.816 + 33.4943yz - 1.402z^2)(41.49 - 16.354Log[x] + 1.653Log[x]^2)$$
$$+ n^2(30.84 + 9.001y^2 - 13.378yz + 14.3985z^2)(68.655 - 28.72Log[x] + 3.07Log[x]^2))$$

A.39

$$\Pi_{314} = \frac{C}{\sigma_0} = (n(378.27 - 62.89y^2 + 111.846yz - 11.1583z^2)(-69.4533 + 26.4896Log[x]$$
$$- 2.51355Log[x]^2) + (14.0156 - 0.473y^2 + 0.5yz + 0.507z^2)(-21.597 + 8.9596Log[x]$$
$$- 0.7174Log[x]^2) + n^2(199.98 + 73.4229y^2 - 103.525yz + 75.404z^2)(220.021$$
$$- 84.545Log[x] + 8.134Log[x]^2))$$

A.40

$$\Pi_{315} = \frac{C}{\sigma_0} = (n(19.33 - 8.098y^2 + 16.234yz - 3.69z^2)(-42.668 + 14.594Log[x] - 1.0367Log[x]^2)$$
$$+ (23.4054 - 0.824y^2 + 0.822yz + 1.33z^2)(27.297 - 10.452Log[x] + 1.1216Log[x]^2)$$
$$+ n^2(13.028 + 19.266y^2 - 34.02yz + 17.182z^2)(95.54 - 40.067Log[x] + 4.3834Log[x]^2))$$

A.41

$$\Pi_{316} = \frac{C}{\sigma_0} = (n^2(90.744 + 98.74y^2 - 135.0867yz + 80.2981z^2)(-218.335 + 86.3119Log[x] - 8.508Log[x]^2) + (23.605 - 0.773y^2 + 0.8935yz + 0.96z^2)(-25.136 + 10.438Log[x] - 0.958Log[x]^2) + n(126.645 - 27.9694y^2 + 45.94yz - 9.5665z^2)(59.095 - 23.9617Log[x] + 2.4617Log[x]^2))$$

A.42

$$\Pi_{321} = \frac{S_m}{\sigma_0} = (1/100)(n^2(-636.665 + 3.5843x)(-10.6856 + 13.737y + 9.4743y^2 - 8.1199y^3) + (-29.3777 + 1.3505x)(4.0227 + 2.056y - 0.1714y^2 - 0.1545y^3) + n(-51.73 + 0.4234x)(-14.6562 - 10.1745y - 5.035y^2 + 5.085y^3))$$

A.43

$$\Pi_{322} = \frac{S_m}{\sigma_0} = (1/100)(n^2(-71.496 + 1.297x)(7.685 - 9.06113y + 5.3444y^2 - 1.0995y^3) + (-9.3294 + 0.9495x)(4.888 + 4.2032y - 1.593y^2 + 0.207) + n(-19.6555 + 0.5043x)(-12.602 + 2.9937y - 1.8045y^2 + 0.449y^3))$$

A.44

$$\Pi_{323} = \frac{S_m}{\sigma_0} = (1/100)(n^2(-90.649 + 1.155x)(4.3139 + 0.64y - 0.2717y^2 - 0.3292y^3) + (-10.921 + 1.0471x)(5.0882 + 1.9874y + 0.2443y^2 - 0.31253y^3) + n(-39.4813 + 0.8429x)(-5.6953 - 1.773y - 0.1754y^2 + 0.5708y^3))$$

A.45

$$\Pi_{324} = \frac{S_m}{\sigma_0} = (1/100)(n^2(1133.337 - 4.5071x)(27.5615 - 56.4473y + 39.05881y^2 - 8.6521y^3) + (-8.8087 + 0.8096x)(7.7353 + 0.609y + 1.17262y^2 - 0.4371y^3) + n(111.634 + 0.9591x)(-12.2534 + 20.6608y - 14.36774y^2 + 3.201877y^3))$$

A.46

$$\Pi_{325} = \frac{S_m}{\sigma_0} = (1/100)(n^2(219.0867 - 1.0412x)(9.2568 + 2.7738y + 0.0434y^2 - 1.08434y^3) + (-22.3769 + 1.1262x)(5.2684 + 1.778y + 0.2544y^2 - 0.3226y^3) + n(43.214 + 0.532x)(-5.2321 - 0.97681y + 0.08065y^2 + 0.4183y^3))$$

A.47

$$\Pi_{326} = \frac{S_m}{\sigma_0} = (1/100)(n^2(559.2 - 2.632x)(6.915 - 11.7656y + 12.634y^2 - 3.6745y^3) + (-14.4947 + 0.8385x)(8.527 - 0.2849y + 1.3448y^2 - 0.397y^3) + n(20.8327 + 0.1733x)(-23.5716 + 17.2385y - 10.8858y^2 + 2.2938y^3))$$

A.48

$$\Pi_{331} = R_w = n(-1.089 + 0.20756y - 0.1706z)(2.487 - 0.4192Log[x]) + (0.1195 - 0.0024y + 0.0024y^2 + 0.01367z - 0.00161yz - 0.005786z^2)(4.5686 + 0.5012Log[x]) + n^2(-1.6328 + 0.2266y - 0.8676z)(-4.3119 + 0.787Log[x]) + n^3(0.161 - 0.129y + 0.5852z)(-74.743 + 23.0371Log[x] - 1.74811Log[x]^2)$$

A.49

$$\Pi_{332} = R_w = n^2(0.0081 - 0.0125y + 0.0405z)(-35.634 + 5.5486Log[x]) + (0.0773 + 0.00215y - 0.00052y^2 - 0.002544z + 0.00038yz + 0.00026z^2)(-7.4983 + 6.1823Log[x] - 0.48Log[x]^2) + n(-0.157 + 0.0746y - 0.0192y^2 - 0.024248z - 0.000174yz + 0.00685z^2)(12.405 - 3.8025Log[x] + 0.3398Log[x]^2)$$

A.50

$$\Pi_{333} = R_w = n^2(-1.2776 + 1.27547y - 1.75103z)(3.5018 - 0.6955Log[x]) + (0.1886 + 0.005925y - 0.000737 + 0.00356z - 0.00296z^2)(2.3249 + 0.4416Log[x]) + n(-0.0696 + 0.01255y - 0.0209z)(0.7338 + 0.4861Log[x]) + n^3(-0.2718 + 0.3438y - 0.5615z)(-71.837 + 22.926Log[x] - 1.678Log[x]^2)$$

A.51

$$\Pi_{334} = R_w = (n^2(1.0326 - 3.2045y + 1.0895y^2 + 3.978z - 0.702yz - 0.23424z^2)(-24.467 + 8.7135Log[x] - 0.7673Log[x]^2) + (0.2288 + 0.0097y - 0.00232y^2 - 0.00771z + 0.001084yz + 0.00089z^2)(-6.885 + 3.7917Log[x] - 0.33Log[x]^2) + n(0.03532 - 0.00927y + 0.000424y^2 + 0.0071z + 0.001628yz - 0.000224)(58.6076 - 25.0304Log[x] + 2.371Log[x]^2) + n^3(-0.069 - 0.9017y + 0.3516 + 1.5964z - 0.266yz - 0.17672z^2)(356.247 - 131.1068Log[x] + 11.979Log[x]^2)$$

A.52

$$\Pi_{335} = R_w = n(3.3327 + 1.0874y - 2.2805y^2 + 1.764z + 3.687yz - 1.978z^2)(-1.10338 + 0.3919Log[x] - 0.03626Log[x]^2) + n^3(1.5959 + 2.4894y + 3.8297y^2 + 1.3586z + 0.2545yz + 1.6684z^2)(0.4167 - 0.234Log[x] + 0.0272Log[x]^2) + n^2(-1.5289 - 0.009863y + 2.2687y^2 + 0.3755z - 17.272yz + 9.621z^2)(0.7918 - 0.3635Log[x] + 0.03985Log[x]^2) + (-0.0157 - 0.00016y^2 - 0.001629z + 0.00079z^2)(-4.7439 - 13.515Log[x] + 0.7875Log[x]^2$$

A.53

$$\Pi_{336} = R_w = (1.776967 + 1.3261n - 7.7316n^2)(-0.2098 + 0.0883y + 0.07y^2 + 0.2304z - 0.1498yz - 0.0471z^2) + (-1.1447 - 0.2898n + 5.6733n^2 - 5.1651n^3)(-0.3045 + 0.0023y + 0.0335y^2 + 0.1231z - 0.0589yz - 0.022z^2)Log[x] + (-0.5494 - 0.874n + 9.5098n^2 - 10.027n^3)(0.03667 + 0.0071y - 0.00417y^2 - 0.01946z + 0.005yz + 0.00292z^2)Log[x]^2$$

A.54

Appendix B: Hardness equations

The equations are listed as Π_{jkl}. Here, j goes from 1 to 2 and signifies the indenter orientation, 1 for perpendicular, and 2 for parallel to the plane of isotropy, k takes values 4 and 5, and conveys the type of dimensionless function, 4 for A_m and 5 for H_m, and lastly l represents the part number and goes from 1 to 6. Also x, y and z represent the properties E_0, E_L/E_T and σ_L/σ_T respectively, n being the strain hardening exponent.

Longitudinal indentation

$$\Pi_{151} = H/\sigma = (n(-0.1272 - 0.6576y^2 + 6.1848yz - 0.06897z^2)(-35.984 + 13.6496Log[x] - 1.2616Log[x]^2) + (2.6054 - 0.1339y^2 + 0.17091yz + 0.1728z^2)(15.98 - 5.678Log[x] + 0.543Log[x]^2) + n^2(17.92 - 3.708y^2 + 0.1982yz - 2.114z^2)(241.1 - 92.884Log[x] + 9.0109))$$

B.1

$$\Pi_{152} = H/\sigma = ((3.6004 - 0.09255y^2 + 0.1296yz + 0.24z^2)(11.91 - 4.1712Log[x] + 0.3902Log[x]^2) + n^2(39.572 + 12.99y^2 - 34.0394yz + 17.8487z^2)(255.369 - 95.334Log[x] + 8.9121Log[x]^2) + n(-9.0044 + 4.2726y^2 - 9.791yz + 3.4731z^2)(263.75 - 98.015Log[x] + 9.0796Log[x]^2))$$

B.2

$$\Pi_{153} = H/\sigma = (n^2(21.469 + 16.295y^2 - 41.696yz + 19.1475z^2)(-334.55 + 127.647Log[x] - 12.1275Log[x]^2) + (1.8505 + 0.01624y^2 - 0.114yz + 0.232z^2)(12.825 - 4.5018Log[x] + 0.4455Log[x]^2) + n(1.2337 - 7.613y^2 + 19.125yz - 7.2672z^2)(65.286 - 25.308Log[x] + 2.488Log[x]^2))$$

B.3

$$\Pi_{154} = H/\sigma = (n^2(20.422 + 5.4588y^2 - 18.283yz + 6.342782z^2)(-229.6853 + 87.3963Log[x] - 8.2544Log[x]^2) + n(1.899 - 4.969y^2 + 14.464yz - 3.966z^2)(-107.43 + 40.915Log[x] - 3.8688Log[x]^2) + (5.423 - 0.1245y^2 + 0.137yz + 0.362z^2)(12.42 - 4.621Log[x] + 0.448Log[x]^2))$$

B.4

$$\Pi_{155} = H/\sigma = (n^2(494.41 - 37.065y^2 + 90.58yz - 13.61z^2)(-40.541 + 15.91Log[x] - 1.559Log[x]^2) + (5.0247 - 0.518 + 0.94yz + 0.277z^2)(19.087 - 7.417Log[x] + 0.739Log[x]^2) + n(117.662 - 9.448y^2 + 24.61yz + 9.04z^2)(42.0957 - 16.539Log[x] + 1.626Log[x]^2))$$

B.5

$$\Pi_{156} = H/\sigma = (n^2(208.264 - 11.76y^2 + 20.3yz + 2.91677z^2)(-143.318 + 56.35Log[x] - 5.5364Log[x]^2) + (11.048 - 0.7239y^2 + 1.2796yz + 0.475z^2)(20.395 - 8.02Log[x] + 0.797Log[x]^2) + n(172.35 - 11.636y^2 + 19.675yz + 4.696z^2)(40.512 - 15.922Log[x] + 1.566Log[x]^2))$$

B.6

Transverse indentation

$$\Pi_{251} = H/\sigma = (n^2(-25.151 - 21.081y^2 + 53.796yz - 20.651z^2)(-498.28 + 185.072Log[x] - 17.18Log[x]^2) + (0.0552 - 0.00059 - 0.000045yz - 0.000163z^2)(2.2336 + 3.985Log[x] - 0.236Log[x]^2) + n(-1.4269 + 1.306y^2 - 4.779yz + 1.895z^2)(58.37 - 21.608Log[x] + 2.001Log[x]^2))$$

B.7

$$\Pi_{252} = H/\sigma = (n^2(-77.197 + 46.043y - 12.1176y^2 + 47.91z - 3.393yz - 12.7135z^2)(-889.5677 + 330.388Log[x] - 30.667Log[x]^2) + (7.626 - 0.273y + 0.025y^2 + 0.0246z + 0.000062yz - 0.03625z^2)(-0.0956 + 0.0706Log[x] - 0.00551Log[x]^2) + n(8.515 - 7.44y + 1.7821y^2 - 5.841z + 0.475yz + 1.5028z^2)(92.0021 - 34.052Log[x] + 3.153Log[x]^2))$$

B.8

$$\Pi_{253} = H/\sigma = ((0.0593 + 0.00043y^2 + 0.000112yz - 0.00066z^2)(0.468 + 4.259Log[x] - 0.271Log[x]^2) + n^2(-0.924 + 0.082y^2 - 0.208yz - 1.0106z^2)(15.435 - 5.798Log[x] + 0.548Log[x]^2) + n(0.633 - 0.0782y^2 + 0.0144yz + 0.0124z^2)(21.15 - 8.272Log[x] + 0.795Log[x]^2))$$

B.9

$$\Pi_{254} = H/\sigma = (n^2(-21.366 - 21.653y + 3.093y^2 + 54.8z + 7.681yz - 25.88z^2)(-196.997 + 75.7Log[x] - 7.27Log[x]^2) + (0.2685 - 0.0173y + 0.0026y^2 + 0.0089z + 0.00077yz - 0.0051z^2)(-10.99 + 5.11Log[x] - 0.446Log[x]^2) + n(0.776 - 1.588y + 0.318y^2 - 2.7141z - 0.0539yz + 1.034z^2)(93.06 - 35.756Log[x] + 3.438Log[x]^2))$$

B.10

$$\Pi_{255} = H/\sigma = (n^2(-2.825 + 0.2225y^2 - 0.416yz - 0.0293z^2)(-94.13 + 37.046Log[x] - 3.641Log[x]^2) + (0.374 - 0.0029y^2 - 0.0037yz + 0.00016z^2)(33.127 - 12.357Log[x] + 1.2423Log[x]^2) + n(-1.7983 - 0.634y^2 + 0.45yz - 0.0861z^2)(52.47 - 20.564Log[x] + 2.018Log[x]^2))$$

B.11

$$\Pi_{256} = H/\sigma = ((0.595 - 0.03y + 0.00033y^2 - 0.0135z + 0.0052yz - 0.0014z^2)(10.06 - 3.535Log[x] + 0.37Log[x]^2) + n(-0.12 - 0.131y + 0.0296y^2 + 0.215z + 0.019874875909881115yz - 0.0945244160732065z^2)(-0.32485697970817407 - 2.33Log[x] + 0.59Log[x]^2) + n^2(1.047 + 3.409y - 0.687y^2 - 8.964z - 1.814yz + 4.83z^2)(34.01 - 12.78Log[x] + 1.2Log[x]^2))$$

B.12

Appendix C: Residual stress equations

The equations are listed as Π_{jk}. Here, j denotes the case II analysis of transversely isotropic materials with residual stress and k conveys the type of dimensionless function, 1 for C/E, 2 for S_m/h_m*E, and 3 for R_w. Also x, y and z represent the properties E/σ_y, σ_r/σ_y and σ_L/σ_T respectively.

$$\Pi_{21} = C/E = (\frac{1}{x}(-135.3 - 4.34y - 171.81y^2 + (64.44 - 12.44y + 56.8y^2)Log[x] + (-5.16 + 1.98y - 4.9y^2)Log[x]^2 + z^2(-32.4 + 40.16y - 60.22y^2 + (11.6 - 15.25y + 21.41y^2)Log[x] + (-1.15 + 1.437y - 1.895y^2)Log[x]^2) + z(50.43 - 49.3y + 271.83y^2 + (-17.55 + 20.33y - 96.45y^2)Log[x] + (2.4 - 2.16y + 8.52y^2)Log[x]^2))$$

C.1

$$\Pi_{22} = S_m/Eh_m = (\frac{1}{x} - 104.21 - 33.18y - 160.41 + x^2(0.00029 + 0.0023y - 0.00118y^2) + x(8.94 - 1.53y + 0.389y^2) + (-38.7 + 48.02y + 252.15y^2 + x(-0.56 + 0.578y - 1.32y^2) + x^2(0.00035 - 0.0016y + 0.0021y^2))z + (12.22 - 4.54y - 67.73y^2 + x^2(-0.00004 + 0.00045y - 0.00054y^2) + x(0.0649 - 0.189y + 0.38y^2))z^2)$$

C.2

$$\Pi_{21} = R_w = (0.146 + 0.34y + 0.12y^2 + (0.24 - 0.1075y - 0.036y^2)\text{Log}[x] + (-0.017 + 0.0084y + 0.00284y^2)\text{Log}[x]^2 + z^2(0.1142 - 0.055y - 0.092y^2 + (-0.037 + 0.02y + 0.032y^2)\text{Log}[x] + (0.003 - 0.0018y - 0.0028y^2)\text{Log}[x]^2) + z(-0.59 + 0.2y + 0.18y^2 + (0.18 - 0.071y - 0.063y^2)\text{Log}[x] + (-0.0145 + 0.0064y + 0.0054y^2)\text{Log}[x]^2))$$

C.3